AFIT/GE/ENG/93D-31

PERFORMANCE COMPARISON OF SHEARING INTERFEROMETER AND HARTMANN WAVE FRONT SENSORS

THESIS

Timothy Lee Pennington
First Lieutenant, USAF

AFIT/GE/ENG/93D-31

AFIT/GE/ENG/93D-31

PERFORMANCE COMPARISON OF SHEARING INTERFEROMETER AND HARTMANN WAVE FRONT SENSORS

THESIS

Presented to the Faculty of the Graduate School of Engineering

of the Air Force Institute of Technology

Air University

In Partial Fulfillment of the

Requirements for the Degree of

Master of Science in Electrical Engineering

Timothy Lee Pennington, B.S.E.E.

First Lieutenant, USAF

December, 1993

Approved for public release; distribution unlimited

Acknowledgments

I would like to take a moment to thank my committee, Dr. Byron Welsh, Dr. Michael Roggemann and Dr. Dennis Ruck for their invaluable guidance during this thesis effort. A special thanks is due to Dr. Welsh for his enthusiasm and advice which surpassed all levels of expectation. I am also indebted to my parents for teaching me that "I can do all things through Christ who strengths me" (Philippians 4:13)–which has provided strength to continue even in the most difficult of times. Most importantly though, a heartfelt thanks to my wife, Amy, for her understanding, support and help during these past eighteen months.

Timothy Lee Pennington

Table of Contents

Abstract

The resolution of optical imaging systems is severely degraded from the diffraction limit by the random effects of the atmosphere. Techniques exist to compensate for the atmospheric turbulence, one of which is adaptive optics. A critical component in the adaptive optics system is the wavefront sensor. Presently, two types of sensors are being used–the Hartmann-Shack Wavefront Sensor and the Shearing Interferometer. Previous studies have compared these two sensors and found them to perform identically for a point source. However, to date, no comparison has been performed for an extended source and subaperture spacing larger than the correlation length of the atmosphere, r_o. This thesis has examined this problem and compared these two sensors for the above conditions. Results indicate that the sensors have comparable performance when an infinite number of photons are available. However, the photon limited cases indicate superior performance by the Hartmann Sensor.

PERFORMANCE COMPARISON OF SHEARING INTERFEROMETER AND HARTMANN WAVE FRONT SENSORS

I. Introduction

The upper bound on the resolution achievable by a ground based imaging system is set by the diffraction limit. This diffraction limit is inversely proportional to the size of the optical system. However, Sir Isaac Newton recognized in 1730 that another, more restrictive limit existed when he wrote:

> If the Theory of making Telescopes could at length be fully brought into Practice, yet there would be certain Bounds beyond which Telescopes could not perform. For the Air through which we look upon the Stars, is in perpetual Tremor; as may be seen by the tremulous Motion of Shadows cast from high Towers, and by the twinkling of the fix'd Stars [16].

This "Tremor" of the air is today known as atmospheric distortion and has been the object of considerable research for the past several decades [2], [9], [10], [14], [19].

1.1 Atmospheric Turbulence and Its Effect

Atmospheric turbulence arises from the sun's uneven heating of the Earth. This differential heating generates pockets of air, called eddies, each a different temperature. Each eddy deflects, or refracts, the light by an amount related to its temperature. Hence, as light passes from one air pocket to the next, it is randomly bent as the temperature changes. As the entire wavefront propagates through the atmosphere, it passes through different "eddies" and hence is bent by different amounts, (see Figure 1.1), creating uneven lines of constant phase. The resulting image formed by a telescope looking through the atmosphere is distorted and blurred.

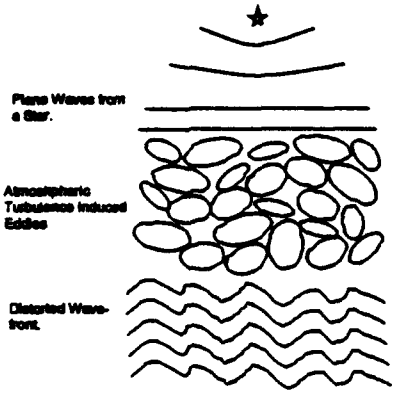

Figure 1.1. Light Experiencing Atmospheric Turbulence.

From a communication theory perspective, the atmospheric turbulence can be thought of as a low pass filter with a spatial frequency cut-off far below the diffraction limit. And just as sharp transitions, such as the corners of a square wave, require high frequencies to pass through a communication channel, so do the sharp transitions that might be present on a satellite in Earth orbit. The atmospheric low pass filter effectively removes these high frequency components, resulting in a blurred image. This cut-off frequency is related to Fried's Coherence Diameter, r_o [2], which can be thought of as the maximum separation of two points for which the field is correlated. This parameter is, of course, related to the strength of the atmospheric turbulence.

1.2 Adaptive Optic Compensation

In 1953, Horace W. Babcock [1] proposed using a mirror coated with an oil film to correct for the phase distortions imposed by atmospheric turbulence. The thickness of the oil film would be altered by electric charge, changing the optical path length such that the effects of atmospheric turbulence would be canceled out. This idea is the basis of current adaptive optic systems. Present day systems are composed of three major components [15]: a phase-shifting optical element, a wavefront sensor, and a servo-control system, (see Figure 1.2). As the light passes through the telescope, the atmospheric phase distortions are compensated for by using the phase-shifting optical

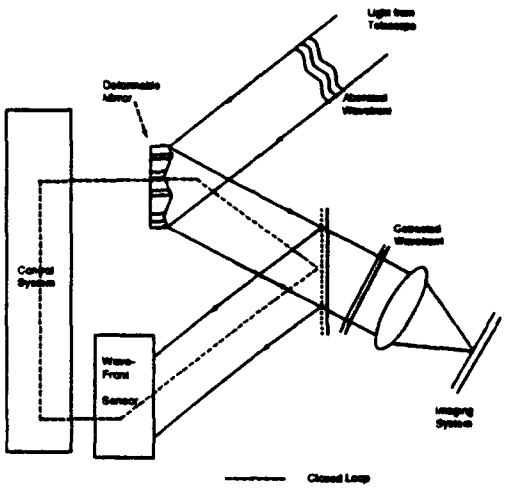

Figure 1.2. Block Diagram of a General Adaptive Optic System.

element, which is usually a deformable mirror. The reflected light is then analyzed with the wavefront sensor which detects the phase along the wavefront. This information is used by the servo-control system, usually a dedicated computer or specialized hardware, to compute the residual phase error and control the deformable mirror, thus closing the loop. Systems using this general approach have been under extensive development for the past twenty to thirty years. Recent declassification of this technology has revealed impressive and tantalizing results [3], [4], [17].

1.3 Measurement of Wavefront Phase

The phase of the incident optical wave cannot be measured directly. One method of indirectly measuring the wavefront phase is to measure the phase slope of small zones of the wavefront. These zones, within the overall aperture of the telescope, will be referred to as "subapertures." These measurements can be used to create a "map" of the slope and hence the phase along the entire wavefront. An illustration of how such a phase map might be constructed is given in Figure 1.3 [19]. Here, s^x or s^y is the phase slope in the x or y direction, respectively, obtained from the wavefront

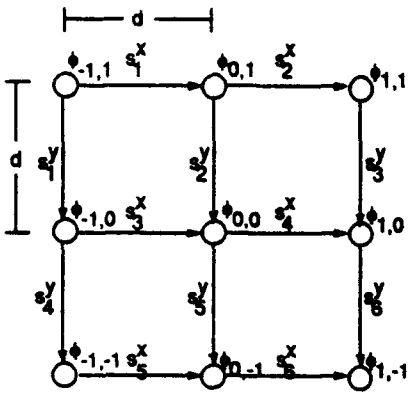

Figure 1.3. Phase Map Reconstruction.

sensor. $\phi_{i,j}$ is the wavefront phase at location i, j. Therefore, the phase slope could be written as:

$$\begin{aligned} s_1^x &= \frac{\phi_{0,1} - \phi_{-1,1}}{d} \\ s_1^y &= \frac{\phi_{-1,1} - \phi_{-1,0}}{d} \\ &\vdots \end{aligned} \tag{1.1}$$

Examination of Figure 1.3 shows that there are more slope measurements than nodes where we wish to determine the phase. Thus, a least squares algorithm can be used to reconstruct the phase wavefront map [10].

Two instruments are commonly used to measure the phase slopes: the Hartmann-Shack Wavefront sensor and the Shearing Interferometer Wavefront sensor. The Hartmann-Shack Wavefront sensor, (see Figure 1.4), measures the slope by focusing the wavefront incident onto each subaperture to form a spot. The slope of the wavefront segment is proportional to the offset of the spot from center. The Shearing Interferometer, (see Figure 1.5), determines the wavefront slope by duplicating the wavefront and shifting, or shearing, it with respect to the original. The two wavefronts are interfered to produce an interferogram. The slope information along the wavefront can be determined from the information in the interferogram. The Hartmann Wavefront sensor

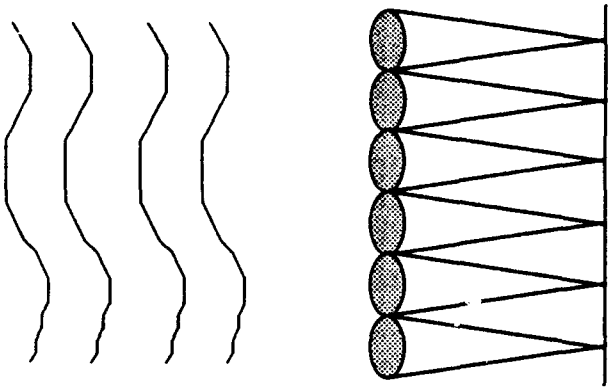

Figure 1.4. Diagram of the Hartmann Wavefront Sensor.

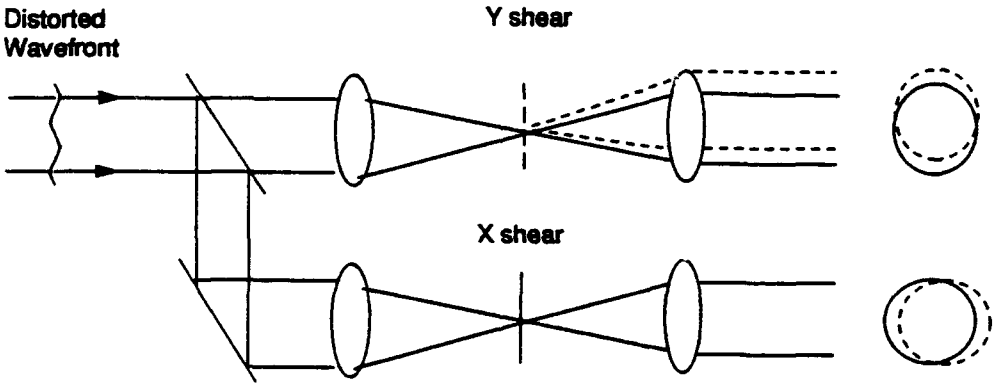

Figure 1.5. Diagram of the Shearing Interferometer.

and Shearing Interferometer, and how each one measures the phase slopes, are discussed in greater detail in Chapter II.

As with all practical systems, the Hartman Wavefront sensor and Shearing Interferometer do not measure the wavefront perfectly. Two significant, and unavoidable, errors associated with wavefront sensing are photon noise effects and sampling errors. As the brightness of the source decreases, photon noise can become a considerable problem. Photon noise results from the uncertainty in the detection of the light due to fluctuations in the photo count statistic, often modeled as a Poisson process [8:pg. 482]. Photon noise can be decreased by either making the light source brighter, increasing the integration time for each sample or making the subaperture larger. Sampling errors occur due to the finite size of the subaperture. Instead of measuring the exact wavefront slope within each subaperture, the *average* wavefront slope, over the subaperture, is measured. Sampling errors can be reduced by either making the subapertures smaller or decreasing the integration time for each sample. A tradeoff must therefore be made between photon noise effects and sampling errors, the optimum condition being when these errors are equal [10:pg. 687].

Previous studies have shown that both of these sensors perform equally well under quasi-ideal conditions, i.e. when imaging a point source and there is little or no atmospheric turbulence [10]. However, no studies have been performed comparing the sensors when using an extended source, and the atmospheric turbulence is such that the correlation length, r_o, is less than the subaperture diameter. As the source becomes larger and r_o smaller, the randomness of the wavefront phase increases–to a point where the phase at one end of the subaperture is not related to the phase at the other end of the subaperture. As r_o decreases, the phase will vary within the subaperture diameter. Thus, the sensor does not "see" the true tilt, (called z-tilt), but instead "sees" the average of the true tilt over the subaperture diameter, (called g or s tilt). Phase measurements under these conditions will not reflect the true wavefront tilt.

This thesis will examine the sensors under these conditions and develop mathematical models to predict their performance.

1.4 Scope

The scope of this thesis will be to develop an expression to model the performance of each of these sensors given the subaperture size, light level, source size and correlation length, r_o. The performance of the two sensor will be compared based upon these models.

1.5 Summary of Key Results

This analysis determines that, as expected, the Hartmann Wavefront Sensor and Shearing Interferometer perform comparably for weak atmospheric turbulence, (large r_o), and very small sources, or very bright sources. However, for strong atmospheric turbulence, extended sources and photon limited conditions, the Hartmann Wavefront Sensor displays better performance.

1.6 Overview

Chapter II briefly summarizes the theory involved with wavefront sensing. Chapter III examines the Hartmann-Shack Wavefront sensor. Performance models for the Hartmann WFS are developed. Chapter IV discusses the Shearing Interferometer Wavefront sensor and performance models are developed. Chapter V compares the sensors based upon the models developed in Chapters III and IV. Results are presented that indicate which sensor performs the best under various situations. Chapter VI gives some conclusions about the results and recommendations for further study.

II. Preliminaries

Before proceeding with an analysis of the errors resulting from wavefront measurements with the Hartmann Wavefront sensor and the Shearing Interferometer, it will be useful to establish how each sensor measures the wavefront. The Hartmann Wavefront sensor will be discussed in Section 2.1 and the Shearing Interferometer in Section 2.2. Finally, Section 2.3 establishes some definitions that will be used throughout this thesis.

2.1 Hartmann Wavefront Sensor

A Hartmann Wavefront sensor is composed of an array of subapertures which segment the wavefront. In each subaperture is a lens which focuses the segmented wavefront onto an array of photo detectors that determine the resulting spot positions. A single element of the lens array, illustrated in Figure 1.4, is depicted in Figure 2.1. By use of simple geometry, we can see that the focused spot centroid, x_c, is easily related to the tilt, α, of the incoming optical wave:

$$\tan(\alpha) = \frac{x_c}{f_l} \qquad \rightarrow \qquad \alpha = \tan^{-1}\left(\frac{x_c}{f_l}\right) \tag{2.1}$$

However, the question as to how the centroid of the intensity pattern is determined still remains. Using a detector array like the one in Figure 2.2, Kane [12] determined that the centroid

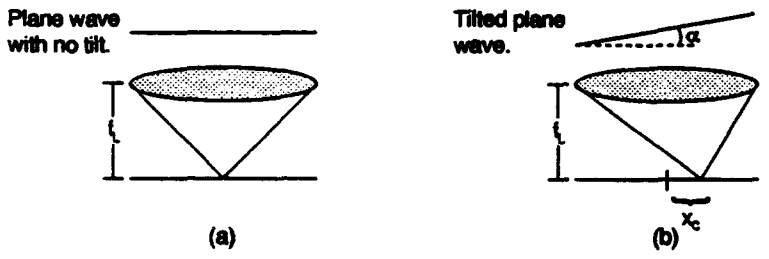

Figure 2.1. One Subaperture of the Hartmann Sensor with (a) a Normally Incident Plane Wave and (b) a Tilted Plane Wave.

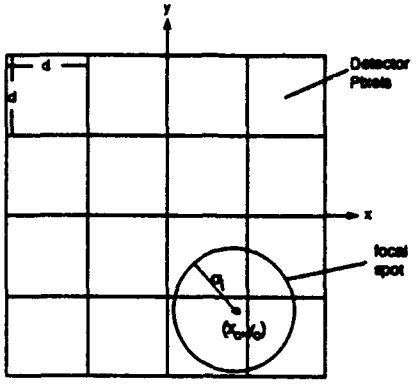

Figure 2.2. Model of Photo Detectors in Focal Plane of the Hartmann Sensor.

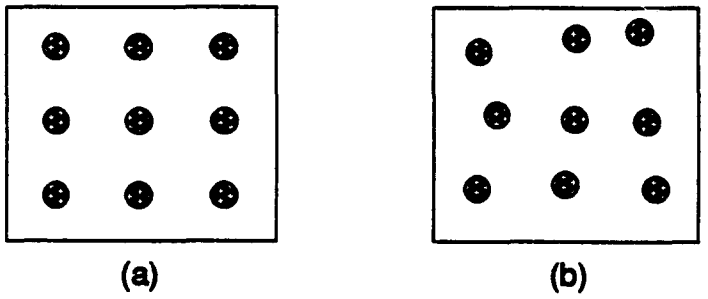

Figure 2.3. (a) Array of Spots from a Plane Wave. (b) Array of Spots from a Distorted Wave.

of the spot could be estimated using:

$$U(x_c, y_c) = \frac{\Sigma_i \Sigma_j x_i P_{i,j}}{\Sigma_i \Sigma_j P_{i,j}} \tag{2.2}$$

where $U(x_c, y_c)$ is the estimate of the centroid in the x direction, x_i is the center of the x_i^{th} detector pixel and $P_{i,j}$ is the number of photon events in the $(i,j)^{th}$ pixel. Note that Equation 2.2 looks very much like a one dimensional centroid definition. Figures 2.1 and 2.2 represented one subaperture. If an array of subapertures is considered, a pattern much like Figure 2.3 might be seen where each spot results from one subaperture. Figure 2.3(a) represents the pattern that might be seen in the detector plane of a Hartmann Sensor illuminated by a plane wave with no atmospheric distortion. Figure 2.3(b) represents the same pattern resulting from a distorted wavefront.

2.2 *Shearing Interferometer*

As discussed in Chapter I, the Shearing Interferometer takes a different approach to wavefront sensing. Instead of spatially segmenting the wavefront, the Shearing Interferometer duplicates the incident wavefront; shifts (shears) it; and interferes it with itself. Several types of Shearing Interferometers exist [11]. For this thesis, a version of the AC Shearing Interferometer is considered– which induces a temporal modulation on one of the sheared beams by use of a rotating diffraction grating [11:pg. 183]. The temporal modulation causes the interference fringes to evolve with time in the subaperture. The phase of the fringes can then be determined from the temporally modulated wavefront. Exactly how the interference fringes are related to the wavefront distortion is discussed in greater detail in Section 2.2.1. Section 2.2.2 describes how the phase can be derived from this intensity pattern using Goodman's Discrete Fourier Transform (DFT) Fringe Estimator [8:pp. 494-501].

2.2.1 Relationship Between Detected Intensity and Wavefront Tilt for the Shearing Interferometer Imperative to understanding how the Shearing Interferometer works is determining how the interference pattern is related to the wavefront tilt. The incident wave, before being sheared, can be expressed as:

$$\mathbf{U}_i(x,y) = \mathbf{E}(x,y)e^{j\phi(x,y)} \tag{2.3}$$

where $\mathbf{E}(x,y)$ is the field from the source and $\phi(x,y)$ is the phase distortion due to atmospheric turbulence. The field from the source, $\mathbf{E}$, is assumed to be complex, so that $\phi(x,y)$ is only the phase due to atmospheric distortion. Recall that the resulting intensity pattern will be sampled temporally. Thus, it is reasonable to assume that the integration time for each sample will be short enough such that Taylor's frozen turbulence hypothesis can be assumed [8:pg. 433]. Hence, $\phi(x,y)$ will be assumed to be deterministic. The two sheared wavefronts are written as:

$$\mathbf{U}_1(x,y) = \mathbf{U}_i\left(x + \frac{\Delta x}{2}, y\right) \qquad \text{and} \qquad \mathbf{U}_2(x,y,t) = \mathbf{U}_i\left(x - \frac{\Delta x}{2}, y\right)e^{j\omega t} \tag{2.4}$$

where the $\exp(j\omega t)$ designates that a temporal modulation has been applied to $\mathbf{U}_2$ using a rotating grating. The total field in the detector plane is:

$$\mathbf{U}_t = \mathbf{U}_1 + \mathbf{U}_2 \tag{2.5}$$

The intensity pattern in the detector plane of the Shearing Interferometer can be described as:

$$I_t(x, y, t) = \langle \mathbf{U}_t \mathbf{U}_t^* \rangle \tag{2.6}$$

where the a^* indicates the complex conjugate of a and the t dependence results from the ac modulation applied to $\mathbf{U}_2$. Substituting Equation 2.5 into Equation 2.6 and expanding gives:

$$I_t(x, y, t) = \left\langle |\mathbf{U}_1|^2 \right\rangle + \left\langle |\mathbf{U}_2|^2 \right\rangle + \langle \mathbf{U}_1 \mathbf{U}_2^* + \mathbf{U}_1^* \mathbf{U}_2 \rangle \tag{2.7}$$

The first two terms are simply:

$$\left\langle |\mathbf{U}_1|^2 \right\rangle = \left\langle |\mathbf{U}_2|^2 \right\rangle = \left\langle |E(x, y)|^2 \right\rangle = I(x, y) \tag{2.8}$$

Therefore, substituting Equation 2.8 into Equation 2.7 we obtain:

$$I_t(x, y, t) = 2I(x, y) + \langle \mathbf{U}_1 \mathbf{U}_2^* + \mathbf{U}_1^* \mathbf{U}_2 \rangle \tag{2.9}$$

Now looking at the cross terms,

$$\begin{aligned} \langle \mathbf{U}_1 \mathbf{U}_2^* + \mathbf{U}_1^* \mathbf{U}_2 \rangle = \Bigg\langle & \mathbf{E}\left(x + \frac{\Delta x}{2}, y\right) e^{j\phi\left(x+\frac{\Delta x}{2}, y\right)} \mathbf{E}^*\left(x - \frac{\Delta x}{2}, y\right) e^{-j\phi\left(x-\frac{\Delta x}{2}, y\right) - j\omega t} \\ & + \mathbf{E}^*\left(x + \frac{\Delta x}{2}, y\right) e^{-j\phi\left(x+\frac{\Delta x}{2}, y\right)} \mathbf{E}\left(x - \frac{\Delta x}{2}, y\right) e^{j\phi\left(x-\frac{\Delta x}{2}, y\right) - j\omega t} \Bigg\rangle \end{aligned} \tag{2.10}$$

Which simplifies to:

$$\langle \mathbf{U}_1\mathbf{U}_2^* + \mathbf{U}_1^*\mathbf{U}_2 \rangle = \left\langle \mathbf{E}\left(x+\frac{\Delta x}{2},y\right)\mathbf{E}^*\left(x-\frac{\Delta x}{2},y\right)e^{-j[\phi(x-\frac{\Delta x}{2},y)-\phi(x+\frac{\Delta x}{2},y)+\omega t]} + \mathbf{E}^*\left(x+\frac{\Delta x}{2},y\right)\mathbf{E}\left(x-\frac{\Delta x}{2},y\right)e^{j[\phi(x-\frac{\Delta x}{2},y)-\phi(x+\frac{\Delta x}{2},y)+\omega t]}\right\rangle \quad (2.11)$$

Note that since $\phi(x,y)$ is deterministic, the expected value operators can be pulled in to include only the source field terms.

$$\langle \mathbf{U}_1\mathbf{U}_2^* + \mathbf{U}_1^*\mathbf{U}_2 \rangle = \left\langle \mathbf{E}\left(x+\frac{\Delta x}{2},y\right)\mathbf{E}^*\left(x-\frac{\Delta x}{2},y\right)\right\rangle e^{-j[\phi(x-\frac{\Delta x}{2},y)-\phi(x+\frac{\Delta x}{2},y)+\omega t]} + \left\langle \mathbf{E}^*\left(x+\frac{\Delta x}{2},y\right)\mathbf{E}\left(x-\frac{\Delta x}{2},y\right)\right\rangle e^{j[\phi(x-\frac{\Delta x}{2},y)-\phi(x+\frac{\Delta x}{2},y)+\omega t]} \quad (2.12)$$

To simplify the notation, define:

$$\Delta\phi(x,y,\Delta x) = \phi\left(x-\frac{\Delta x}{2},y\right) - \phi\left(x+\frac{\Delta x}{2},y\right) \quad (2.13)$$

Further, referencing Goodman [8:pg. 174], the mutual coherence function can be defined for this case as:

$$\Gamma(\Delta x,0) = \left\langle \mathbf{E}^*\left(x+\frac{\Delta x}{2},y\right)\mathbf{E}\left(x-\frac{\Delta x}{2},y\right)\right\rangle \quad (2.14)$$

Thus Equation 2.12 becomes:

$$\langle \mathbf{U}_1\mathbf{U}_2^* + \mathbf{U}_1^*\mathbf{U}_2 \rangle = \Gamma(\Delta x,0)e^{[j\Delta\phi(x,y,\Delta x)+\omega t]} + \Gamma^*(\Delta x,0)e^{-j[\Delta\phi(x,y,\Delta x)+\omega t]} \quad (2.15)$$

Again referencing Goodman [8:pg. 180], for quasimonochromatic conditions, the mutual coherence function can be written as:

$$\Gamma(\Delta x,\Delta y) = \mathbf{J}(\Delta x,\Delta y) \quad (2.16)$$

where J is the mutual intensity and can be found from the Van Cittert-Zernike Theorem. From Van Cittert Zernike, we can relate J to the intensity distribution of the source, I_s, by [8:pg. 209]:

$$\mathbf{J}(\Delta x, \Delta y) = \mathbf{K} \iint I_s(\zeta, \eta) \exp\left[\jmath \frac{2\pi}{\lambda z} (\Delta x \zeta + \Delta y \eta)\right] \mathrm{d}\zeta \mathrm{d}\eta \tag{2.17}$$

where K is some, possibly complex, constant. Thus, J can be found by taking the Fourier Transform of the intensity distribution of the source. It should be noted that a Shearing Interferometer will consist of two sections. One will shear in the Δx direction and the other in the Δy direction. As both legs are otherwise identical, only the Δx shear will be considered and Δy can be assumed to be zero. Further note that for the situations of interest, the source distributions will be assumed to be symmetric about the center of the source, (e.g. circular, rectangular or Gaussian). Thus by Fourier Transform properties [6:Table 7-1], if $f(x)$ and $F(\zeta)$ are Fourier Transform pairs, and if $f(x)$ is real and even, then $F(\zeta)$ will be real and even. Hence, for the situations of interest, J is assumed to be real and

$$\mathbf{J}^* = \mathbf{J} = J \tag{2.18}$$

Thus, Equation 2.15 can be written as:

$$\begin{aligned} \langle \mathbf{U}_1 \mathbf{U}_2^* + \mathbf{U}_1^* \mathbf{U}_2 \rangle &= J(\Delta x, 0) \left[e^{\jmath[\Delta\phi(x,y,\Delta x)+\omega t]} + e^{-\jmath[\Delta\phi(x,y,\Delta x)+\omega t]} \right] \\ &= J(\Delta x, 0) \left[2\cos\left(\Delta\phi(x, y, \Delta x) + \omega t\right) \right] \end{aligned} \tag{2.19}$$

Here, I will continue to follow Goodman and define the normalized mutual coherence function, or degree of coherence function, as:

$$\mu(\Delta x, \Delta y) = \frac{\Gamma(\Delta x, \Delta y)}{\Gamma(0, 0)} \tag{2.20}$$

Recall that:

$$J(0,0) = \left\langle |E(x,y)|^2 \right\rangle = I(x,y) \tag{2.21}$$

and Equation 2.20 can be written as:

$$J(\Delta x, 0) = I(x,y)\mu(\Delta x, 0) \tag{2.22}$$

Substituting Equation 2.22 into Equation 2.19 yields:

$$\langle \mathrm{U}_1 \mathrm{U}_2^* + \mathrm{U}_1^* \mathrm{U}_2 \rangle = 2I(x,y)\mu(\Delta x, 0)\cos(\Delta\phi(x,y,\Delta x) + \omega t) \tag{2.23}$$

If the fields U_1 and U_2 are assumed to have equal amplitude, then the complex coherence factor is equal to the visibility, $\mathcal{V}$, of the fringes formed by the interference [8:pg. 163]. Equation 2.23 can be substituted back into Equation 2.9 to yield an intensity pattern of:

$$I_t(x,y,t) = 2I(x,y)[1 + \mathcal{V}\cos(\Delta\phi(x,y,\Delta x) + \omega t)] \tag{2.24}$$

Equation 2.24 shows that the wavefront difference, $\Delta\phi$, is encoded in the phase of the ac modulated fringe pattern. Therefore, to determine the wavefront tilt, the phase of the fringe pattern needs to be determined. That process is discussed in Section 2.2.2.

2.2.2 Shearing Interferometer Detector Model The problem of retrieving the phase from an ac signal, such as Equation 2.24, is a common one in communication systems [18]. One method is the Discrete Fourier Transform (DFT) Estimator [20], [8:pp. 494-501]. Before describing the DFT Estimator in detail, a discrete representation of the detector plane intensity pattern, Equation 2.24, is needed. Equation 2.24 can be written as:

$$I_t(x,y,t) = 2I\left[1 + \mathcal{V}\cos\left(\frac{2\pi t}{T} + \Delta\phi(x,y,\Delta x)\right)\right] \tag{2.25}$$

where T is the temporal period of the fringe pattern and I is the intensity of each sheared beam in the detector plane. The detector plane is segmented, (as for the Hartmann sensor), into discrete detectors or subapertures. Here, it is assumed that each subaperture is small enough such that $I(x,y)$ is essentially constant across the subaperture. The intensity in each of these subapertures, defined by $W_s(x,y)$, will be integrated for a time, τ, to form a vector of discrete photon count values, see Figure 2.4. Through this count vector, and Goodman's DFT Fringe Estimator, the phase of the fringes can be determined.

Using Equation 2.25, the count vector, $K(n)$, could be described as:

$$K(n) = \alpha \iiint I(x,y,\Delta x,t) W_s(x,y) W_t(t) \mathrm{d}t\mathrm{d}x\mathrm{d}y \tag{2.26}$$

where α is a proportionality constant that converts energy to photo events and is given by [8:Equation 9.1-9], W_s is the aperture function defining the detector pixel and W_t is the temporal windowing function of each measurement interval. $W_s(x,y)$ and W_t can be described by:

$$W_s(x,y) = \mathrm{rect}\left(\frac{x}{d}\right)\mathrm{rect}\left(\frac{y}{d}\right) = \begin{cases} 1 & -\frac{d}{2} \le x \le \frac{d}{2} \text{ and } -\frac{d}{2} \le y \le \frac{d}{2} \\ 0 & \text{otherwise} \end{cases} \tag{2.27}$$

$$W_t(t) = \mathrm{rect}\left(\frac{t-\tau n}{\tau}\right) = \begin{cases} 1 & \tau n - \frac{\tau}{2} \le x \le \tau n + \frac{\tau}{2} \\ 0 & \text{otherwise} \end{cases} \tag{2.28}$$

where d is the width of the detector and τ is the integration time for each intensity measurement, n. Substituting Equation 2.25 into Equation 2.26 yields:

$$K(n) = 2I\alpha \iiint \left[1 + \mathcal{V}\cos\left(\frac{2\pi t}{T} + \Delta\phi(x,y,\Delta x)\right)\right] W_s(x,y) W_t(t) \mathrm{d}t\mathrm{d}x\mathrm{d}y \tag{2.29}$$

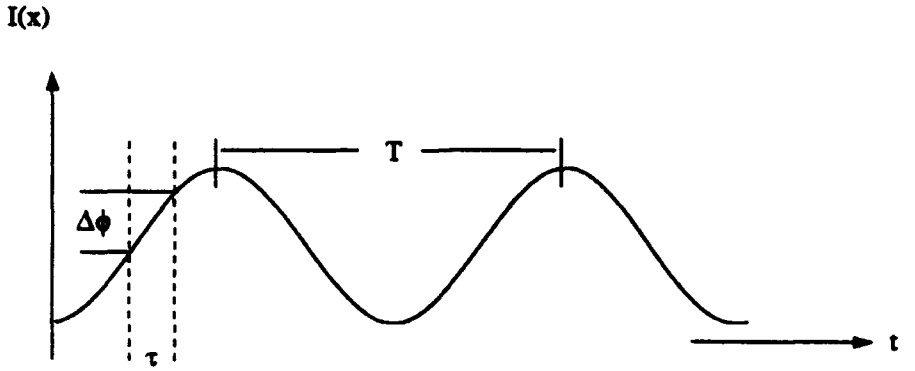

Figure 2.4. Fringe Pattern being Sampled Temporally.

Equation 2.29 is evaluated in Appendix B and shown to be:

$$\overline{K}(n) = 2I\alpha\tau A\left[1 + \mathcal{V}\cos\left(\frac{2\pi p_o n}{N} + 2\overline{\Delta\phi}(\Delta x)\right)\right] \tag{2.30}$$

where $\overline{\Delta\phi}$ was defined as:

$$A\overline{\Delta\phi}(\Delta x) = \iint \Delta\phi(x, y, \Delta x)W_s(x, y)\mathrm{d}x\mathrm{d}y \tag{2.31}$$

and the relationship:

$$\tau \cdot N = p_o \cdot T \tag{2.32}$$

was used where τ is the integration time, N is the number of samples in the count vector, $K(n)$, i.e. $0 \leq n \leq N-1$, p_o is the number of fringes embraced by the count vector and T is the period of the fringe. Equation 2.30 describes the photon count vector. This is, of course, a discrete representation of the fringe pattern. However, we still need to determine $\overline{\Delta\phi}$ from this count vector.

The Shearing Interferometer can be set up such that p_o is an integer number of fringes. The phase difference, $\overline{\Delta\phi}$, can then be determined from $\overline{K}(n)$ using Goodman's DFT fringe estimator.

The DFT of Equation 2.30 is:

$$\mathcal{H}(p) = \frac{1}{N}\sum_{n=0}^{N-1} \overline{K}(n) e^{j(2\pi np/N)} \tag{2.33}$$

Define the real and imaginary components of the DFT evaluated at p_o as:

$$\mathcal{H}_R \equiv \mathrm{Re}\{\mathcal{H}(p_o)\} = \frac{1}{N}\sum_{n=0}^{N-1} \overline{K}(n) \cos\frac{2\pi np_o}{N} \tag{2.34}$$

$$\mathcal{H}_I \equiv \mathrm{Im}\{\mathcal{H}(p_o)\} = \frac{1}{N}\sum_{n=0}^{N-1} \overline{K}(n) \sin\frac{2\pi np_o}{N} \tag{2.35}$$

Using Equation 2.30, the mean values of Equations 2.34 and 2.35 can be evaluated to be:

$$\overline{\mathcal{H}}_R = \frac{2I\alpha A\tau}{2}\mathcal{V}\cos(\overline{\Delta\phi}) \tag{2.36}$$

$$\overline{\mathcal{H}}_I = \frac{2I\alpha A\tau}{2}\mathcal{V}\sin(\overline{\Delta\phi}) \tag{2.37}$$

From which we can easily see that:

$$\frac{\overline{\mathcal{H}}_I}{\overline{\mathcal{H}}_R} = \tan(\overline{\Delta\phi}) \qquad \rightarrow \qquad \overline{\Delta\phi} = \tan^{-1}\left(\frac{\overline{\mathcal{H}}_I}{\overline{\mathcal{H}}_R}\right) \tag{2.38}$$

It should be noted that my model is slightly different from Goodman's. I have assumed the fringes are modulated and hence pass by a single detector. Goodman assumed that the fringes are stationary and an array of detectors spatially sample the fringe pattern. However, Equation 2.30 matches Goodman's Equation (9.4-2). Therefore, the statistics Goodman develops for his DFT Estimator are valid for my model as well. These statistics will be used in Chapter IV.

2.3 Definitions

2.3.1 z-tilt z-tilt, $\vec{\theta}_t$, is the wavefront slope, or tilt, over a subaperture. z-tilt is defined as [24]:

$$\vec{\theta}_t = \frac{\iint (x \cdot \hat{x} + y \cdot \hat{y})\, \phi(x,y) W(x,y) \mathrm{d}x\mathrm{d}y}{\frac{1}{2} k \iint (x^2 + y^2)\, W(x,y) \mathrm{d}x\mathrm{d}y} \tag{2.39}$$

where $W(x,y)$ defines the subaperture over which we are considering the wavefront tilt; $\hat{x}$ and $\hat{y}$ are unit vectors in orthogonal directions; $k = 2\pi/\lambda$, where λ is the optical wavelength; and ϕ is the turbulence induced phase distortion.

2.3.2 g-tilt g-tilt, $\vec{\theta}_c$, is the wavefront slope, or tilt, as measured by the Hartmann-Shack Wavefront sensor. It is directly related to the instantaneous angular position of the centroid of the intensity distribution in the focal plane of the Hartmann Sensor. g-tilt is defined as [24]:

$$\vec{\theta}_c = \frac{\iint \nabla \phi(x,y)\, |W(x,y)|^2 \, \mathrm{d}x\mathrm{d}y}{k \iint |W(x,y)|^2 \, \mathrm{d}x\mathrm{d}y} \tag{2.40}$$

where ∇ is the gradient operator.

2.3.3 s-tilt s-tilt, $\vec{\theta}_s$, is the wavefront slope, or tilt, as measured by the Shearing Interferometer. $\vec{\theta}_s$ is defined by:

$$\vec{\theta}_s = \frac{\hat{x} \iint \frac{\Delta\phi(x,y,\Delta x)}{\Delta x} W(x,y) \mathrm{d}x\mathrm{d}y + \hat{y} \iint \frac{\Delta\phi(x,y,\Delta x)}{\Delta y} W(x,y) \mathrm{d}x\mathrm{d}y}{k \iint W(x,y) \mathrm{d}x\mathrm{d}y} \tag{2.41}$$

where Δx and Δy is the amount of shear in the x and y direction respectively. Note, in Equation 2.41, that as $\Delta x, \Delta y \to 0$ then $\vec{\theta}_s \to \vec{\theta}_c$ defined in Equation 2.40.

2.3.4 Subaperture The Hartmann Wavefront sensor and the Shearing Interferometer measures the wavefront tilt over some finite area. That area is the subaperture which is defined as:

$$W(x,y) = \text{rect}\left(\frac{x}{d}\right)\text{rect}\left(\frac{y}{d}\right) = \begin{cases} 1 & -\frac{d}{2} \le x \le \frac{d}{2} \text{ and } -\frac{d}{2} \le y \le \frac{d}{2} \\ 0 & \text{otherwise} \end{cases} \tag{2.42}$$

With this subaperture definition, several items about Equations 2.39, 2.40 and 2.41 can be noted. First, in Equation 2.40, since $W(x,y)$ is real and only takes values of one or zero:

$$|W(x,y)|^2 = W(x,y) \tag{2.43}$$

Further the denominators of Equations 2.39, 2.40 and 2.41 can be evaluated as:

$$\frac{1}{2}k\iint (x^2+y^2)\,W(x,y)\mathrm{d}x\mathrm{d}y = \frac{kd^4}{12}, \tag{2.44}$$

$$k\iint W(x,y)\mathrm{d}x\mathrm{d}y = kd^2 \tag{2.45}$$

and

$$k\iint W(x,y)\mathrm{d}x\mathrm{d}y = kd^2, \tag{2.46}$$

respectively.

2.3.5 Normalized Shear In the Shearing Interferometer, the wavefront is sheared by a distance Δx before being interfered with itself. Let the normalized shear be defined as:

$$s \equiv \frac{\Delta x}{r_o} \tag{2.47}$$

where r_o is the atmospheric correlation length.

III. Hartmann-Shack Wavefront Sensor

Two major sources of error have been assumed for the Hartmann Wavefront Sensor. Those two sources can be described by the error between g-tilt and z-tilt in the wavefront measurement and the photon or shot noise effects. These two effects are independent and hence can simply be added to give the total mean square (MS) error. For notational simplicity, the total MS error for the Hartmann sensor will be defined as:

$$E_H \equiv E_{Hp} + E_{Hgz} \tag{3.1}$$

where E_{Hp} is the MS error resulting from the detectors inability to accurately determine the true centroid due to photon noise effects and E_{Hgz} is the MS error due to the difference between the true wavefront tilt, z-tilt, and the tilt seen by the Hartmann Sensor, g-tilt. E_H will be manipulated to have units of (radians/r_o cell)^2.

3.1 Shot Noise, E_{Hp}

An optical wave passing through a positive lens will be Fourier transformed at the lens' back focal plane. Thus, one would assume that an incident plane wave will form an impulse function at the back focal plane. However, this would require the lens to have an infinite spatial bandwidth, which is not the case. Hence we must take diffraction effects into account. Diffraction will result in a plane wave being transformed to a finite width spot. Kane [12] has shown that the width of this spot is related to the MS error in determining the spot centroid by:

$$E\left[(\hat{x}_c - x_c)^2\right] = \sigma_{\Delta x}^2 = \left(\frac{\eta\sigma_i}{\sqrt{N}}\right)^2 \tag{3.2}$$

where x_c is the true centroid location, $\hat{x}_c$ is the centroid estimate given by Equation 2.2, η is related to the detector efficiency, N is the total photon count and σ_i is the RMS width of the intensity

pattern in the detector plane. σ_i will be determined for two cases. Section 3.1.1 will determine the RMS spot width for a point source and Section 3.1.2 will determine σ_i for an extended source.

3.1.1 RMS Spot Width for a Point Source The RMS spot width for a point source is needed for two reasons. First, as indicated by Equation 3.2, the MS error in determining the spot centroid is proportional to the RMS spot width. By finding the RMS width for a point source, the MS shot noise error, due solely to diffraction, can be determined. Second, the intensity pattern resulting from a point source also gives the diffraction limited Point Spread Function, (PSF), for a Hartmann subaperture. This relationship will be used later in Section 3.1.2.

The diffraction pattern for a square lens of width d is given by [7: pg. 63]:

$$I(x_o, y_o) = \frac{A^2}{(\lambda f_l)^2} \text{sinc}^2\left(\frac{dx_o}{\lambda f_l}\right) \text{sinc}^2\left(\frac{dy_o}{\lambda f_l}\right) \tag{3.3}$$

where x_o and y_o are points in the focal plane and $\text{sinc}(x)$ is defined as $\text{sinc}(x) = \sin(\pi x)/\pi x$ [6:pg. 45]. By defining:

$$x = \frac{dx_o}{\lambda f_l} \qquad \text{and} \qquad y = \frac{dy_o}{\lambda f_l} \tag{3.4}$$

and normalizing I to one at $x, y = 0$, Equation 3.3 can be written as:

$$I'(x, y) = \text{sinc}^2(x)\text{sinc}^2(y) \tag{3.5}$$

which represents the normalized intensity pattern for a point source with no atmospheric distortion. Analytical and numerical computations with a sinc^2 function can be difficult. To ease the computations, the approach taken by Kane [12] is followed, and this distribution is approximated by a normalized Gaussian function having the same width at the e^{-1} points.

Examination of Figure 3.1(a) shows that $I'(x)$ has a value of e^{-1} at $x = 0.5234$. A normalized Gaussian curve can be matched to the sinc^2 pattern by finding a variance, σ^2, that forces the

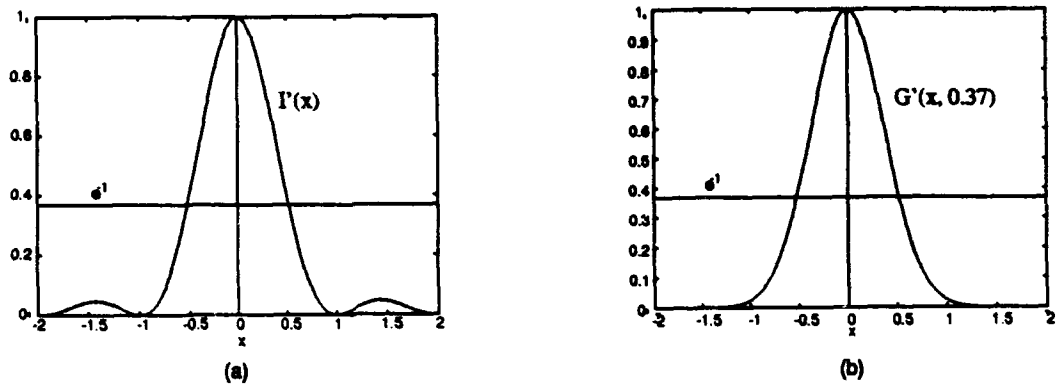

Figure 3.1. Plot of sinc^2 and Gaussian function for $\sigma^2 = 0.37^2$.

normalized Gaussian function to have a value of e^{-1} at $x = 0.5234$. The Gaussian curve is given by:

$$G(x,\sigma) = \frac{1}{\sqrt{2\pi}\sigma} \exp\left(-\frac{x^2}{\sigma^2}\right) \tag{3.6}$$

and the normalized Gaussian function by:

$$G'(x,\sigma) = \frac{G(x,\sigma)}{G(0,\sigma)} = \exp\left(-\frac{x^2}{\sigma^2}\right) \tag{3.7}$$

It can easily be shown that a variance of $\sigma^2 = (0.37)^2$ will match the two functions at the e^{-1} points. A normalized Gaussian function with such a variance is plotted in Figure 3.1(b) for comparison. Accounting for the variable change in Equation 3.4, the approximated intensity pattern can be expressed as:

$$I''(x_o, y_o) = \exp\left(-\frac{x_o^2 + y_o^2}{2(0.37)^2\left(\frac{f_L\lambda}{d}\right)^2}\right) \tag{3.8}$$

which also represents the diffraction limited PSF for the Hartmann subaperture.

To determine the shot noise error, E_{Hp}, the RMS width of the approximated intensity distribution, described by Equation 3.8, needs to be determined. However, since Equation 3.8 is a

Gaussian function, the RMS width is simply its standard deviation; hence:

$$\sigma_i = 0.37\frac{\lambda f_L}{d} \tag{3.9}$$

This result is similar to one obtained by Kane [13] for a circular aperture.

3.1.2 RMS spot width due to Extended Source The analysis in Section 3.1.1 gave the RMS spot width for a point source. However, we are also interested in the effects due to an extended source. The source intensity, I_s, is modeled as an elliptical Gaussian distribution. This distribution is expected to be formed from a laser guide star [5:pg 1722].

$$I_s(\zeta,\eta) = I_o \exp\left[-\frac{\zeta^2 + (b\eta)^2}{2\sigma_s^2}\right] \tag{3.10}$$

where the constant b is added in to make the distribution "elliptical." The intensity in the detector plane is given by the convolution of the source intensity with the diffraction limited PSF, (Equation 3.8):

$$I_d(x',y') = \exp\left[-\frac{x'^2 + y'^2}{2(0.37)^2\left(\frac{f_1\bar{\lambda}}{d}\right)^2}\right] * \exp\left[-\frac{x'^2 + (by')^2}{2\left(\frac{f_1\sigma_s}{z}\right)^2}\right] \tag{3.11}$$

where the constants have been ignored. This is essentially the convolution of two 2-D Gaussian functions, which can easily be evaluated to be:

$$I_d(x',y') = \exp\left[-\frac{x'^2}{2\left(\sigma_{DL}^2 + \left(\frac{f_1\sigma_s}{z}\right)^2\right)} - \frac{y'^2}{2\left(\sigma_{DL}^2 + \left(\frac{f_1\sigma_s}{zb}\right)^2\right)}\right] \tag{3.12}$$

where:

$$\sigma_{DL}^2 = (0.37)^2\left(\frac{f_1\bar{\lambda}}{d}\right)^2 \tag{3.13}$$

is the diffraction limited spot width for a square aperture, determined in Section 3.1.1, and the factor of f_l/z converts the source RMS width, σ_s, from object space to image space. Thus we see that the intensity distribution in the detector plane of the Hartmann sensor is Gaussian with MS width equal to the sum of the diffraction limited MS width and the MS width of the source in image space. Hence the RMS spot width is given by:

$$\sigma_{i_x} = \sqrt{\sigma_{DL}^2 + \left(\frac{f_l \sigma_s}{z}\right)^2} \quad \text{and} \quad \sigma_{i_y} = \sqrt{\sigma_{DL}^2 + \left(\frac{f_l \sigma_s}{zb}\right)^2} \tag{3.14}$$

and in general:

$$\sigma_i^2 = (0.37)^2 \left(\frac{f_l \lambda}{d}\right)^2 + \left(\frac{f_l}{z}\right)^2 \sigma_s^2 \tag{3.15}$$

3.1.3 Mean Square Error Due to Finite Spot Size Recalling Equation 3.2, the RMS spot width, given by Equation 3.14, is related to a centroid location MS error. Using simple geometry, (see Figure 3.2), this location MS error can be related to a MS error in the wavefront slope measurement by:

$$\Delta\phi = \frac{dx_c}{f_l} \quad \rightarrow \quad \sigma_{\Delta\phi}^2 = 2\left(\frac{d}{f_l}\right)^2 \sigma_{\Delta x}^2 = 2\left(\frac{d}{f_l}\right)^2 \left(\frac{\sigma_i}{\sqrt{N}}\right)^2 \tag{3.16}$$

where $\sigma_{\Delta x}^2$ is given by Equation 3.2, $\Delta\phi$ is assumed to represent the change in phase of the wavefront over the subaperture and the factor of two accounts for an identical error in the y direction. Note that σ_i has units of meters, as does f_l and d (or meters per diameter). Thus Equation 3.16 has units of (meter/diameter)^2. To transform these units to (radians/$r_o$cell)^2, a multiplication by $(kr_o/d)^2$, which has units of

$$\left(\frac{kr_o}{d}\right)^2 \quad \rightarrow \quad \left(\frac{\text{radians}}{\text{meter}}\right)^2 \left(\frac{\text{meter}}{r_o \text{ cell}}\right)^2 \left(\frac{\text{diameter}}{\text{meter}}\right)^2 \quad \rightarrow \quad \left(\frac{\text{radians} \cdot \text{diameter}}{\text{meter} \cdot r_o \text{ cell}}\right)^2, \tag{3.17}$$

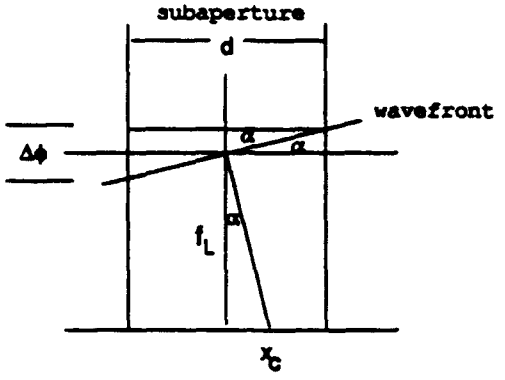

Figure 3.2. Diagram of a Hartmann Sensor Subaperture

is required. Thus

$$\left(\frac{kr_o}{d}\right)^2 \sigma^2_{\Delta\phi} = \frac{2}{N}\left(\frac{kr_o}{f_l}\right)^2 \sigma_i^2 \tag{3.18}$$

and the shot noise MS error for the Hartmann Wavefront Sensor can be defined as:

$$E_{Hp} \equiv \left(\frac{kr_o}{d}\right)^2 \sigma^2_{\Delta\phi} = \frac{2}{N}\left(\frac{kr_o}{f_l}\right)^2 \sigma_i^2 \left(\frac{\text{radians}}{r_o \text{ cell}}\right)^2 \tag{3.19}$$

Substituting in Equation 3.15 for σ_i^2 and simplifying, we obtain:

$$E_{Hp} = \frac{2}{N}\left(\frac{k}{f_l}\right)^2 \left[\left(\frac{f_l r_o}{z}\right)^2 \sigma_s^2 + \left(\frac{0.37 f_l \bar{\lambda}}{d/r_o}\right)^2\right] \tag{3.20}$$

For analysis of arbitrary subaperture sizes and seeing conditions, it is important to note that the second term in Equation 3.20 is only valid for $d/r_o \leq 1$, where r_o is Fried's coherence diameter [2]. The term $0.37 f_l \bar{\lambda}/d$ represents the diffraction limited spot size in the detector plane. However, as the diameter, d, gets larger, the spot size does not shrink in a proportional way—instead, it is limited by the atmospheric correlation length, r_o [8:pp. 431-432]. Thus, for $d/r_o > 1$, the d in the

second term needs to be replaced by a r_o. Equation 3.20 can more accurately be written as:

$$E_{Hp} = \begin{cases} \frac{2}{N}\left(\frac{k}{f_l}\right)^2\left[\left(\frac{f_l r_a}{z}\right)^2\sigma_s^2 + \left(\frac{0.37 f_l \bar{\lambda}}{d/r_o}\right)^2\right] & \text{for } \frac{d}{r_o} \le 1 \\ \frac{2}{N}\left(\frac{k}{f_l}\right)^2\left[\left(\frac{f_l r_a}{z}\right)^2\sigma_s^2 + (0.37 f_l \bar{\lambda})^2\right] & \text{for } \frac{d}{r_o} > 1 \end{cases} \tag{3.21}$$

Performing algebraic simplification, recalling that $k = 2\pi/\lambda$, Equation 3.21 becomes:

$$E_{Hp} = \begin{cases} 2\frac{(2\pi)^2}{N}\left[\left(\frac{\sigma_s}{z}\cdot\frac{r_a}{\lambda}\right)^2 + (0.37)^2\left(\frac{r_a}{d}\right)^2\right] & \text{for } \frac{d}{r_o} \le 1 \\ 2\frac{(2\pi)^2}{N}\left[\left(\frac{\sigma_s}{z}\cdot\frac{r_a}{\lambda}\right)^2 + (0.37)^2\right] & \text{for } \frac{d}{r_o} > 1 \end{cases} \tag{3.22}$$

Note that σ_s/z is equivalent to the angular size of the source, while λ/r_o is the angular resolution limit induced by the atmosphere. The ratio of the angular size of the source to the angular resolution of the unaided optical system is defined by:

$$\beta \equiv \frac{\frac{\sigma_s}{z}}{\frac{\lambda}{r_o}} = \frac{\sigma_s}{z}\cdot\frac{r_o}{\lambda} \tag{3.23}$$

Using Equation 3.23, Equation 3.22 can be written as:

$$E_{Hp} = \begin{cases} 2\frac{(2\pi)^2}{N}\left[\beta^2 + (0.37)^2\left(\frac{r_a}{d}\right)^2\right]\left(\frac{\text{radians}}{r_o \text{ cell}}\right)^2 & \text{for } \frac{d}{r_o} \le 1 \\ 2\frac{(2\pi)^2}{N}\left[\beta^2 + (0.37)^2\right]\left(\frac{\text{radians}}{r_o \text{ cell}}\right)^2 & \text{for } \frac{d}{r_o} > 1 \end{cases} \tag{3.24}$$

3.2 Mean Square Error between z-tilt and g-tilt, E_{Hgz}

In this section, the MS error resulting from the error between the true wavefront tilt, $\vec{\theta}_t$, and the wavefront tilt "seen" by the subaperture is computed using a method similar to that of Yura and Tavis [24]. The Hartmann sensor averages the wavefront tilt, $\nabla\phi$, over the subaperture. In doing so, the phase slope is approximated in a piecewise linear fashion. As can be seen from Figure 3.3(a), this is a good approximation when r_o is large. However, as r_o decreases, the averaged wavefront tilt diverges from the true wavefront tilt, as can be seen from Figure 3.3(b).

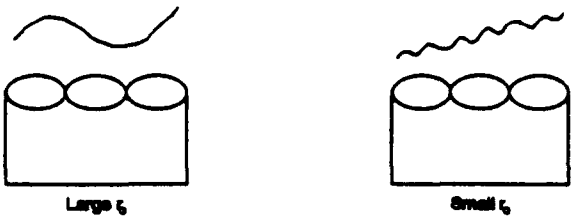

Figure 3.3. Hartmann Sensor with (a) large r_o and (b) small r_o

The MS error between the z-tilt and the estimated tilt can be expressed as [24]:

$$\left\langle \left(\vec{\theta}_t - \hat{\theta}_t \right)^2 \right\rangle \tag{3.25}$$

where $\vec{\theta}_t$ is the true wavefront tilt, called z-tilt, over the entire aperture and $\hat{\theta}_t$ is the estimate of this tilt. This estimate, $\hat{\theta}_t$, is assumed to be equal to the instantaneous angular position of the centroid, $\vec{\theta}_c$, which is equivalent to the α in Figure 3.2. $\vec{\theta}_c$ is commonly called the g-tilt. Expanding Equation 3.25, we obtain:

$$\left\langle \left(\vec{\theta}_t - \vec{\theta}_c \right)^2 \right\rangle = \left\langle \vec{\theta}_t^2 - 2\vec{\theta}_t \cdot \vec{\theta}_c + \vec{\theta}_c^2 \right\rangle \tag{3.26}$$

Recall that $\vec{\theta}_t$ and $\vec{\theta}_c$ were defined in Section 2.3. These definitions will be used to evaluate each of these three terms individually.

Using Equations 2.39, 2.40, 2.44 and 2.45, the cross correlation between g-tilt and z-tilt, $\left\langle \vec{\theta}_t \cdot \vec{\theta}_c \right\rangle$ can be expressed as:

$$\left\langle \vec{\theta}_t \cdot \vec{\theta}_c \right\rangle = \frac{12}{k^2 d^6} \left\langle \iint \left(x \cdot \hat{x} + y \cdot \hat{y} \right) W(x,y) \phi(x,y) \mathrm{d}x\mathrm{d}y \cdot \iint W(x,y) \nabla\phi(x,y) \mathrm{d}x\mathrm{d}y \right\rangle \tag{3.27}$$

Using integration by parts, this becomes:

$$\left\langle \vec{\theta}_t \cdot \vec{\theta}_c \right\rangle = \frac{12}{k^2 d^6} \left\langle \iint \left(x_1 \hat{x} + y_1 \hat{y} \right) W(x_1,y_1) \phi(x_1,y_1) \mathrm{d}x_1 \mathrm{d}y_1 \cdot \left(- \iint \nabla_2 W(x_2,y_2) \phi(x_2,y_2) \mathrm{d}x_2 \mathrm{d}y_2 \right) \right\rangle \tag{3.28}$$

Using the definition of the gradient operator in Equation A.3, performing the dot product and simplifying yields:

$$\left\langle \vec{\theta}_t \cdot \vec{\theta}_c \right\rangle = \frac{24}{k^2 d^6} \left\langle \iiint x_1 W(x_1, y_1) \phi(x_1, y_1) \phi(x_2, y_2) \right.$$
$$\left. \times \left[\delta\left(x_2 - \frac{d}{2}\right) - \delta\left(x_2 + \frac{d}{2}\right) \right] \text{rect}\left(\frac{y_2}{d}\right) dx_1 dx_2 dy_1 dy_2 \right\rangle \quad (3.29)$$

since all terms in Equation 3.29 are deterministic *except* ϕ, the expected value operator can be taken inside the integrals to yield:

$$\left\langle \vec{\theta}_t \cdot \vec{\theta}_c \right\rangle = \frac{24}{k^2 d^6} \iiint x_1 W(x_1, y_1) \left\langle \phi(x_1, y_1) \phi(x_2, y_2) \right\rangle$$
$$\times \left[\delta\left(x_2 - \frac{d}{2}\right) - \delta\left(x_2 + \frac{d}{2}\right) \right] \text{rect}\left(\frac{y_2}{d}\right) dx_1 dx_2 dy_1 dy_2 \quad (3.30)$$

An expression for the correlation function, $\langle \phi(x_1, y_1) \phi(x_2, y_2) \rangle$, is needed to continue. It is shown in Appendix A.1, that, using the Kolmogorov structure function as described by Wallner [21:pg. 1774]:

$$D\left(\vec{x}, \vec{x'}\right) = 6.88 \left| \frac{\left(\vec{x} - \vec{x'}\right)}{r_o} \right|^{\frac{5}{3}} \quad (3.31)$$

the correlation function can be expressed as:

$$\left\langle \phi(x_1, y_1) \phi(x_2, y_2) \right\rangle = -\frac{6.88}{2} \left(\frac{\sqrt{(x_2 - x_1)^2 + (y_2 - y_1)^2}}{r_o} \right)^{5/3} + \Gamma_\phi(0, 0) \quad (3.32)$$

Substitution of Equation 3.32 into Equation 3.30 yields:

$$\left\langle \vec{\theta}_t \cdot \vec{\theta}_c \right\rangle = \frac{24}{k^2 d^6} \iiint x_1 W(x_1, y_1) \left(-\frac{1}{2} 6.88 \left(\frac{\sqrt{(x_2 - x_1)^2 + (y_2 - y_1)^2}}{r_o} \right)^{5/3} + \Gamma_\phi(0, 0) \right)$$
$$\times \left[\delta\left(x_2 - \frac{d}{2}\right) - \delta\left(x_2 + \frac{d}{2}\right) \right] \text{rect}\left(\frac{y_2}{d}\right) dx_1 dx_2 dy_1 dy_2 \quad (3.33)$$

Using the sifting property of delta functions to integrate over x_2, making the variable substitutions

given by Equations A.17 and A.18 and using Fourier Transform analysis, Equation 3.33 becomes:

$$\left\langle \vec{\theta}_t \cdot \vec{\theta}_c \right\rangle = \frac{24}{k^2 d^5} \left[\frac{6.88}{2r_o^{5/3}} \iint x_1 \mathrm{tri}\left(\frac{\Delta y}{d}\right) \mathrm{rect}\left(\frac{x_1}{d}\right) \left(\sqrt{\left(\frac{d}{2} + x_1\right)^2 + (\Delta y)^2} \right)^{5/3} \mathrm{d}x_1 \mathrm{d}\Delta y \right.$$
$$\left. - \frac{6.88}{2r_o^{5/3}} \iint x_1 \mathrm{tri}\left(\frac{\Delta y}{d}\right) \mathrm{rect}\left(\frac{x_1}{d}\right) \left(\sqrt{\left(\frac{d}{2} - x_1\right)^2 + (\Delta y)^2} \right)^{5/3} \mathrm{d}x_1 \mathrm{d}\Delta y \right] \quad (3.34)$$

Substituting in for the definitions of the tri and rect functions, setting the limits on the integrals using these definitions and performing numerical integration, Equation 3.34 can be expressed as:

$$\left\langle \vec{\theta}_t \cdot \vec{\theta}_c \right\rangle = \frac{13.0934}{k^2 r_o^{5/3} d^{1/3}} \quad (3.35)$$

Recalling the definition of $\vec{\theta}_t$, Equation 2.39, and also recalling Equation 2.44, the mean square value of the z-tilt, $< \vec{\theta}_t^2 >$, can be written as:

$$\left\langle \vec{\theta}_t^2 \right\rangle = \left(\frac{12}{kd^4}\right)^2 \left\langle \left(\iint (x \cdot \hat{x} + y \cdot \hat{y})\, \phi(x,y) W(x,y) \mathrm{d}x \mathrm{d}y \right)^2 \right\rangle \quad (3.36)$$

Using a very similar analysis as that used to determine $\left\langle \vec{\theta}_t \cdot \vec{\theta}_c \right\rangle$, it is shown in Appendix A.2 that Equation 3.36, becomes:

$$\left\langle \vec{\theta}_t^2 \right\rangle = \frac{13.6183}{k^2 r_0^{5/3} d^{1/3}} \quad (3.37)$$

Likewise, the MS value of g-tilt, $< \vec{\theta}_c^2 >$ can be expressed using Equations 2.40 and 2.45 as:

$$\left\langle \vec{\theta}_c^2 \right\rangle = \left\langle \left(\frac{1}{kd^2} \iint \nabla \phi(x,y) W(x,y) \mathrm{d}x \mathrm{d}y \right)^2 \right\rangle \quad (3.38)$$

Equation 3.38 is also evaluated in Appendix A.3, using a similar approach, and becomes:

$$\left\langle \vec{\theta}_c^2 \right\rangle = \frac{12.803}{k^2 r_0^{5/3} d^{1/3}} \quad (3.39)$$

3.2.1 Combining $< \vec{\theta}_t^2 >$, $< \vec{\theta}_c^2 >$ and $< \vec{\theta}_t \cdot \vec{\theta}_t >$ to Find E_{Hgz} Substituting Equations 3.35, 3.37 and 3.39 into Equation 3.26, will result in:

$$\left\langle \left(\vec{\theta}_t - \vec{\theta}_c \right)^2 \right\rangle = \frac{0.235}{k^2 r_0^{5/3} d^{1/3}} \tag{3.40}$$

which has the same functional dependence as a similar quantity determined by Yura and Tavis [24] for a circular aperture. Equation 3.40 can also be written as:

$$\left\langle \left(\vec{\theta}_t - \vec{\theta}_c \right)^2 \right\rangle = 0.235 \left(\frac{d}{r_o} \right)^{-\frac{1}{3}} \left(\frac{1}{k r_o} \right)^2 \tag{3.41}$$

Equation 3.41 has units of dimensionless slope (meters over meters). However, the $(kr_o)^2$ term has units of:

$$(kr_o)^2 \quad \rightarrow \quad \left(\frac{\text{radians}}{\text{meter}} \right)^2 \left(\frac{\text{meters}}{r_o \text{ cell}} \right)^2 \quad \rightarrow \quad \left(\frac{\text{radians}}{r_o \text{ cell}} \right)^2 \tag{3.42}$$

Hence, the product, $< (\vec{\theta}_t - \vec{\theta}_c)^2 > (kr_o)^2$ will have units of (radians/r_o cell)^2, which is desired. Therefore, define:

$$E_{Hgz} \equiv \left\langle \left(\vec{\theta}_t - \vec{\theta}_c \right)^2 \right\rangle (kr_o)^2 = 0.235 \left(\frac{d}{r_o} \right)^{-\frac{1}{3}} \left(\frac{\text{radians}}{r_o \text{ cell}} \right)^2 \tag{3.43}$$

3.2.2 Total Hartmann Mean Square Error Combining Equations 3.24 and 3.43 will give the total MS error for the Hartmann Sensor due to both shot noise and the error between g-tilt and z-tilt.

$$E_H = \begin{cases} 2\frac{(2\pi)^2}{N} \left[\beta^2 + (0.37)^2 \left(\frac{r_o}{d} \right)^2 \right] + 0.235 \left(\frac{d}{r_o} \right)^{-\frac{1}{3}} \left(\frac{\text{radians}}{r_o \text{ cell}} \right)^2 & \text{for } \frac{d}{r_o} \leq 1 \\ 2\frac{(2\pi)^2}{N} \left[\beta^2 + (0.37)^2 \right] + 0.235 \left(\frac{d}{r_o} \right)^{-\frac{1}{3}} \left(\frac{\text{radians}}{r_o \text{ cell}} \right)^2 & \text{for } \frac{d}{r_o} > 1 \end{cases} \tag{3.44}$$

Some observations regarding Equation 3.44 are in order. First, this result shows that some error is inherent, even for "perfect" seeing conditions, i.e. $d/r_o \ll 1$. That error is determined by the

amount of light, N, and the diffraction limited spot size in the detector plane. Second, the shot noise portion of the error is strongly dependent on the angular size of the source, β. Hence, as the source becomes larger, i.e. an artificial guide star as opposed to a natural star, the error will increase. And third, the error is dependent on the seeing conditions, given by the factor d/r_o.

IV. Shearing Interferometer Wavefront Sensor

As for the Hartmann Wavefront Sensor, two major sources of error will be examined for the Shearing Interferometer. Those two sources can be described by the error between s-tilt and z-tilt in the wavefront measurement and the shot noise effects. These two effects are independent and hence can simply be added to give the total mean square (MS) error. For notation simplicity, the total MS error for the Shearing Interferometer will be defined as:

$$E_S \equiv E_{Sp} + E_{Ssz} \tag{4.1}$$

E_{Sp} is the MS error due to the photon, or shot, noise effects. E_{Ssz} is the MS error due to the difference between the true wavefront tilt, and the tilt "seen" by the Shearing Interferometer. A similar argument as given in Section 3.2 applies. To match units with the Hartmann analysis, E_S will be manipulated to have units of (radians/$r_o$cell)^2. An expression for E_{Sp} is derived in Section 4.1. Likewise, an expression for E_{Ssz} is derived in Section 4.2.

4.1 Shot Noise, E_{Sp}

It was shown in Chapter II that the count vector statistics for our AC lateral Shearing Interferometer model match those of Goodman's DFT Fringe Estimator. Thus, the result derived by Goodman [8] for the RMS error in estimating $\Delta\phi$ due to shot noise can be used for our model as well:

$$\sigma_{\Delta\phi|x} = \sqrt{\frac{2}{\alpha A \tau N (I_1 + I_2)}} \cdot \frac{1}{\mathcal{V}} \tag{4.2}$$

where α is the quantum efficiency of the detector, A is the area of the detector element, τ is the integration time of the measurement, I_i is the intensity of each sheared beam and $\mathcal{V}$ is the visibility. The notation $\Delta\phi|_x$ indicates this is the RMS error for the x shear section of the Shearing Interferometer.

It is important to relate I_1 and I_2 to the incident beam intensity. The light coming into the Shearing Interferometer must be split at least twice. The first split divides the light between the x and y shear sections of the Shearing Interferometer. The second beam splitter divides the light into two beams which are sheared and interfered. Assuming 50-50 beam splitters, the individual beam intensities can be described as:

$$I_1 = I_2 = \frac{I}{4} \qquad \rightarrow \qquad I_1 + I_2 = \frac{I}{2} \tag{4.3}$$

Since the two beam intensities are equal, the visibility is equal to the complex coherence factor [8:pg. 163]. The complex coherence factor for a Gaussian source of RMS width σ_s was found in Chapter III to be:

$$\mu_{12}(\Delta x, \Delta y) = \exp\left[-\pi \frac{2\pi\sigma_s^2}{(\bar{\lambda}z)^2}\left(\Delta x^2 + \Delta y^2\right)\right] \tag{4.4}$$

where Δx and Δy, are the separations of the points in the x and y direction. Therefore Equation 4.4 can be used to write the visibility as a function of d, the aperture size, and $s = \Delta x/r_o$, the normalized shear.

$$\mathcal{V}(s, r_o) = \exp\left[-2\left(\frac{\pi\sigma_s}{\bar{\lambda}z}\right)^2 (sr_o)^2\right] \tag{4.5}$$

where $\bar{\lambda}$ is the mean optical wavelength and z is the distance from the source. Substituting Equations 4.3 and 4.5 into Equation 4.2 yields:

$$\sigma_{\Delta\phi|x} = \sqrt{\frac{4}{\alpha A \tau N I}} \cdot \frac{1}{\exp\left[-2\left(\frac{\pi\sigma_s}{\bar{\lambda}z}\right)^2 (sr_o)^2\right]} \tag{4.6}$$

which has units of radians. To effectively compare this with the results for the Hartmann sensor, the units on Equation 4.6 need to be converted to (radians/$r_o$cell)^2. First, Equation 4.6 needs to be converted to a slope. This is done by dividing Equation 4.6 by Δx, which gives the phase change, (in radians) per amount of shear, (in meters). Further, squaring Equation 4.6, to make it a MS

error instead of a RMS error, produces:

$$\frac{\sigma^2_{\Delta\phi|x}(s,r_o)}{\Delta x^2} = \frac{4}{N_{tot}\Delta x^2}\exp\left[4\left(\frac{\pi\sigma_s}{\lambda z}\right)^2(sr_o)^2\right] \tag{4.7}$$

where $N_{tot} = \alpha A \tau N I$, which represents the total average photon count over the aperture for each integration time. N_{tot} is comparable to N used for the Hartmann sensor. Equation 4.7 has units of (radians/meter)^2. Thus, by dividing by $1/r_o^2$ (or effectively multiplying by r_o^2), which has units of (meters/r_o cell)^2, the desired units will be obtained:

$$\frac{\sigma^2_{\Delta\phi|x}(s,r_o)r_o^2}{\Delta x^2} = \frac{4r_o^2}{N_{tot}\Delta x^2}\exp\left[4\left(\frac{\pi\sigma_s}{\lambda z}\right)^2(sr_o)^2\right]\left(\frac{\text{radians}}{r_o\text{ cell}}\right)^2 \tag{4.8}$$

In Equations 4.6–4.8, the $|x$ designates that this is the error in the x direction. If we assume that an identical error will occur in the y shear section of the Shearing Interferometer, then the total error will be twice that indicated in Equation 4.8. Further, recalling that the $s = \Delta x/r_o$, Equation 4.8 becomes:

$$\frac{\sigma^2_{\Delta\phi}(s,r_o)}{s^2} = 2\frac{4}{N_{tot}s^2}\exp\left[4\left(\frac{\pi\sigma_s}{\lambda z}\right)^2(sr_o)^2\right] \tag{4.9}$$

Thus, the MS error due to the shot noise can now be defined as:

$$E_{Sp} \equiv \frac{\sigma^2_{\Delta\phi}(s,r_o)}{s^2} = \frac{8}{N_{tot}s^2}\exp\left[4\left(\frac{\pi\sigma_s}{\lambda z}\right)^2(sr_o)^2\right]\left(\frac{\text{radians}}{r_o\text{ cell}}\right)^2 \tag{4.10}$$

The terms in the exponent can be rearranged to yield:

$$E_{Sp} = \frac{8}{N_{tot}s^2}\exp\left[(2\pi)^2\left(\frac{\sigma_s r_o}{z\lambda}\right)^2 s^2\right] \tag{4.11}$$

Recalling Equation 3.23, Equation 4.11 becomes:

$$E_{Sp} = \frac{8}{N_{tot}s^2}\exp\left[(2\pi)^2\beta^2 s^2\right]\left(\frac{\text{radians}}{r_o\text{ cell}}\right)^2 \tag{4.12}$$

4.2 Mean Square Error between z-tilt and s-tilt, E_{Sz_s}

This section examines the second of the two major sources of error in the Shearing Interferometer. As for the Hartmann Wavefront Sensor, we are interested in the MS error between the true tilt and the tilt estimate given by the sensor:

$$\left\langle \left(\vec{\theta}_t - \hat{\theta}_t \right)^2 \right\rangle \tag{4.13}$$

where $\vec{\theta}_t$ is the true wavefront tilt over the aperture and $\hat{\theta}_t$ is its estimate. In the Hartmann Sensor, it was assumed that $\hat{\theta}_t = \vec{\theta}_c$, where $\vec{\theta}_c$ is the instantaneous angular position of the centroid in the Hartmann subaperture. A similar approach will be taken for the Shearing Interferometer. The estimate of the wavefront tilt, $\hat{\theta}_t$ will be assumed to be equivalent to $\vec{\theta}_s$ which is the tilt measured by the Shearing Interferometer. Expanding Equation 4.13 then yields:

$$\left\langle \left(\vec{\theta}_t - \vec{\theta}_s \right)^2 \right\rangle = \left\langle \vec{\theta}_t^2 - 2\vec{\theta}_t \cdot \vec{\theta}_s + \vec{\theta}_s^2 \right\rangle \tag{4.14}$$

The mean square value of $\vec{\theta}_t$ was evaluated in Section 3.2 and found to be:

$$\left\langle \vec{\theta}_t^2 \right\rangle = \frac{13.6183}{k^2 r_o^{5/3} d^{1/3}} \tag{4.15}$$

The terms in Equation 4.14 that remain to be evaluated are the mean square value of s-tilt, $< \vec{\theta}_s^2 >$, and the cross–correlation between z-tilt and s-tilt, $< \vec{\theta}_t \cdot \vec{\theta}_s >$.

Using Equations 2.41 and 2.46, the mean square value of s-tilt, $< \vec{\theta}_s^2 >$, can be expressed as:

$$\left\langle \vec{\theta}_s^2 \right\rangle = \left\langle \left(\frac{1}{kd} \right)^2 \left(\hat{x} \iint \frac{\Delta\phi(x,y,\Delta x)}{\Delta x} W(x,y) \mathrm{d}x\mathrm{d}y + \hat{y} \iint \frac{\Delta\phi(x,y,\Delta x)}{\Delta y} W(x,y) \mathrm{d}x\mathrm{d}y \right)^2 \right\rangle \tag{4.16}$$

It is shown in Appendix B.2 that evaluating Equation 4.16 yields:

$$\left\langle \vec{\theta}_s^2 \right\rangle = \frac{2}{k^2 d^4 \Delta x^2} \iiint \langle \Delta\phi(x_1, y_1, \Delta x) \Delta\phi(x_2, y_2, \Delta x) \rangle \, W(x_1, y_1) W(x_2, y_2) \mathrm{d}x_1 \mathrm{d}y_1 \mathrm{d}x_2 \mathrm{d}y_2 \quad (4.17)$$

An expression for $\langle \Delta\phi(x_1, y_1, \Delta x) \Delta\phi(x_2, y_2, \Delta x) \rangle$ is therefore needed. Recalling the definition for $\Delta\phi$:

$$\Delta\phi(x, y, \Delta x) = \phi(x - \frac{\Delta x}{2}, y) - \phi(x + \frac{\Delta x}{2}, y) \quad (4.18)$$

and using the structure function given by Equation 3.32, Equation 4.18 becomes:

$$\left\langle \vec{\theta}_s^2 \right\rangle = \frac{6.88}{k^2 d^4 \Delta x^2 r_o^{5/3}} \iiint \left[\sqrt{(x_2 - x_1 + \Delta x)^2 + (y_2 - y_1)^2}^{\frac{5}{3}} + \sqrt{(x_2 - x_1 - \Delta x)^2 + (y_2 - y_1)^2}^{\frac{5}{3}} \right.$$
$$\left. -2\sqrt{(x_2 - x_1)^2 + (y_2 - y_1)^2}^{\frac{5}{3}} \right]$$
$$\times \mathrm{rect}\left(\frac{x_1}{d}\right) \mathrm{rect}\left(\frac{x_2}{d}\right) \mathrm{rect}\left(\frac{y_1}{d}\right) \mathrm{rect}\left(\frac{y_2}{d}\right) \mathrm{d}x_1 \mathrm{d}y_1 \mathrm{d}x_2 \mathrm{d}y_2 \quad (4.19)$$

A variable substitution can be made so that the integral in Equation 4.19 will be in dimensionless form. This includes a substitution of $s = \Delta x / r_o$, which is defined as the normalized shear. Using these substitutions and Fourier Transform analysis, Appendix B shows that Equation 4.19 becomes:

$$\left\langle \vec{\theta}_s^2 \right\rangle = \frac{0.13544 f_v\left(s\frac{r_o}{d}\right)}{k^2 d^{1/3} r_o^{5/3}} \quad (4.20)$$

where $f_v\left(s\frac{r_o}{d}\right)$ is defined to be:

$$f_v(x) \equiv (x)^{-2} \int_{-2}^{2} \int_{-2}^{2} (2 - |\Delta\xi|)(2 - |\Delta\psi|) \left[\left| ((\Delta\xi + 2x)^2 + \Delta\psi^2 \right|^{\frac{5}{6}} \right.$$
$$\left. + \left| ((\Delta\xi - 2x)^2 + \Delta\psi^2 \right|^{\frac{5}{6}} - 2 \left| (\Delta\xi^2 + \Delta\psi^2 \right|^{\frac{5}{6}} \right] \mathrm{d}\Delta\xi \mathrm{d}\Delta\psi \quad (4.21)$$

and is plotted in Figure 4.1. Equation 4.20 is the simplest analytical solution than can be obtained. Note that any numerical solutions of Equation 4.21 must be for a given value of $\frac{s}{d/r_o}$. Also, note

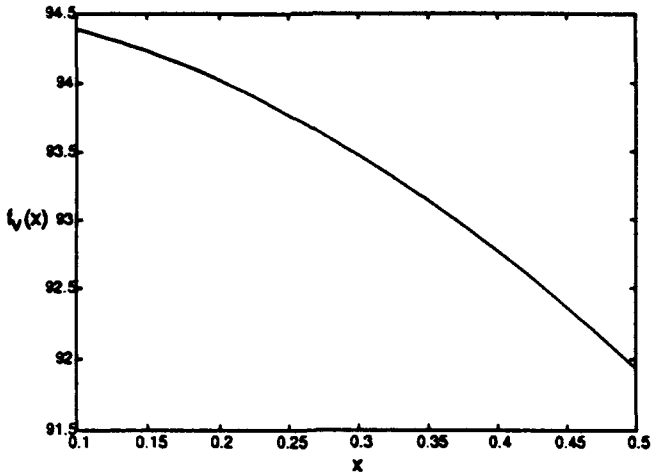

Figure 4.1. Plot of $f_v(x)$.

that from Equation 2.47

$$\frac{s}{d/r_o} = \frac{\Delta x}{d} \tag{4.22}$$

Hence, Equation 4.20 will be solved for a family of $\frac{s}{d/r_o}$ values from, $0 \leq \frac{s}{d/r_o} \leq 1/2$, as it is unreasonable to assume that the wavefronts would be sheared more than one half the subaperture diameter.

Attention is now turned to the middle term of Equation 4.14, $\left\langle \vec{\theta}_t \cdot \vec{\theta}_s \right\rangle$. By use of Equations 2.39, 2.41, 2.44 and 2.46, this can be expressed as:

$$\begin{aligned} \left\langle \vec{\theta}_t \cdot \vec{\theta}_s \right\rangle = & \left\langle \left[\hat{x} \frac{\int x\phi(x,y)W(x,y)\mathrm{d}x\mathrm{d}y}{\frac{kd^4}{12}} + \hat{y} \frac{\int y\phi(x,y)W(x,y)\mathrm{d}x\mathrm{d}y}{\frac{kd^4}{12}} \right] \right. \\ & \left. \cdot \left[\hat{x} \frac{\int \Delta\phi(x,y,\Delta x)W(x,y)\mathrm{d}x\mathrm{d}y}{\Delta x k d^2} + \hat{y} \frac{\int \Delta\phi(x,y,\Delta y)W(x,y)\mathrm{d}x\mathrm{d}y}{\Delta y k d^2} \right] \right\rangle \end{aligned} \tag{4.23}$$

Using a very similar analysis as that used to determine $\left\langle \vec{\theta}_s^2 \right\rangle$, Equation 4.23 is evaluated in Appendix B.3 and is found to be:

$$\left\langle \vec{\theta}_t \cdot \vec{\theta}_s \right\rangle = \frac{0.406325 f_c \left(s \frac{r_o}{d} \right)}{k^2 d^{1/3} r_o^{5/3}} \tag{4.24}$$

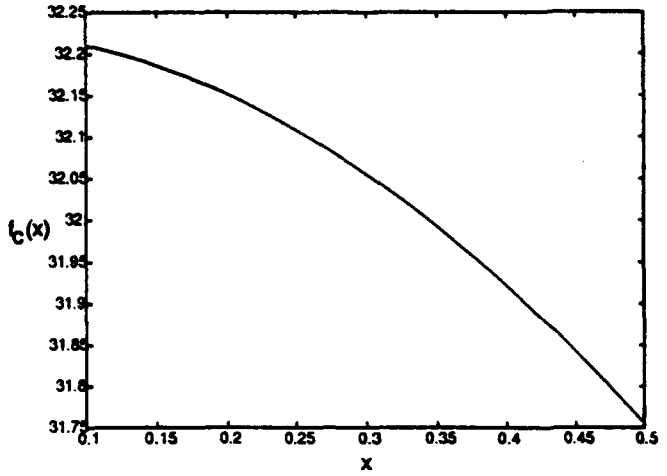

Figure 4.2. Plot of $f_c(x)$.

where $f_c\left(s\frac{r_o}{d}\right)$ is defined as:

$$f_c(x) = x^{-1}\int_{-2}^{2}\int_{-2}^{2}\Delta\xi\,(2-|\Delta\xi|)\,(2-|\Delta\psi|) \times\left[\left|(\Delta\xi+x)^2+\Delta\psi^2\right|^{\frac{5}{6}}-\left|(\Delta\xi-x)^2+\Delta\psi^2\right|^{\frac{5}{6}}\right]\mathrm{d}\Delta\xi\mathrm{d}\Delta\psi \tag{4.25}$$

and is plotted in Figure 4.2. Equation 4.24 is the simplest analytical form of an expression for the cross correlation between z-tilt and s-tilt. To proceed from here, a value for $\frac{s}{d/r_o}$, the normalized shear, must be specified and Equation 4.25 solved numerically.

4.2.1 Mean Square Error Between z-tilt and s-tilt, $E_{S_{zz}}$ Recalling Equation 4.14, the total MS error due to the difference between z-tilt and s-tilt can be obtained by combining Equations 4.15, 4.20 and 4.24. Doing so yields:

$$\left\langle\left(\vec{\theta}_t-\vec{\theta}_s\right)^2\right\rangle = \frac{13.6183}{k^2r_o^{5/3}d^{1/3}} - \frac{2\cdot 0.406325 f_c\left(s\frac{r_o}{d}\right)}{k^2d^{1/3}r_o^{5/3}} + \frac{0.13544 f_v\left(s\frac{r_o}{d}\right)}{k^2d^{1/3}r_o^{5/3}} \tag{4.26}$$

where $f_v\left(s\frac{r_o}{d}\right)$ and $f_c\left(s\frac{r_o}{d}\right)$ are defined by Equations 4.21 and 4.25 respectively. Note that Equation 4.26 can be re-written as:

$$\left\langle \left(\vec{\theta}_t - \vec{\theta}_s\right)^2 \right\rangle = \left[13.6183 - 0.8126 f_c\left(s\frac{r_o}{d}\right) + 0.1354 f_v\left(s\frac{r_o}{d}\right)\right]\left(\frac{d}{r_o}\right)^{-\frac{1}{3}}\left(\frac{1}{kr_o}\right)^2 \qquad (4.27)$$

which gives the MS error in terms of slope, (meters/meters). Therefore, as in Section 3.2.1, to convert the units to (radians/r_o cell)^2, a multiplication of $(kr_o)^2$ is required. Thus:

$$E_{Sxz} \equiv \left\langle \left(\vec{\theta}_t - \vec{\theta}_s\right)^2 \right\rangle (kr_o)^2 = \left[13.6183 - 0.8126 f_c\left(s\frac{r_o}{d}\right) + 0.1354 f_v\left(s\frac{r_o}{d}\right)\right]\left(\frac{d}{r_o}\right)^{-\frac{1}{3}}\left(\frac{\text{radians}}{r_o \text{ cell}}\right)^2 \qquad (4.28)$$

4.3 Total Shearing Mean Square Error

Using Equations 4.1, 4.12 and 4.28, the total MS error for the Shearing Interferometer can be described as:

$$E_S = \frac{8}{N_{tot}s^2}\exp\left[(2\pi)^2\beta^2 s^2\right] + \left[13.6183 - 0.8126 f_c\left(s\frac{r_o}{d}\right) + 0.1354 f_v\left(s\frac{r_o}{d}\right)\right]\left(\frac{d}{r_o}\right)^{-\frac{1}{3}}\left(\frac{\text{radians}}{r_o \text{ cell}}\right)^2 \qquad (4.29)$$

Some comments about this result are in order. First, as in Equation 3.44, Equation 4.29 shows that some error is inherent even for "perfect" seeing conditions, $d/r_o \ll 1$. This minimum error is determined by the total photon count, N_{tot}, and the shear, s. Figures 4.1 and 4.2 show that the $f_c\left(s\frac{r_o}{d}\right)$ and $f_v\left(s\frac{r_o}{d}\right)$ change very little over the range of $\frac{s}{d/r_o}$ values we are interested in. Thus the MS error between s-tilt and z-tilt is only weakly dependent on the shear.

V. *Comparison of Hartmann and Shearing Wavefront Sensors*

The total error variance for the Hartmann Wavefront Sensor, found in Chapter III, is:

$$E_H = \begin{cases} 2\frac{(2\pi)^2}{N}\left[\beta^2 + (0.37)^2\left(\frac{r_o}{d}\right)^2\right] + 0.235\left(\frac{d}{r_o}\right)^{-\frac{1}{3}}\left(\frac{\text{radians}}{r_o \text{ cell}}\right)^2 & \text{for } \frac{d}{r_o} \leq 1 \\ 2\frac{(2\pi)^2}{N}\left[\beta^2 + (0.37)^2\right] + 0.235\left(\frac{d}{r_o}\right)^{-\frac{1}{3}}\left(\frac{\text{radians}}{r_o \text{ cell}}\right)^2 & \text{for } \frac{d}{r_o} > 1 \end{cases} \tag{5.1}$$

Likewise, the total error variance for the Shearing Interferometer, found in Chapter IV, is:

$$E_S = \frac{8}{Ns^2}\exp\left[(2\pi)^2\beta^2 s^2\right] + \left[13.6183 - 0.8126 f_c\left(s\frac{r_o}{d}\right) + 0.1354 f_v\left(s\frac{r_o}{d}\right)\right]\left(\frac{d}{r_o}\right)^{-\frac{1}{3}}\left(\frac{\text{radians}}{r_o \text{ cell}}\right)^2 \tag{5.2}$$

Recall that the N in Equations 5.1 and 5.2 represents the total number of photon events within the subaperture during the integration time. The ratio of the angular size of the source to the angular resolution of the optical system, limited by the atmosphere, was defined in Equation 3.23 to be:

$$\beta \equiv \frac{\frac{\sigma_s}{z}}{\frac{\lambda}{r_o}} = \frac{\sigma_s}{z}\cdot\frac{r_o}{\lambda} \tag{5.3}$$

The normalized shear, s, was defined as the ratio of the absolute shear, Δx, to the atmospheric correlation length, r_o.

$$s = \frac{\Delta x}{r_o} \tag{5.4}$$

The functions $f_v\left(s\frac{r_o}{d}\right)$ and $f_c\left(s\frac{r_o}{d}\right)$ are given by Equations 4.21 and 4.25 respectively and are plotted in Figures 4.1 and 4.2, respectively. And, finally, d/r_o is the ratio of the subaperture diameter to the atmospheric correlation length.

Several items about Equations 5.1 and 5.2 should be noted. First, some error is inherent in wavefront measurements, even for "perfect" seeing conditions, i.e. $d/r_o \ll 1$. This minimum error is determined by the total photon count, N, and the source size, β. Second, examination of Figure 5.8 reveals that the term $\left[13.6183 - 0.8126 f_c\left(s\frac{r_o}{d}\right) + 0.1354 f_v\left(s\frac{r_o}{d}\right)\right]$ is approximately equal to 0.235

for most values of $\frac{s}{d/r_o}$ of interest. Hence, the error due to the difference between g-z-tilt and s-z-tilt, given by the second term in each equation, is relatively the same for both wavefront sensors. Third, due to the source size term in the exponent of Equation 5.2, the Shearing Interferometer is much more sensitive to changes in the source size than is the Hartmann Wavefront sensor.

The total RMS error for the Hartmann Wavefront Sensor and Shearing Interferometer is plotted in Figure 5.1 versus d/r_o for $N = 2$; $s = 0.1, 0.2, 0.3, 0.4$ and 0.5; and $\beta = 0.01, 0.10, 0.50$ and 1.00. Looking first at the $\beta = 0.01$ plot, recall that this source size represents a very small (almost a point) source. Notice that the Hartmann Sensor performance improves significantly as d/r_o increases, for $d/r_o < 1$ and then flattens out for further increases in d/r_o. This results from the spot size in the detector plane of the Hartmann being inversely proportional to the subaperture diameter. As the spot size decreases, the Hartmann sensor determines the centroid more accurately, and hence the shot noise decreases. However, for $d/r_o > 1$, the spot size is limited by r_o instead of d and no further reduction in the spot size occurs. We also notice that the RMS error for the Shearing Interferometer decreases with increasing shear. As the shear increases, the phase difference will also increase while the noise in the measurement will remain relatively the same. Hence, the signal to noise ratio will increase causing the shot noise portion of the error to decrease. This is represented by the s^{-2} in the first term of Equation 5.2.

Now, looking at the $\beta = 0.10$ plot, we see the same trends observed for the $\beta = 0.01$ plot. However, close examination shows that all the curves have been shifted up slightly, indicating that the RMS error increases for increasing source size. This is more easily seen in the plots for $\beta = 0.5$ and 1.00. However, in these last two plots, we also notice that the consistent decrease in RMS error for increasing shear no longer occurs. Instead, error decreases until some "optimum" shear is reached and then begins to increase again. This results from the Shearing Interferometer's sensitivity to the fringe visibility, which is inversely proportional to the size of the source.

The total RMS error is again plotted in Figures 5.2 and 5.3 for the same conditions as above

except for $N = 5$ and 10, respectively. The same trends as mentioned in the above paragraphs are noticed. However, we see that the total RMS error decreases with increasing photon count since the shot noise error is inversely proportional to N.

Figure 5.4 is a plot of the RMS error for $N = \infty$. This plot represents the portion of the total RMS error due only to the difference between g-tilt and z-tilt for the Hartmann Sensor and the difference between s-tilt and z-tilt for the Shearing Interferometer. We can clearly see that, in the absence of shot noise effects, the two sensors show nearly identical performance.

Likewise, Figures 5.5–5.7 represent only the shot noise portion of the total error for the Hartmann and Shearing Interferometer–given by the first term in Equations 5.1 and 5.2 respectively. Comparing Figure 5.5 with Figure 5.1 we see that they are nearly identical, indicating that shot noise effects are the dominate noise source for both the Hartmann Wavefront Sensor and the Shearing Interferometer, for the photon count values examined. This same conclusion can be drawn by comparing Figures 5.6 and 5.2; and Figures 5.7 and 5.3.

As mentioned above, there seems to be some "optimum" shear, at which the RMS error for the Shearing Interferometer is a minimum. Since Figures 5.5–5.7 indicate that the majority of the error results from the shot noise component, that term will be examined to determine the optimum shear. Recalling Equation 4.12, the shot noise component of the total Shearing MS error; taking its derivative with respect to s; setting it equal to zero and solving for s gives the optimum shear as a function of source size:

$$s_{opt} = \frac{1}{2\pi\beta} \tag{5.5}$$

Hence, as expected, the optimum shear is inversely proportional to the source size. Equation 5.5 is plotted in Figure 5.9.

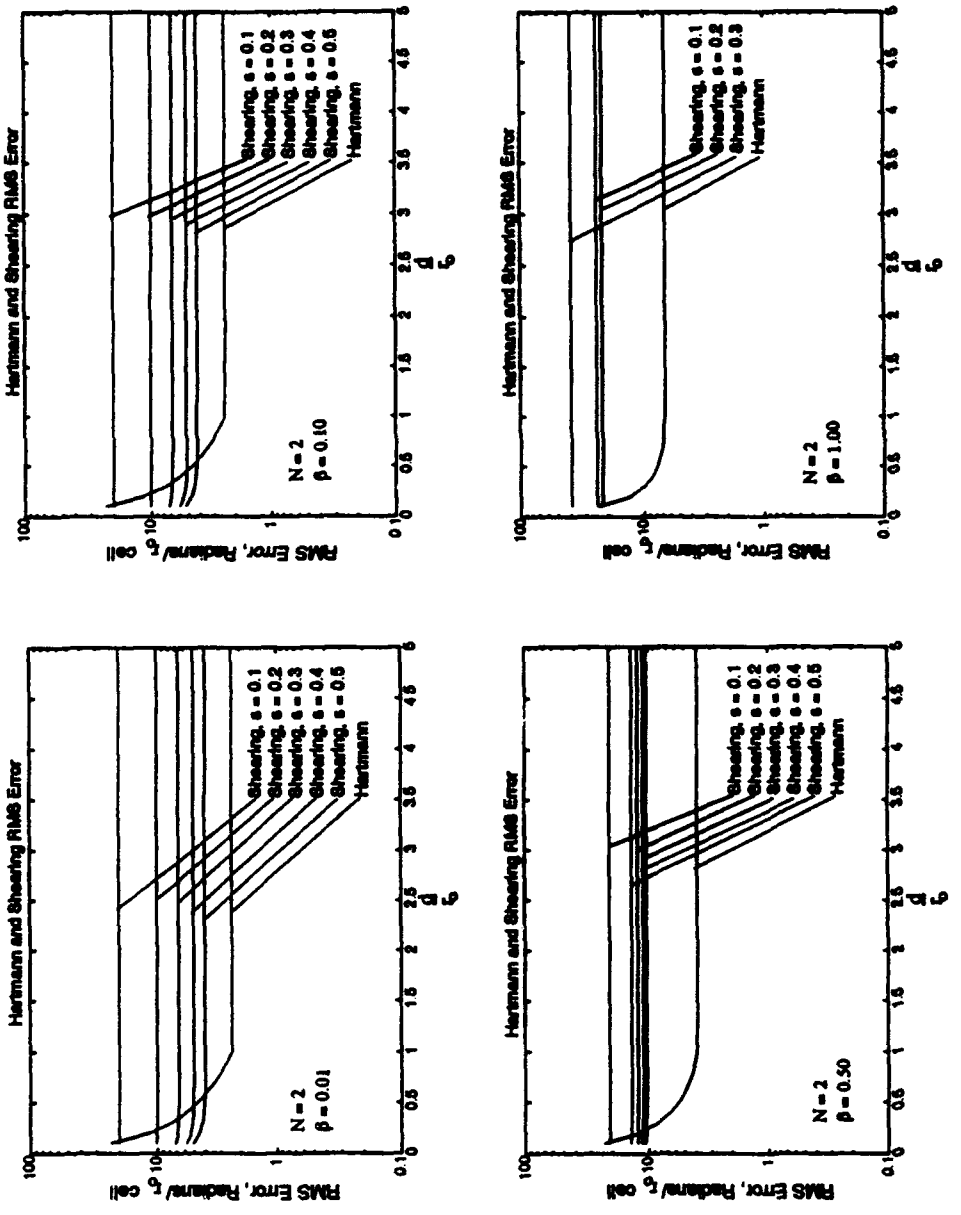

Figure 5.1. RMS Error vs d/r_o for $N = 2$

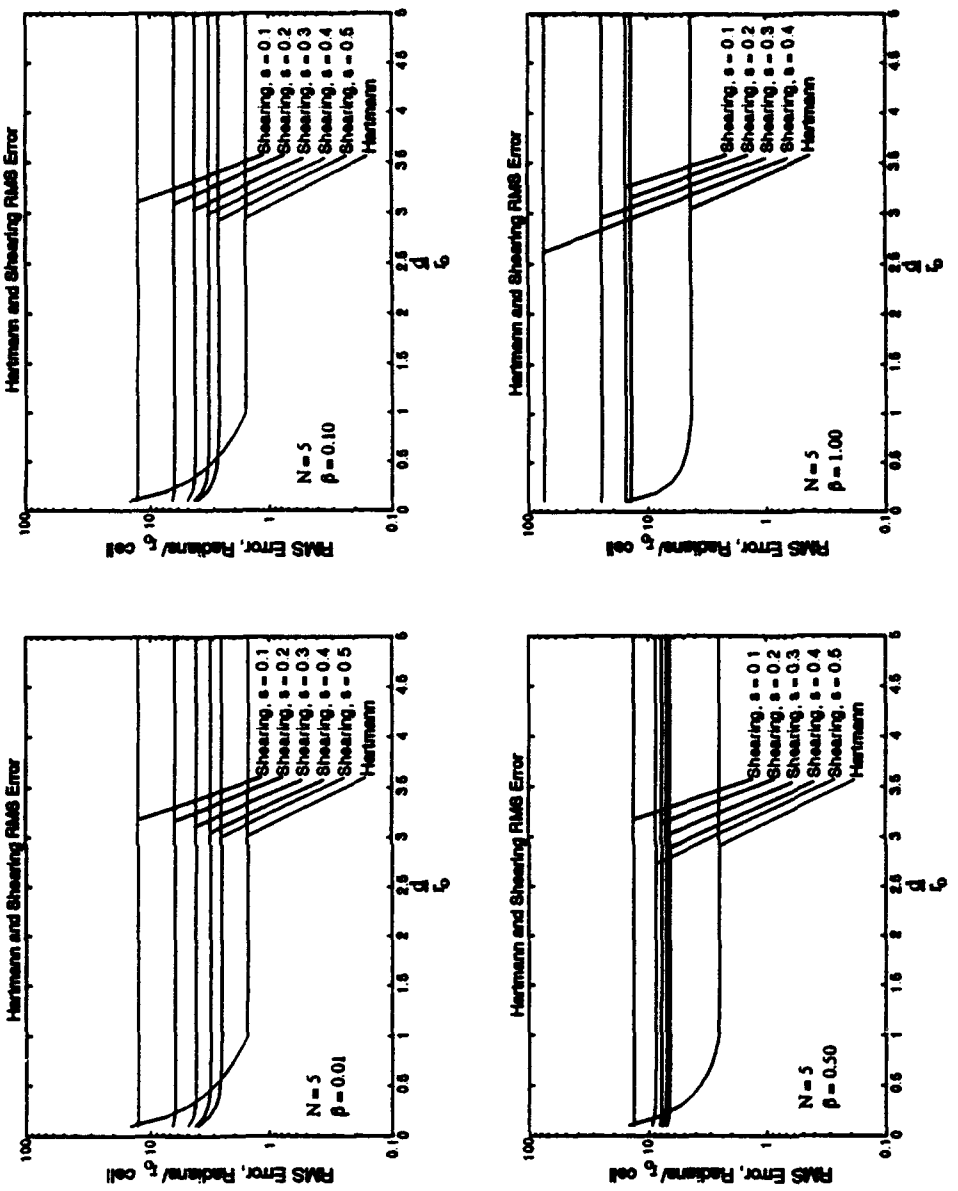

Figure 5.2. RMS Error vs d/r_o for $N = 5$

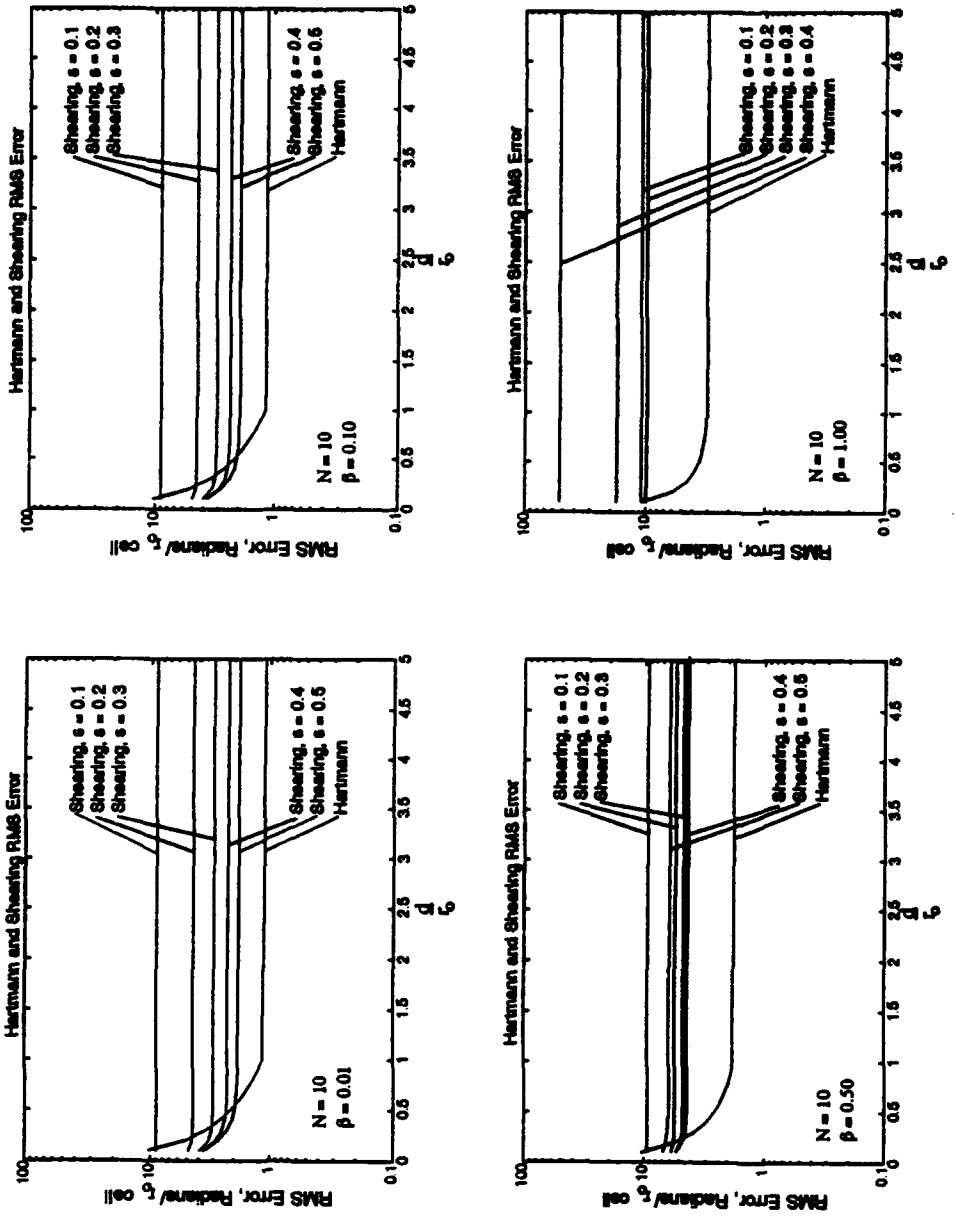

Figure 5.3. RMS Error vs d/r_o for $N = 10$

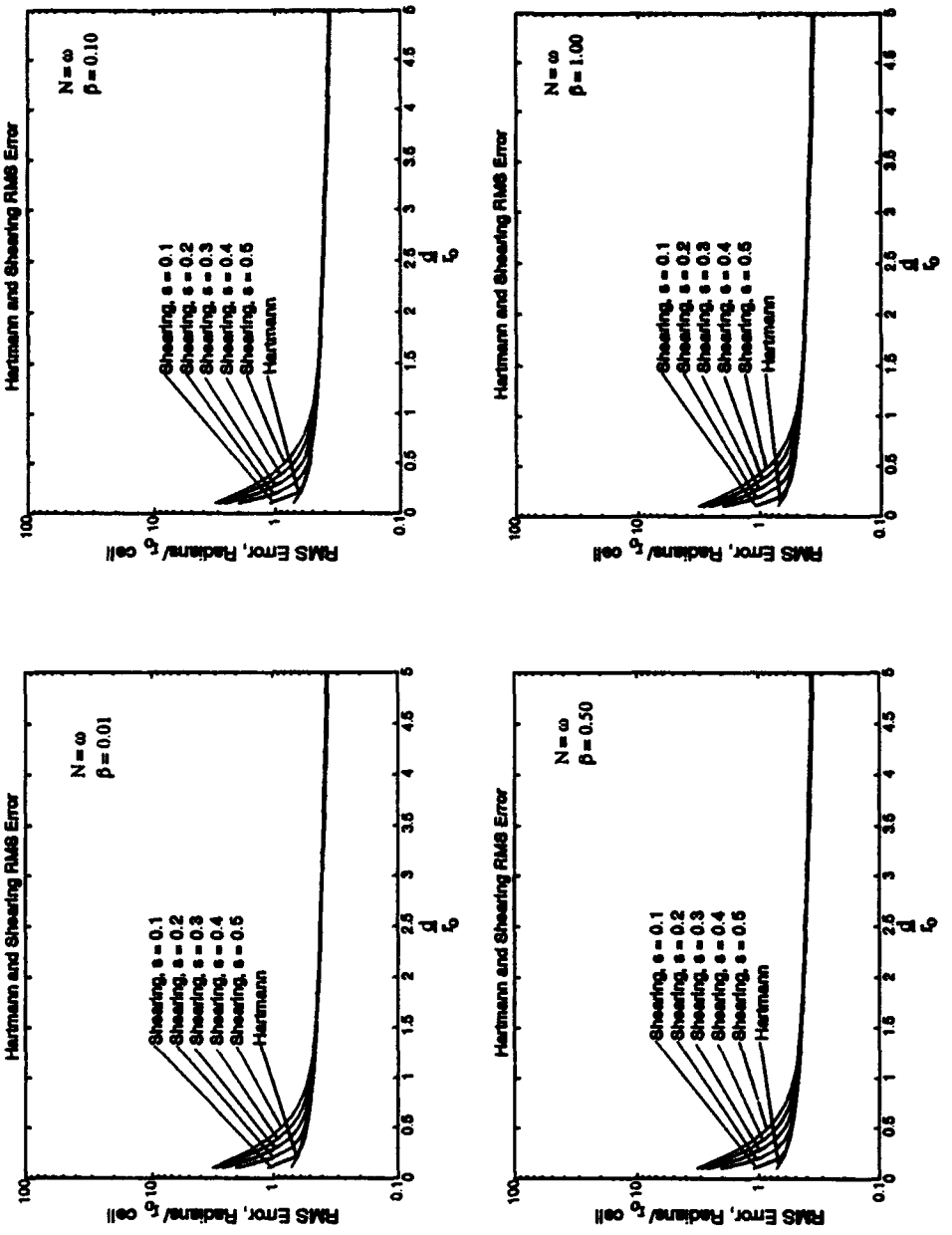

Figure 5.4. RMS Error vs d/r_o for $N = \infty$

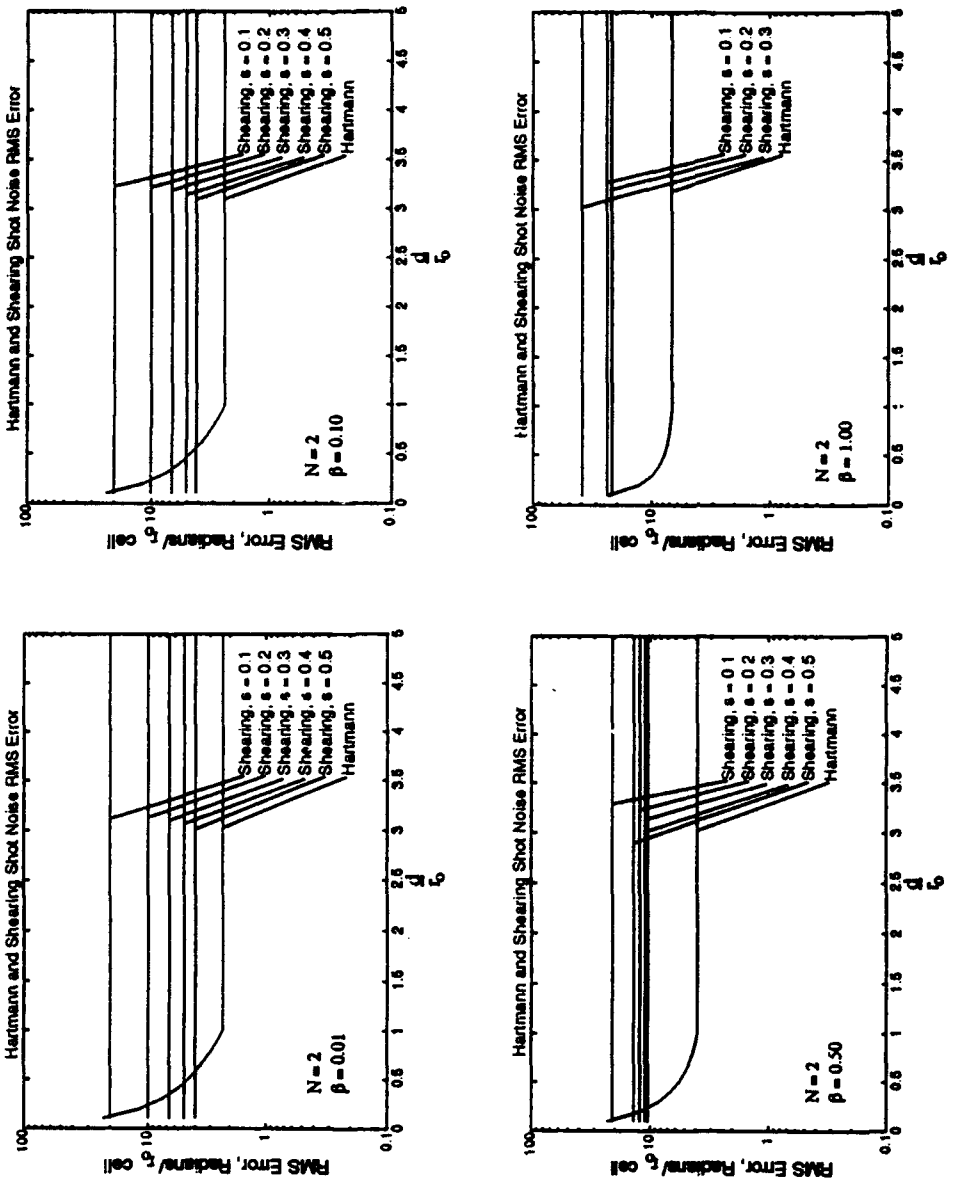

Figure 5.5. RMS Shot Noise Error vs d/r_o for $N = 2$

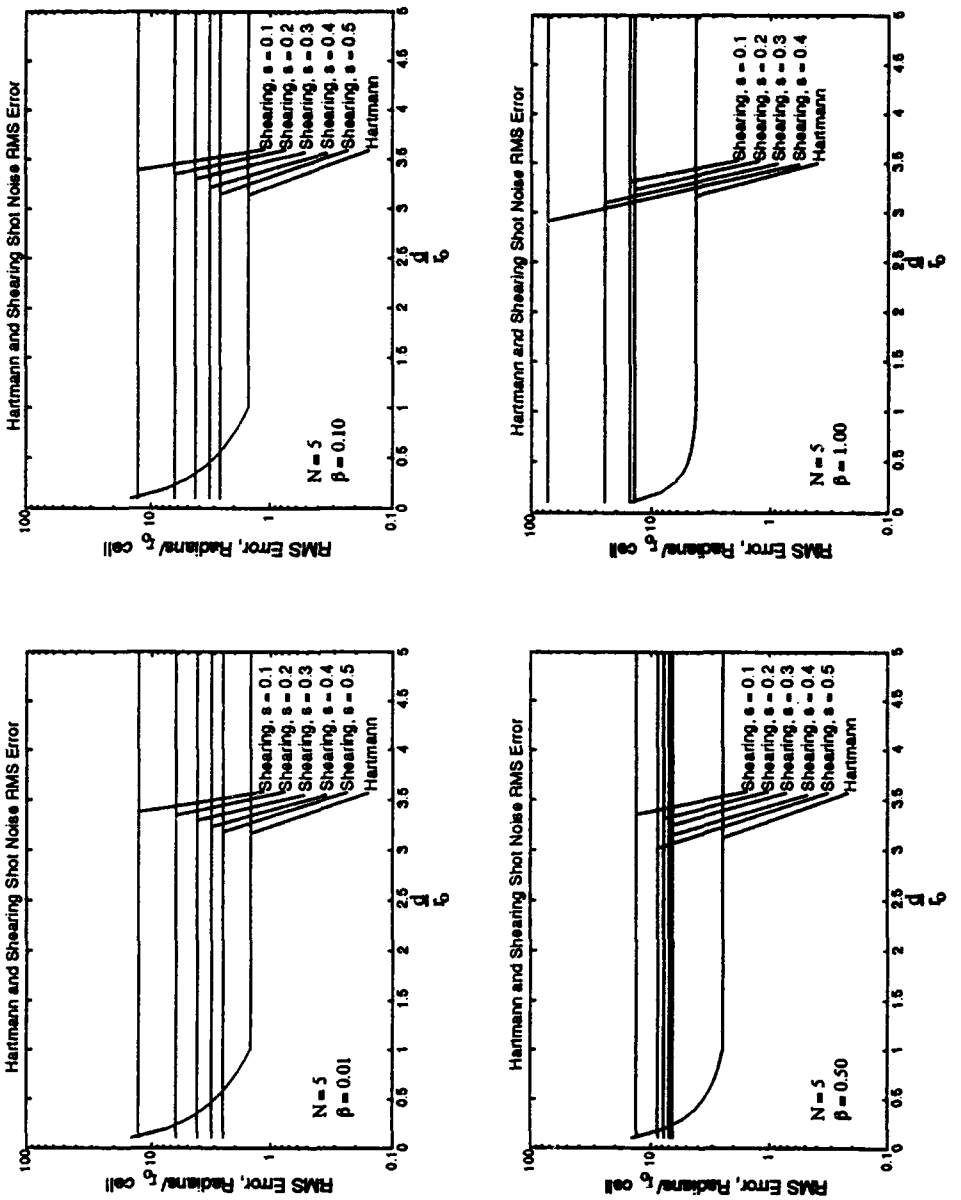

Figure 5.6. RMS Shot Noise Error vs d/r_o for $N = 5$

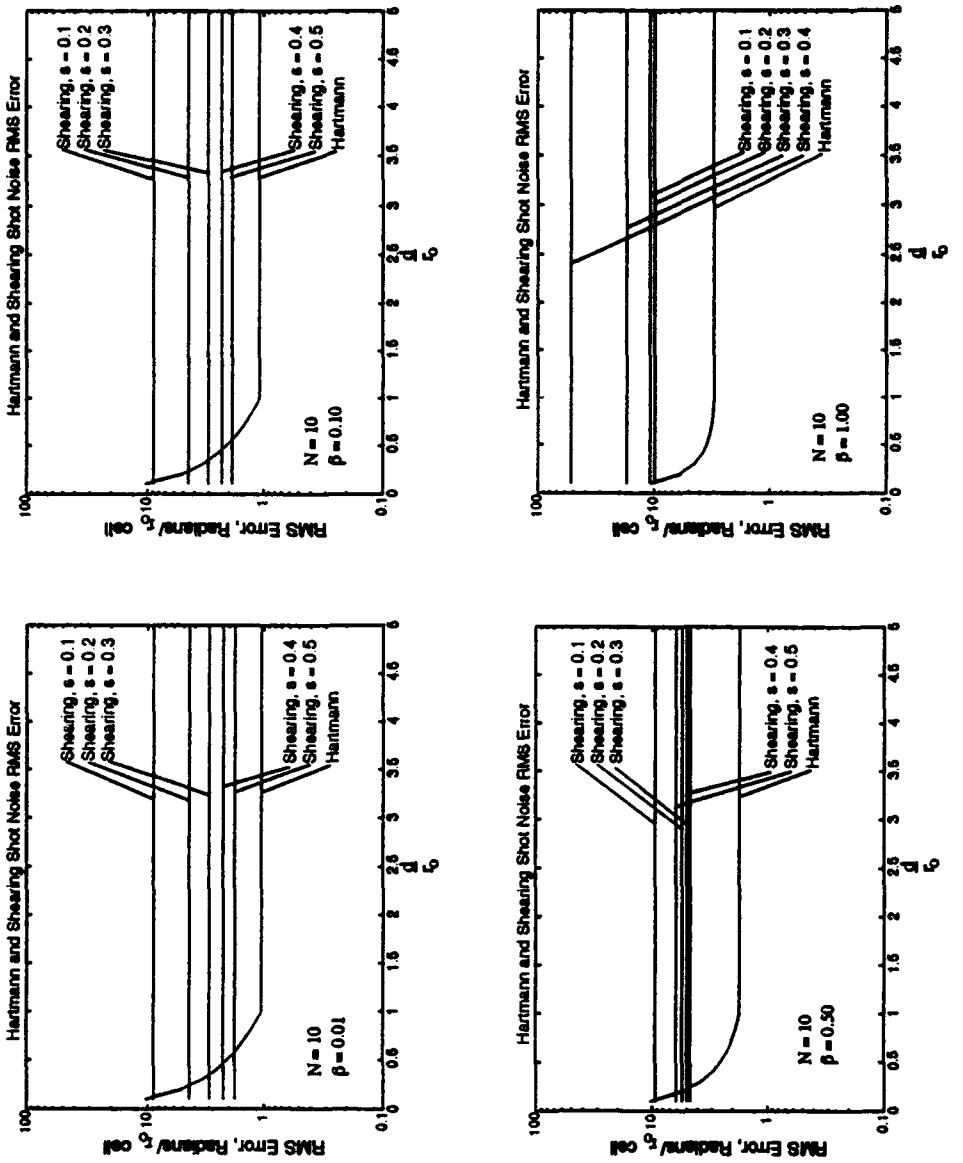

Figure 5.7. RMS Shot Noise Error vs d/r_o for $N = 10$

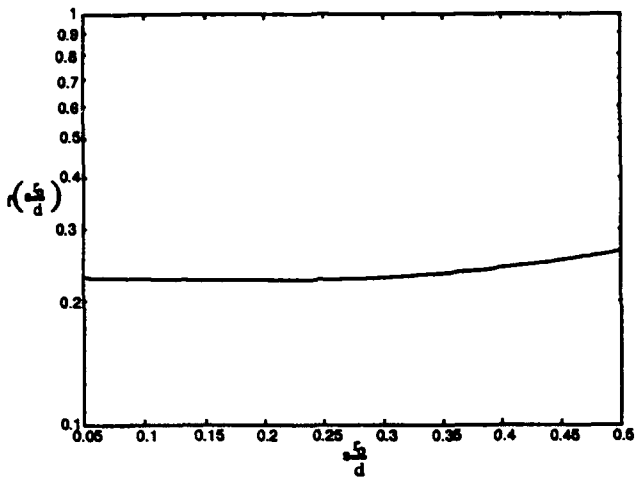

Figure 5.8. Plot of $13.6183 - 0.8126 f_c(x) + 0.1354 f_v(x)$.

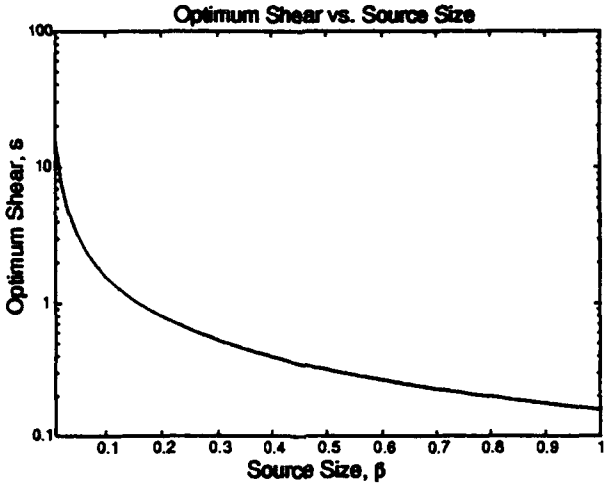

Figure 5.9. Plot of Optimum Shear, s, vs. Source Size, β.

VI. Conclusions and Recommendations

6.1 Conclusions

This research has conducted an analysis of the mean square error resulting from wavefront measurements obtained from the Hartmann Wavefront Sensor and the Shearing Interferometer when viewing extended objects through a turbulent atmosphere. Two sources of error were considered: the shot noise error and the g-z-tilt and s-z-tilt error. The shot noise error results from inaccuracies in determining the spot centroid, for the Hartmann Sensor, and the phase of the fringe pattern, for the Shearing Interferometer. Likewise, the g-z-tilt error and the s-z-tilt error results from the difference between the true wavefront tilt and the averaged wavefront tilt over the finite sized subaperture.

Results indicated that the major contributor to the total error, for the photon counts examined, was the shot noise effects. The shot noise error had a strong dependance on the source size, in addition to dependencies on the photon count and amount of shear, (for the Shearing Interferometer). When the shot noise error was not considered, the two detectors performed nearly identically.

However, for the more realistic–photon limited–cases, the Hartmann Wavefront sensor showed much better error performance than the Shearing Interferometer. The only exceptions were for small source sizes and small d/r_o.

6.2 Recommendations for Further Study

The model used for the Shearing Interferometer encoded the wavefront tilt in the phase of an ac modulated fringe pattern. Goodman's DFT Fringe Estimator was then used to extract the phase from this fringe pattern. The results indicate that the major error resulted from this portion of the wavefront detection process. However, there are versions of the Shearing Interferometer that do not use ac modulation and fringe detection [11]. It is therefore recommended that the

analysis presented in Chapter IV be repeated for one of these other configurations, without the ac modulation. This would establish whether the unusually large error is a result of the shearing process or the ac modulation and fringe detection process.

Appendix A. *Derivation Details for Hartmann Wavefront Sensor*

This appendix provides details of the derivations presented in Chapter III.

A.1 Derivation of Cross Correlation between g-tilt and z-Tilt, $\left\langle \vec{\theta}_t \cdot \vec{\theta}_c \right\rangle$

From Equation 3.27

$$\left\langle \vec{\theta}_t \cdot \vec{\theta}_c \right\rangle = \frac{12}{k^2 d^6} \left\langle \iint (x \cdot \hat{x} + y \cdot \hat{y})\, W(x,y)\phi(x,y)\mathrm{d}x\mathrm{d}y \cdot \iint W(x,y)\nabla\phi(x,y)\mathrm{d}x\mathrm{d}y \right\rangle \tag{A.1}$$

This second integral is very similar to one evaluated by Welsh and Gardner [23:pg. 1914] using integration by parts. This approach yields:

$$\left\langle \vec{\theta}_t \cdot \vec{\theta}_c \right\rangle = \frac{12}{k^2 d^6} \left\langle \iint (x_1\hat{x} + y_1\hat{y})\, W(x_1,y_1)\phi(x_1,y_1)\mathrm{d}x_1\mathrm{d}y_1 \cdot \left(- \iint \nabla_2 W(x_2,y_2)\phi(x_2,y_2)\mathrm{d}x_2\mathrm{d}y_2 \right) \right\rangle \tag{A.2}$$

Note that in Equation A.2, dummy variables, denoted by subscripts 1 or 2, are used to indicate the separate integrals. Further, note that ∇_2 indicates that the gradient operator only operates on functions of x_2 and y_2.

Recalling the definition of the subaperture, $W(x,y)$ (Equation 2.42), and recalling the definition of the gradient operator:

$$\nabla = \hat{x}\frac{\partial}{\partial x} + \hat{y}\frac{\partial}{\partial y}, \tag{A.3}$$

$\nabla W(x,y)$ becomes:

$$\begin{aligned} \nabla W(x,y) &= \frac{\partial}{\partial x}\left[\mathrm{rect}\left(\frac{x}{d}\right)\mathrm{rect}\left(\frac{y}{d}\right)\right]\hat{x} + \frac{\partial}{\partial y}\left[\mathrm{rect}\left(\frac{x}{d}\right)\mathrm{rect}\left(\frac{y}{d}\right)\right]\hat{y} \\ &= \left[-\delta\left(x - \frac{d}{2}\right) + \delta\left(x + \frac{d}{2}\right)\right]\mathrm{rect}\left(\frac{y}{d}\right)\hat{x} \\ &\quad + \left[-\delta\left(y - \frac{d}{2}\right) + \delta\left(y + \frac{d}{2}\right)\right]\mathrm{rect}\left(\frac{x}{d}\right)\hat{y} \end{aligned} \tag{A.4}$$

Substituting this relationship into Equation A.2 yields:

$$\left\langle \vec{\theta}_t \cdot \vec{\theta}_c \right\rangle = \frac{12}{k^2 d^6} \Bigg\langle \iint (x_1 \hat{x} + y_1 \hat{y})\, W(x_1, y_1) \phi(x_1, y_1) \mathrm{d}x_1 \mathrm{d}y_1 \cdot \Bigg(- \iint \phi(x_2, y_2) \Bigg\{ \left[\delta\left(x_2 + \frac{d}{2}\right) - \delta\left(x_2 - \frac{d}{2}\right) \right] \mathrm{rect}\left(\frac{y_2}{d}\right) \hat{x} + \left[\delta\left(y_2 + \frac{d}{2}\right) - \delta\left(y_2 - \frac{d}{2}\right) \right] \mathrm{rect}\left(\frac{x_2}{d}\right) \hat{y} \Bigg\} \mathrm{d}x_2 \mathrm{d}y_2 \Bigg) \Bigg\rangle \qquad \text{(A.5)}$$

Separating each integral in Equation A.5 into its x and y components and performing the dot product results in:

$$\left\langle \vec{\theta}_t \cdot \vec{\theta}_c \right\rangle = \frac{12}{k^2 d^6} \Bigg\langle \iint x_1 W(x_1, y_1) \phi(x_1, y_1) \mathrm{d}x_1 \mathrm{d}y_1 \times \iint \phi(x_2, y_2) \left[\delta\left(x_2 - \frac{d}{2}\right) - \delta\left(x_2 + \frac{d}{2}\right) \right] \mathrm{rect}\left(\frac{y_2}{d}\right) \mathrm{d}x_2 \mathrm{d}y_2 + \iint y_1 W(x_1, y_1) \phi(x_1, y_1) \mathrm{d}x_1 \mathrm{d}y_1 \times \iint \phi(x_2, y_2) \left[\delta\left(y_2 - \frac{d}{2}\right) - \delta\left(y_2 + \frac{d}{2}\right) \right] \mathrm{rect}\left(\frac{x_2}{d}\right) \mathrm{d}x_2 \mathrm{d}y_2 \Bigg\rangle \qquad \text{(A.6)}$$

Note that all actions of the first two integral pairs will be duplicated on the second two integral pairs. Thus, the second two integral pairs are dropped and the entire expression is multiplied by two to account for them. This yields:

$$\left\langle \vec{\theta}_t \cdot \vec{\theta}_c \right\rangle = \frac{2 \cdot 12}{k^2 d^6} \Bigg\langle \iint x_1 W(x_1, y_1) \phi(x_1, y_1) \mathrm{d}x_1 \mathrm{d}y_1 \times \iint \phi(x_2, y_2) \left[\delta\left(x_2 - \frac{d}{2}\right) - \delta\left(x_2 + \frac{d}{2}\right) \right] \mathrm{rect}\left(\frac{y_2}{d}\right) \mathrm{d}x_2 \mathrm{d}y_2 \Bigg\rangle \qquad \text{(A.7)}$$

Combining the integrals in Equation A.7, produces:

$$\left\langle \vec{\theta}_t \cdot \vec{\theta}_c \right\rangle = \frac{24}{k^2 d^6} \Bigg\langle \iiint x_1 W(x_1, y_1) \phi(x_1, y_1) \phi(x_2, y_2) \times \left[\delta\left(x_2 - \frac{d}{2}\right) - \delta\left(x_2 + \frac{d}{2}\right) \right] \mathrm{rect}\left(\frac{y_2}{d}\right) \mathrm{d}x_1 \mathrm{d}x_2 \mathrm{d}y_1 \mathrm{d}y_2 \Bigg\rangle \qquad \text{(A.8)}$$

Note that all terms in Equation A.8 are deterministic *except* ϕ. Thus, the expected value operator can be taken inside the integrals. This results in:

$$\left\langle \vec{\theta}_t \cdot \vec{\theta}_c \right\rangle = \frac{24}{k^2 d^6} \iiint x_1 W(x_1, y_1) \left\langle \phi(x_1, y_1) \phi(x_2, y_2) \right\rangle \times \left[\delta\left(x_2 - \frac{d}{2}\right) - \delta\left(x_2 + \frac{d}{2}\right) \right] \text{rect}\left(\frac{y_2}{d}\right) dx_1 dx_2 dy_1 dy_2 \tag{A.9}$$

An expression for the correlation function, $\langle \phi(x_1, y_1) \phi(x_2, y_2) \rangle$, is needed to continue. However, in atmospheric optics, it is more common to use structure functions rather than correlation functions [22]. The correlation functions and structure functions are related by:

$$\langle \phi(x_1, y_1) \phi(x_2, y_2) \rangle = -\frac{1}{2} D_\phi(x_1, y_1; x_2, y_2) + \Gamma_\phi(0, 0) \tag{A.10}$$

where $\Gamma_\phi(0,0) = \frac{1}{2} \left\langle \phi^2(x_1, y_1) \right\rangle + \frac{1}{2} \left\langle \phi^2(x_2, y_2) \right\rangle$ and is constant since the phase is assumed to be wide sense stationary [8:pg. 376]. The structure function, D_ϕ, has been determined by Wallner [21:pg. 1774] to be:

$$D\left(\vec{x}, \vec{x'}\right) = 6.88 \left| \frac{\left(\vec{x} - \vec{x'}\right)}{r_o} \right|^{\frac{5}{3}} \tag{A.11}$$

Therefore, the correlation function can be expressed as:

$$\langle \phi(x_1, y_1) \phi(x_2, y_2) \rangle = -\frac{6.88}{2} \left(\frac{\sqrt{(x_2 - x_1)^2 + (y_2 - y_1)^2}}{r_o} \right)^{5/3} + \Gamma_\phi(0, 0) \tag{A.12}$$

Substituting Equation A.12 into Equation A.9, produces:

$$\left\langle \vec{\theta}_t \cdot \vec{\theta}_c \right\rangle = \frac{24}{k^2 d^6} \iiint x_1 W(x_1, y_1) \left(-\frac{1}{2} 6.88 \left(\frac{\sqrt{(x_2 - x_1)^2 + (y_2 - y_1)^2}}{r_o} \right)^{5/3} + \Gamma_\phi(0, 0) \right) \times \left[\delta\left(x_2 - \frac{d}{2}\right) - \delta\left(x_2 + \frac{d}{2}\right) \right] \text{rect}\left(\frac{y_2}{d}\right) dx_1 dx_2 dy_1 dy_2 \tag{A.13}$$

Note, if Γ_ϕ is separated out from the rest of the integrals and the limits imposed by the subaperture

are set, the resulting integral will be a constant multiplied by an odd function integrated from $-\frac{d}{2}$ to $\frac{d}{2}$ and hence will become zero. Therefore, the Γ_ϕ term can be dropped. Recalling the definition of the subaperture function, Equation 2.42, Equation A.13 becomes:

$$\left\langle \vec{\theta}_t \cdot \vec{\theta}_c \right\rangle = \frac{24}{k^2 d^6} \iiint x_1 \text{rect}\left(\frac{x_1}{d}\right) \text{rect}\left(\frac{y_1}{d}\right) \left[\delta\left(x_2 - \frac{d}{2}\right) - \delta\left(x_2 + \frac{d}{2}\right)\right] \text{rect}\left(\frac{y_2}{d}\right) \times \left[-\frac{6.88}{2}\left(\frac{\sqrt{(x_2 - x_1)^2 + (y_2 - y_1)^2}}{r_o}\right)^{5/3}\right] dx_1 dx_2 dy_1 dy_2 \quad \text{(A.14)}$$

Using the sifting property of delta functions to integrate over x_2, [6:page 53],

$$\int f(\alpha)\delta(\alpha - x_o)d\alpha = f(x_o) \quad \text{(A.15)}$$

Equation A.14 becomes:

$$\left\langle \vec{\theta}_t \cdot \vec{\theta}_c \right\rangle = \frac{24}{k^2 d^6} \iiint x_1 \text{rect}\left(\frac{x_1}{d}\right) \text{rect}\left(\frac{y_1}{d}\right) \text{rect}\left(\frac{y_2}{d}\right) \left[-\frac{6.88}{2}\left(\frac{\sqrt{\left(\frac{d}{2} - x_1\right)^2 + (y_2 - y_1)^2}}{r_o}\right)^{5/3} + \frac{6.88}{2}\left(\frac{\sqrt{\left(-\frac{d}{2} - x_1\right)^2 + (y_2 - y_1)^2}}{r_o}\right)^{5/3}\right] dx_1 dy_1 dy_2 \quad \text{(A.16)}$$

To proceed, the following variable substitutions are defined:

$$\Delta y = y_2 - y_1 \qquad \text{and} \qquad \Sigma y = \frac{y_2 + y_1}{2} \quad \text{(A.17)}$$

Thus,

$$y_2 = \frac{1}{2}\Delta y + \Sigma y \qquad \text{and} \qquad y_1 = \Sigma y - \frac{1}{2}\Delta y \quad \text{(A.18)}$$

This choice allows the Jacobian to be one. Equation A.16 then becomes:

$$\left\langle \vec{\theta}_t \cdot \vec{\theta}_c \right\rangle = \frac{24}{k^2 d^6} \iiint x_1 \text{rect}\left(\frac{x_1}{d}\right) \text{rect}\left(\frac{\Sigma y - \frac{1}{2}\Delta y}{d}\right) \text{rect}\left(\frac{\frac{1}{2}\Delta y + \Sigma y}{d}\right)$$
$$\times \left[-\frac{6.88}{2} \left(\frac{\sqrt{\left(\frac{d}{2} - x_1\right)^2 + (\Delta y)^2}}{r_o} \right)^{5/3} + \frac{6.88}{2} \left(\frac{\sqrt{\left(-\frac{d}{2} - x_1\right)^2 + (\Delta y)^2}}{r_o} \right)^{5/3} \right]$$
$$\times dx_1 d\Delta y d\Sigma y \tag{A.19}$$

Note, only two terms in Equation A.19 depend on Σy. Thus, for a moment, just look at:

$$\int \text{rect}\left(\frac{\frac{1}{2}\Delta y + \Sigma y}{d}\right) \text{rect}\left(\frac{\Sigma y - \frac{1}{2}\Delta y}{d}\right) d\Sigma y \tag{A.20}$$

Define:

$$\alpha = \frac{\frac{1}{2}\Delta y + \Sigma y}{d} \qquad \rightarrow \qquad d\alpha = \frac{1}{d} d\Sigma y \tag{A.21}$$

Then Equation A.20 becomes:

$$d \int \text{rect}(\alpha) \text{rect}\left(\alpha - \frac{\Delta y}{d}\right) d\alpha \tag{A.22}$$

which, since $\Delta y/d$ is a constant for this integral, is immediately recognized as the correlation of two rect functions. Thus, Equation A.20 can be evaluated by referencing Gaskill [6:page 172] and using Fourier transform analysis.

$$\int \text{rect}\left(\frac{\frac{1}{2}\Delta y + \Sigma y}{d}\right) \text{rect}\left(\frac{\Sigma y - \frac{1}{2}\Delta y}{d}\right) d\Sigma y = d \text{ tri}\left(\frac{\Delta y}{d}\right) \tag{A.23}$$

Substituting the result of Equation A.23 into Equation A.19 results in:

$$\left\langle \vec{\theta}_t \cdot \vec{\theta}_c \right\rangle = \frac{24}{k^2 d^6} \iint x_1 \text{rect}\left(\frac{x_1}{d}\right) \left[d \text{ tri}\left(\frac{\Delta y}{d}\right)\right] \left[-\frac{6.88}{2}\left(\frac{\sqrt{\left(\frac{d}{2}-x_1\right)^2+(\Delta y)^2}}{r_o}\right)^{5/3}\right.$$
$$\left. +\frac{6.88}{2}\left(\frac{\sqrt{\left(\frac{d}{2}+x_1\right)^2+(\Delta y)^2}}{r_o}\right)^{5/3}\right] dx_1 d\Delta y \qquad \text{(A.24)}$$

This double integral can be broken into two double integrals yielding:

$$\left\langle \vec{\theta}_t \cdot \vec{\theta}_c \right\rangle = \frac{24}{k^2 d^6} \left[\frac{6.88}{2r_o^{5/3}} \iint x_1 \text{tri}\left(\frac{\Delta y}{d}\right) \text{rect}\left(\frac{x_1}{d}\right) \left(\sqrt{\left(\frac{d}{2}+x_1\right)^2+(\Delta y)^2}\right)^{5/3} dx_1 d\Delta y\right.$$
$$\left. -\frac{6.88}{2r_o^{5/3}} \iint x_1 \text{tri}\left(\frac{\Delta y}{d}\right) \text{rect}\left(\frac{x_1}{d}\right) \left(\sqrt{\left(\frac{d}{2}-x_1\right)^2+(\Delta y)^2}\right)^{5/3} dx_1 d\Delta y\right] \text{(A.25)}$$

Recalling that:

$$\text{rect}\left(\frac{x_1}{d}\right) = \begin{cases} 1 & -\frac{d}{2} \le x_1 \le \frac{d}{2} \\ 0 & \text{otherwise} \end{cases} \qquad \text{(A.26)}$$

and,

$$\text{tri}\left(\frac{\Delta y}{d}\right) = \begin{cases} \frac{d-|\Delta y|}{d} & -d \le \Delta y \le d \\ 0 & \text{otherwise} \end{cases} \qquad \text{(A.27)}$$

the limits on the integrals in Equation A.25 can be set as:

$$-\frac{d}{2} \le x_1 \le \frac{d}{2} \qquad \text{and} \qquad -d \le \Delta y \le d \qquad \text{(A.28)}$$

and Equation A.25 becomes:

$$\left\langle \vec{\theta}_t \cdot \vec{\theta}_c \right\rangle = \frac{24 \cdot 6.88}{2k^2 d^5 r_o^{5/3}} \left[\int_{-d}^{d} \int_{-\frac{d}{2}}^{\frac{d}{2}} x_1 \left(\frac{d-|\Delta y|}{d}\right) \left(\left(\frac{d}{2}+x_1\right)^2+(\Delta y)^2\right)^{5/6} dx_1 d\Delta y\right.$$
$$\left. -\int_{-d}^{d} \int_{-\frac{d}{2}}^{\frac{d}{2}} x_1 \left(\frac{d-|\Delta y|}{d}\right) \left(\left(\frac{d}{2}-x_1\right)^2+(\Delta y)^2\right)^{5/6} dx_1 d\Delta y\right] \qquad \text{(A.29)}$$

Numerical techniques must be used to proceed from this point. However, Equation A.29 will first be written in terms of dimensionless quantities to facilitate the numerical integration. To do so, let:

$$\xi = \frac{x_1}{d/2} \qquad \rightarrow \qquad \mathrm{d}\xi = \frac{2}{d}\mathrm{d}x_1 \tag{A.30}$$

with limits:

$$-1 \leq \xi \leq 1 \tag{A.31}$$

And let:

$$\Delta y' = \frac{\Delta y}{d} \qquad \rightarrow \qquad \mathrm{d}\Delta y' = \frac{1}{d}\mathrm{d}\Delta y \tag{A.32}$$

with limits:

$$-1 \leq \Delta y' \leq 1 \tag{A.33}$$

Substituting Equations A.30, A.31, A.32 and A.33 into Equation A.29, produces:

$$\left\langle \vec{\theta}_t \cdot \vec{\theta}_c \right\rangle = \frac{12 \cdot 6.88}{k^2 d^5 r_o^{5/3}} \left[\int_{-1}^{1} \int_{-1}^{1} \frac{d}{2}\xi \left(\frac{d - |d\Delta y'|}{d} \right) \left(\left(\frac{d}{2} + \frac{d}{2}\xi \right)^2 + (d\Delta y')^2 \right)^{5/6} \left(\frac{d}{2}\mathrm{d}\xi \right) (d \cdot \mathrm{d}\Delta y') \right.$$
$$\left. - \int_{-1}^{1} \int_{-1}^{1} \frac{d}{2}\xi \left(\frac{d - |d\Delta y'|}{d} \right) \left(\left(\frac{d}{2} - \frac{d}{2}\xi \right)^2 + (d\Delta y')^2 \right)^{5/6} \left(\frac{d}{2} \cdot \mathrm{d}\xi \right) (d\mathrm{d}\Delta y') \right] \tag{A.34}$$

Performing algebraic simplification yields:

$$\left\langle \vec{\theta}_t \cdot \vec{\theta}_c \right\rangle = \frac{6.50119}{k^2 r_o^{5/3} d^{1/3}} \left[\int_{-1}^{1} \int_{-1}^{1} x_1' \left(1 - |\Delta y'|\right) \left((1 + x_1')^2 + (2\Delta y')^2 \right)^{5/6} \mathrm{d}x_1' \mathrm{d}\Delta y' \right.$$
$$\left. - \int_{-1}^{1} \int_{-1}^{1} x_1' \left(1 - |\Delta y'|\right) \left((1 - x_1')^2 + (2\Delta y')^2 \right)^{5/6} \mathrm{d}x_1' \mathrm{d}\Delta y' \right] \tag{A.35}$$

Using numerical integration, the difference of these two integrals is found to be 2.014. Thus the

cross-correlation for a square subaperture can then be expressed as:

$$\left\langle \vec{\theta}_t \cdot \vec{\theta}_c \right\rangle = \frac{13.0934}{k^2 r_o^{5/3} d^{1/3}} \tag{A.36}$$

A.2 Derivation of Mean Square Value of z-Tilt, $< \vec{\theta}_t^2 >$

From Equation 3.36:

$$\left\langle \vec{\theta}_t^2 \right\rangle = \left(\frac{12}{kd^4} \right)^2 \left\langle \left(\iint (x \cdot \hat{x} + y \cdot \hat{y})\, \phi(x,y) W(x,y) \mathrm{d}x\mathrm{d}y \right)^2 \right\rangle \tag{A.37}$$

Which can be written as:

$$\left\langle \vec{\theta}_t^2 \right\rangle = \frac{12^2}{k^2 d^8} \left\langle \iint (x_1 \hat{x} + y_1 \hat{y})\, \phi(x_1, y_1)\, W(x_1, y_1)\, \mathrm{d}x_1 \mathrm{d}y_1 \cdot \iint (x_2 \hat{x} + y_2 \hat{y})\, \phi(x_2, y_2)\, W(x_2, y_2)\, \mathrm{d}x_2 \mathrm{d}y_2 \right\rangle \tag{A.38}$$

Next, the dot product will be performed which will eliminate the unit vectors. Further, just as in Section A.1, the dot product will form two integrals which will be identical except for different variables. This duplicate integral can be accounted for by multiplying one of the resulting integrals by two and dropping the second. Doing this results in:

$$\left\langle \vec{\theta}_t^2 \right\rangle = \frac{2 \cdot 12^2}{k^2 d^8} \left\langle \iiii x_1 x_2 \phi(x_1, y_1)\, \phi(x_2, y_2)\, W(x_1, y_1)\, W(x_2, y_2)\, \mathrm{d}x_1 \mathrm{d}y_1 \mathrm{d}x_2 \mathrm{d}y_2 \right\rangle \tag{A.39}$$

Since ϕ is the only random process in Equation A.39, the expected value operators can be moved inside the integral yielding:

$$\left\langle \vec{\theta}_t^2 \right\rangle = \frac{2 \cdot 12^2}{k^2 d^8} \iiii x_1 x_2 \left\langle \phi(x_1, y_1)\, \phi(x_2, y_2) \right\rangle W(x_1, y_1)\, W(x_2, y_2)\, \mathrm{d}d x_1 \mathrm{d}y_1 \mathrm{d}x_2 \mathrm{d}y_2 \tag{A.40}$$

In Section A.1, Equation A.12, the correlation function, $\langle \phi(x_1, y_1)\, \phi(x_2, y_2) \rangle$, was found to be:

$$\langle \phi(x_1, y_1)\, \phi(x_2, y_2) \rangle = -\frac{6.88}{2} \left(\frac{\sqrt{(x_2 - x_1)^2 + (y_2 - y_1)^2}}{r_o} \right)^{5/3} + \Gamma_\phi(0,0) \qquad \text{(A.41)}$$

Note that if the $\Gamma_\phi(0,0)$ term is separated out from the rest of the integrals and the limits imposed by the subaperture are set, the resulting integral will be a constant multiplied by an odd function integrated over symmetric limits and hence will become zero. Thus the $\Gamma_\phi(0,0)$ term can dropped here as well. Including these substitutions and taking out the constants produces:

$$\left\langle \vec{\theta}_t^2 \right\rangle = \frac{-6.88 \cdot 12^2}{k^2 r_0^{5/3} d^8} \iiint\!\!\iint x_1 x_2 \left((x_2 - x_1)^2 + (y_2 - y_1)^2 \right)^{5/6} W(x_1, y_1)\, W(x_2, y_2)\, \mathrm{d}x_1 \mathrm{d}y_1 \mathrm{d}x_2 \mathrm{d}y_2 \qquad \text{(A.42)}$$

The subaperture function, $W(x, y)$, serves only to set the limits on the integration. Setting those limits yields:

$$\left\langle \vec{\theta}_t^2 \right\rangle = \frac{-6.88 \cdot 12^2}{k^2 r_0^{5/3} d^8} \int_{-d/2}^{d/2} \int_{-d/2}^{d/2} \int_{-d/2}^{d/2} \int_{-d/2}^{d/2} x_1 x_2 \left((x_2 - x_1)^2 + (y_2 - y_1)^2 \right)^{5/6} \mathrm{d}x_1 \mathrm{d}y_1 \mathrm{d}x_2 \mathrm{d}y_2 \qquad \text{(A.43)}$$

Equation A.43 can be written in terms of dimensionless quantities to facilitate the numerical integration. Let:

$$\begin{aligned}
\xi_1 &= \frac{x_1}{d/2} \quad \rightarrow \quad \mathrm{d}\xi_1 = \frac{d}{2}\mathrm{d}x_1 && -1 \le \xi_1 \le 1 \\
\xi_2 &= \frac{x_2}{d/2} \quad \rightarrow \quad \mathrm{d}\xi_2 = \frac{d}{2}\mathrm{d}x_2 && -1 \le \xi_2 \le 1 \\
\psi_1 &= \frac{y_1}{d/2} \quad \rightarrow \quad \mathrm{d}\psi_1 = \frac{d}{2}\mathrm{d}y_1 && -1 \le \psi_1 \le 1 \\
\psi_2 &= \frac{y_2}{d/2} \quad \rightarrow \quad \mathrm{d}\psi_2 = \frac{d}{2}\mathrm{d}y_2 && -1 \le \psi_2 \le 1
\end{aligned} \qquad \text{(A.44)}$$

Using these variable substitutions and performing some simplification yields:

$$\left\langle \vec{\theta}_t^2 \right\rangle = \frac{-6.88 \cdot 12^2}{2^6 2^{5/3} k^2 r_0^{5/3} d^{1/3}} \int_{-1}^{1}\int_{-1}^{1}\int_{-1}^{1}\int_{-1}^{1} \xi_1\xi_2 \left((\xi_2-\xi_1)^2+(\psi_2-\psi_1)^2\right)^{5/6} \mathrm{d}\xi_1\mathrm{d}\psi_1\mathrm{d}\xi_2\mathrm{d}\psi_2 \tag{A.45}$$

Using numerical integration to solve this 4-D integral results in:

$$\left\langle \vec{\theta}_t^2 \right\rangle = \frac{13.6183}{k^2 r_0^{5/3} d^{1/3}} \tag{A.46}$$

A.3 Derivation of Mean Square Value of g-Tilt, $< \vec{\theta}_c^2 >$

From Equation 3.38:

$$\left\langle \vec{\theta}_c^2 \right\rangle = \left\langle \left(\frac{1}{kd^2} \iint \nabla\phi(x,y)W(x,y)\mathrm{d}x\mathrm{d}y \right)^2 \right\rangle \tag{A.47}$$

Which becomes:

$$\left\langle \vec{\theta}_c^2 \right\rangle = \left(\frac{1}{kd^2}\right)^2 \left\langle \iint \nabla_1\phi(x_1,y_1)W(x_1,y_1)\mathrm{d}x_1\mathrm{d}y_1 \cdot \iint \nabla_2\phi(x_2,y_2)W(x_2,y_2)\mathrm{d}\mathrm{d}x_2\mathrm{d}y_2 \right\rangle \tag{A.48}$$

Welsh and Gardner [23:page 1914], have shown that:

$$\iint W(x,y)\nabla\phi(x,y)\mathrm{d}x\mathrm{d}y = -\iint \nabla W(x,y)\phi(x,y)\mathrm{d}x\mathrm{d}y \tag{A.49}$$

Therefore, Equation A.48 becomes:

$$\left\langle \vec{\theta}_c^2 \right\rangle = \frac{1}{k^2 d^4} \left\langle \iint \nabla_1 W(x_1,y_1)\phi(x_1,y_1)\mathrm{d}x_1\mathrm{d}y_1 \cdot \iint \nabla_2 W(x_2,y_2)\phi(x_2,y_2)\mathrm{d}x_2\mathrm{d}y_2 \right\rangle \tag{A.50}$$

Combining the integrals, results in:

$$\left\langle \vec{\theta}_c^2 \right\rangle = \frac{1}{k^2 d^4} \left\langle \iiiint \nabla_1 W(x_1, y_1) \cdot \nabla_2 W(x_2, y_2) \phi(x_1, y_1) \phi(x_2, y_2) \mathrm{d}x_1 \mathrm{d}y_1 \mathrm{d}x_2 \mathrm{d}y_2 \right\rangle \qquad \text{(A.51)}$$

Again, since ϕ is the only random variable, the expected value operators can be moved inside to yield:

$$\left\langle \vec{\theta}_c^2 \right\rangle = \frac{1}{k^2 d^4} \iiiint \nabla_1 W(x_1, y_1) \cdot \nabla_2 W(x_2, y_2) \left\langle \phi(x_1, y_1) \phi(x_2, y_2) \right\rangle \mathrm{d}x_1 \mathrm{d}y_1 \mathrm{d}x_2 \mathrm{d}y_2 \qquad \text{(A.52)}$$

Equation A.12 transforms the correlation function to a structure function, resulting in:

$$\left\langle \vec{\theta}_c^2 \right\rangle = \frac{1}{k^2 d^4} \iiiint \nabla_1 W(x_1, y_1) \cdot \nabla_2 W(x_2, y_2) \left(\Gamma_\phi(0,0) - \frac{6.88}{2} \left(\frac{\sqrt{(x_2 - x_1)^2 + (y_2 - y_1)^2}}{r_o} \right)^{5/3} \right) \mathrm{d}x_1 \mathrm{d}y_1 \mathrm{d}x_2 \mathrm{d}y_2 \qquad \text{(A.53)}$$

Recalling Equation A.4, which expands out $\nabla W(x, y)$, Equation A.53 can be written as:

$$\begin{aligned} \left\langle \vec{\theta}_c^2 \right\rangle = \frac{1}{k^2 d^4} \iiiint & \left(\Gamma_\phi(0,0) - \frac{6.88}{2} \left(\frac{\sqrt{(x_2 - x_1)^2 + (y_2 - y_1)^2}}{r_o} \right)^{5/3} \right) \\ & \times \left\{ \left(\left[\delta\left(x_1 + \frac{d}{2}\right) - \delta\left(x_1 - \frac{d}{2}\right) \right] \mathrm{rect}\left(\frac{y_1}{d}\right) \hat{x} + \left[\delta\left(y_1 + \frac{d}{2}\right) - \delta\left(y_1 - \frac{d}{2}\right) \right] \mathrm{rect}\left(\frac{x_1}{d}\right) \hat{y} \right) \right. \\ & \left. \cdot \left(\left[\delta\left(x_2 + \frac{d}{2}\right) - \delta\left(x_2 - \frac{d}{2}\right) \right] \mathrm{rect}\left(\frac{y_2}{d}\right) \hat{x} + \left[\delta\left(y_2 + \frac{d}{2}\right) - \delta\left(y_2 - \frac{d}{2}\right) \right] \mathrm{rect}\left(\frac{x_2}{d}\right) \hat{y} \right) \right\} \\ & \times \mathrm{d}x_1 \mathrm{d}y_1 \mathrm{d}x_2 \mathrm{d}y_2 \end{aligned} \qquad \text{(A.54)}$$

Performing the dot product yields:

$$\left\langle \vec{\theta}_c^2 \right\rangle = \frac{1}{k^2 d^4} \iiiint \left(\Gamma_\phi(0,0) - \frac{6.88}{2} \left(\frac{\sqrt{(x_2-x_1)^2+(y_2-y_1)^2}}{r_o} \right)^{5/3} \right)$$
$$\times \left\{ \left[\delta\left(x_1 + \frac{d}{2}\right) - \delta\left(x_1 - \frac{d}{2}\right) \right] \left[\delta\left(x_2 + \frac{d}{2}\right) - \delta\left(x_2 - \frac{d}{2}\right) \right] \text{rect}\left(\frac{y_1}{d}\right) \text{rect}\left(\frac{y_2}{d}\right) \right.$$
$$\left. + \left[\delta\left(y_1 + \frac{d}{2}\right) - \delta\left(y_1 - \frac{d}{2}\right) \right] \left[\delta\left(y_2 + \frac{d}{2}\right) - \delta\left(y_2 - \frac{d}{2}\right) \right] \text{rect}\left(\frac{x_1}{d}\right) \text{rect}\left(\frac{x_2}{d}\right) \right\}$$
$$\times dx_1 dy_1 dx_2 dy_2 \qquad \text{(A.55)}$$

Examination of Equation A.55 reveals that it can be split into two 4-D integrals differing only by what is an x in one delta or rect function is a y in the other. Thus, as before, the second integral can be dropped and accounted for by multiply the remaining integral by two, yielding:

$$\left\langle \vec{\theta}_c^2 \right\rangle = \frac{2}{k^2 d^4} \iiiint \left(\Gamma_\phi(0,0) - \frac{6.88}{2} \left(\frac{\sqrt{(x_2-x_1)^2+(y_2-y_1)^2}}{r_o} \right)^{5/3} \right)$$
$$\times \left\{ \left[\delta\left(x_1 + \frac{d}{2}\right) - \delta\left(x_1 - \frac{d}{2}\right) \right] \left[\delta\left(x_2 + \frac{d}{2}\right) - \delta\left(x_2 - \frac{d}{2}\right) \right] \text{rect}\left(\frac{y_1}{d}\right) \text{rect}\left(\frac{y_2}{d}\right) \right\}$$
$$\times dx_1 dy_1 dx_2 dy_2 \qquad \text{(A.56)}$$

Multiplying out the delta functions will result in:

$$\left\langle \vec{\theta}_c^2 \right\rangle = \frac{2}{k^2 d^4} \iiiint \text{rect}\left(\frac{y_1}{d}\right) \text{rect}\left(\frac{y_2}{d}\right) \left(\Gamma_\phi(0,0) - \frac{6.88}{2} \left(\frac{\sqrt{(x_2-x_1)^2+(y_2-y_1)^2}}{r_o} \right)^{5/3} \right)$$
$$\times \left[\delta\left(x_1 + \frac{d}{2}\right) \delta\left(x_2 + \frac{d}{2}\right) - \delta\left(x_1 + \frac{d}{2}\right) \delta\left(x_2 - \frac{d}{2}\right) \right.$$
$$\left. - \delta\left(x_1 - \frac{d}{2}\right) \delta\left(x_2 + \frac{d}{2}\right) + \delta\left(x_1 - \frac{d}{2}\right) \delta\left(x_2 - \frac{d}{2}\right) \right] dx_1 dy_1 dx_2 dy_2 \qquad \text{(A.57)}$$

To make the next few steps easier to visualize, Equation A.57 can be written as:

$$\left\langle \vec{\theta}_c^2 \right\rangle = \left(\frac{2}{k^2 d^4}\right)\Bigg\{ \iiiint \operatorname{rect}\left(\frac{y_1}{d}\right)\operatorname{rect}\left(\frac{y_2}{d}\right)\left[\Gamma_\phi(0,0) - \frac{6.88}{2}\left(\frac{\sqrt{(x_2-x_1)^2+(y_2-y_1)^2}}{r_o}\right)^{5/3}\right]$$
$$\times\delta\left(x_1+\frac{d}{2}\right)\delta\left(x_2+\frac{d}{2}\right)\mathrm{d}x_1\mathrm{d}y_1\mathrm{d}x_2\mathrm{d}y_2$$
$$-\iiiint \operatorname{rect}\left(\frac{y_1}{d}\right)\operatorname{rect}\left(\frac{y_2}{d}\right)\left[\Gamma_\phi(0,0) - \frac{6.88}{2}\left(\frac{\sqrt{(x_2-x_1)^2+(y_2-y_1)^2}}{r_o}\right)^{5/3}\right]$$
$$\times\delta\left(x_1+\frac{d}{2}\right)\delta\left(x_2-\frac{d}{2}\right)\mathrm{d}x_1\mathrm{d}y_1\mathrm{d}x_2\mathrm{d}y_2$$
$$-\iiiint \operatorname{rect}\left(\frac{y_1}{d}\right)\operatorname{rect}\left(\frac{y_2}{d}\right)\left[\Gamma_\phi(0,0) - \frac{6.88}{2}\left(\frac{\sqrt{(x_2-x_1)^2+(y_2-y_1)^2}}{r_o}\right)^{5/3}\right]$$
$$\times\delta\left(x_1-\frac{d}{2}\right)\delta\left(x_2+\frac{d}{2}\right)\mathrm{d}x_1\mathrm{d}y_1\mathrm{d}x_2\mathrm{d}y_2$$
$$+\iiiint \operatorname{rect}\left(\frac{y_1}{d}\right)\operatorname{rect}\left(\frac{y_2}{d}\right)\left[\Gamma_\phi(0,0) - \frac{6.88}{2}\left(\frac{\sqrt{(x_2-x_1)^2+(y_2-y_1)^2}}{r_o}\right)^{5/3}\right]$$
$$\times\delta\left(x_1-\frac{d}{2}\right)\delta\left(x_2-\frac{d}{2}\right)\mathrm{d}x_1\mathrm{d}y_1\mathrm{d}x_2\mathrm{d}y_2\Bigg\} \tag{A.58}$$

It can be observed that if the integrals were further split to separate the Γ functions, all integrals with Γ_ϕ functions would subtract out. Hence, we can drop those terms. Now using the sifting property of delta functions to integrate over x_1 and x_2 and recalling Equation A.15, we get:

$$\left\langle \vec{\theta}_c^2 \right\rangle = \left(\frac{-6.88}{k^2 r_o^{5/3} d^4}\right)\Bigg\{ \iint \operatorname{rect}\left(\frac{y_1}{d}\right)\operatorname{rect}\left(\frac{y_2}{d}\right)\left(\left(-\frac{d}{2}-\left(-\frac{d}{2}\right)\right)^2+(y_2-y_1)^2\right)^{5/6}\mathrm{d}y_1\mathrm{d}y_2$$
$$-\iint \operatorname{rect}\left(\frac{y_1}{d}\right)\operatorname{rect}\left(\frac{y_2}{d}\right)\left(\left(\frac{d}{2}-\left(-\frac{d}{2}\right)\right)^2+(y_2-y_1)^2\right)^{5/6}\mathrm{d}y_1\mathrm{d}y_2$$
$$-\iint \operatorname{rect}\left(\frac{y_1}{d}\right)\operatorname{rect}\left(\frac{y_2}{d}\right)\left(\left(-\frac{d}{2}-\frac{d}{2}\right)^2+(y_2-y_1)^2\right)^{5/6}\mathrm{d}y_1\mathrm{d}y_2$$
$$+\iint \operatorname{rect}\left(\frac{y_1}{d}\right)\operatorname{rect}\left(\frac{y_2}{d}\right)\left(\left(\frac{d}{2}-\frac{d}{2}\right)^2+(y_2-y_1)^2\right)^{5/6}\mathrm{d}y_1\mathrm{d}y_2\Bigg\} \tag{A.59}$$

Note that in integral pairs 1 and 4, the $\frac{d}{2}$ terms cancel out, where as in integral pairs 2 and 3, the $\frac{d}{2}$ terms add to form d. Thus integral pairs 1 and 4; and 2 and 3 are identical. Once again, the

duplicate integral pairs will be deleted and the remaining integrals will be multiplied by two to account for them. Further, the rect functions serve only to set limits on the integration:

$$\left\langle \vec{\theta}_c^2 \right\rangle = \left(\frac{-6.88 \cdot 2}{k^2 r_o^{5/3} d^4} \right) \int_{-d/2}^{d/2} \int_{-d/2}^{d/2} \left[\left((y_2 - y_1)^2 \right)^{5/6} - \left(d^2 + (y_2 - y_1)^2 \right)^{5/6} \right] \mathrm{d}y_1 \mathrm{d}y_2 \qquad \text{(A.60)}$$

Equation A.60 can be written in terms of dimensionless quantities with the following variable changes:

$$\begin{aligned} \psi_1 = \frac{y_1}{d/2} \quad &\rightarrow \quad \mathrm{d}y_1 = \frac{d}{2}\mathrm{d}\psi_1 \qquad -1 \le \psi_1 \le 1 \\ \psi_2 = \frac{y_2}{d/2} \quad &\rightarrow \quad \mathrm{d}y_2 = \frac{d}{2}\mathrm{d}\psi_2 \qquad -1 \le \psi_2 \le 1 \end{aligned} \qquad \text{(A.61)}$$

which after simplification yields:

$$\left\langle \vec{\theta}_c^2 \right\rangle = \left(\frac{6.88}{2 \cdot 2^{5/3} k^2 r_o^{5/3} d^{1/3}} \right) \left[\int_{-1}^{1} \int_{-1}^{1} \left(4 + (\psi_2 - \psi_1)^2 \right)^{5/6} - |\psi_2 - \psi_1|^{5/3} \, \mathrm{d}\psi_1 \mathrm{d}\psi_2 \right] \qquad \text{(A.62)}$$

Using numerical integration to solve this 2-D integral results in:

$$\left\langle \vec{\theta}_c^2 \right\rangle = \frac{12.803}{k^2 r_0^{5/3} d^{1/3}} \qquad \text{(A.63)}$$

Appendix B. *Derivation Details for Shearing Interferometer*

This appendix provides details of the derivations for the Shearing Interferometer.

B.1 Derivation of Count Vector, $K(n)$

From Equation 2.29:

$$K(n) = 2I\alpha \iiint \left[1 + \mathcal{V}\cos\left(\frac{2\pi t}{T} + \Delta\phi(x, y, \Delta x)\right)\right] W_s(x, y) W_t(t) \mathrm{d}t\mathrm{d}x\mathrm{d}y \tag{B.1}$$

which can be separated to obtain:

$$K(n) = 2I\alpha \left[\iiint W_s(x, y) W_t(t) \mathrm{d}t\mathrm{d}x\mathrm{d}y + \mathcal{V} \iiint \cos\left(\frac{2\pi t}{T} + \Delta\phi(x, y, \Delta x)\right) W_s(x, y) W_t(t) \mathrm{d}t\mathrm{d}x\mathrm{d}y\right] \tag{B.2}$$

The first triple integral is trivial and simplifies to:

$$K(n) = 2I\alpha \left[A\tau + \mathcal{V} \iiint \cos\left(\frac{2\pi t}{T} + \Delta\phi(x, y, \Delta x)\right) W_s(x, y) W_t(t) \mathrm{d}t\mathrm{d}x\mathrm{d}y\right] \tag{B.3}$$

where $A = d^2$ has been defined as the area of the detector element. Now, using the relationships:

$$\cos\alpha = \frac{e^{j\alpha} + e^{-j\alpha}}{2} \qquad \text{and} \qquad e^{(a+b)} = e^a e^b \tag{B.4}$$

Equation B.3 becomes:

$$K(n) = 2I\alpha \left[A\tau + \frac{\mathcal{V}}{2} \iiint \left(e^{j\frac{2\pi t}{T}} e^{j\Delta\phi(x,y,\Delta x)} + e^{-j\frac{2\pi t}{T}} e^{-j\Delta\phi(x,y,\Delta x)}\right) W_s(x, y) W_t(t) \mathrm{d}t\mathrm{d}x\mathrm{d}y\right] \tag{B.5}$$

which becomes:

$$K(n) = 2I\alpha\Big[A\tau + \frac{\nu}{2}\int e^{\jmath\frac{2\pi t}{T}}W_t(t)\mathrm{d}t \iint e^{\jmath\Delta\phi(x,y,\Delta x)}W_s(x,y)\mathrm{d}x\mathrm{d}y + \frac{\nu}{2}\int e^{-\jmath\frac{2\pi t}{T}}W_t(t)\mathrm{d}t \iint e^{-\jmath\Delta\phi(x,y,\Delta x)}W_s(x,y)\mathrm{d}x\mathrm{d}y\Big] \tag{B.6}$$

For a moment, just look at the term:

$$\iint e^{\jmath\Delta\phi(x,y,\Delta x)}W_s(x,y)\mathrm{d}x\mathrm{d}y \tag{B.7}$$

which represents the component of the measurement proportional to the change in wavefront phase. Assuming that Δx, the shear, will be adjusted such that $\Delta\phi(x,y,\Delta x) \ll 2\pi$, which will be required for accuracy, then the approximation,

$$e^{\jmath x} \approx 1 + \jmath x \qquad \text{for small } x \tag{B.8}$$

can be used and Equation B.7 becomes:

$$\iint W_s(x,y)\mathrm{d}x\mathrm{d}y + \jmath\iint \Delta\phi(x,y,\Delta x)W_s(x,y)\mathrm{d}x\mathrm{d}y \tag{B.9}$$

Defining:

$$A\overline{\Delta\phi}(\Delta x) = \iint \Delta\phi(x,y,\Delta x)W_s(x,y)\mathrm{d}x\mathrm{d}y \tag{B.10}$$

and using the definition in Equation B.10, Equation B.9 becomes:

$$A - \jmath A\overline{\Delta\phi}(\Delta x) = A\left(1 + \jmath\overline{\Delta\phi}(\Delta x)\right) \tag{B.11}$$

And using Equation B.8 in reverse, Equation B.7 becomes:

$$\iint e^{j\Delta\phi(x,y,\Delta x)} W_s(x,y)\mathrm{d}x\mathrm{d}y = Ae^{j\overline{\Delta\phi}(\Delta x)} \tag{B.12}$$

Substituting Equation B.12 into Equation B.6 the count vector becomes:

$$\overline{K}(n) = 2I\alpha\left[A\tau + A\frac{\mathcal{V}}{2}\int e^{j\overline{\Delta\phi}(\Delta x)}e^{j\frac{2\pi t}{T}}W_t(t)\mathrm{d}t + A\frac{\mathcal{V}}{2}\int e^{-j\overline{\Delta\phi}(\Delta x)}e^{-j\frac{2\pi t}{T}}W_t(t)\mathrm{d}t\right] \tag{B.13}$$

which can be recombined to form:

$$\overline{K}(n) = 2I\alpha A\left[\tau + \mathcal{V}\int \cos\left(\frac{2\pi t}{T} + \overline{\Delta\phi}(\Delta x)\right)W_t(t)\mathrm{d}t\right] \tag{B.14}$$

Recalling Equation 2.28, the limits in the integral can be set as:

$$\overline{K}(n) = 2I\alpha A\left[\tau + \mathcal{V}\int_{\tau n-\frac{\tau}{2}}^{\tau n-\frac{\tau}{2}} \cos\left(\frac{2\pi t}{T} + \overline{\Delta\phi}(\Delta x)\right)\mathrm{d}t\right] \tag{B.15}$$

Performing the integration results in:

$$\overline{K}(n) = 2I\alpha A\left[\tau + \frac{\mathcal{V}T}{2\pi}\left[\sin\left(\frac{2\pi\tau n}{T} + \frac{\pi\tau}{T} + \overline{\Delta\phi}(\Delta x)\right) - \sin\left(\frac{2\pi\tau n}{T} - \frac{\pi\tau}{T} + \overline{\Delta\phi}(\Delta x)\right)\right]\right] \tag{B.16}$$

Using the relationship:

$$\sin\alpha - \sin\beta = 2\cos\frac{1}{2}(\alpha+\beta)\sin\frac{1}{2}(\alpha-\beta) \tag{B.17}$$

Equation B.16 simplifies to:

$$\overline{K}(n) = 2I\alpha A\left[\tau + \frac{\mathcal{V}T}{\pi}\sin\left(\frac{\pi\tau}{T}\right)\cos\left(\frac{2\pi\tau n}{T} + \overline{\Delta\phi}(\Delta x)\right)\right] \tag{B.18}$$

Assuming that the sampling rate is such that:

$$\frac{\pi\tau}{T} \ll 1 \qquad \rightarrow \qquad \tau \ll \frac{T}{\pi} \tag{B.19}$$

(note that Nyquist criteria requires $\tau < T/2$) then the small angle approximation can be used for sine:

$$\sin(x) \approx x \qquad \text{for } x \ll 1 \tag{B.20}$$

and Equation B.18 simplifies further to:

$$\overline{K}(n) = 2I\alpha A\left[\tau + \mathcal{V}\tau\cos\left(\frac{2\pi\tau n}{T} + \overline{\Delta\phi}(\Delta x)\right)\right] \tag{B.21}$$

By using the relationship:

$$\tau \cdot N = p_o \cdot T \tag{B.22}$$

where τ is the integration time, N is the number of samples in the count vector, $K(n)$, i.e. $0 \leq n \leq N-1$, p_o is the number of fringes embraced by the count vector and T is the period of the fringe. Then Equation B.21 can be written as:

$$\overline{K}(n) = 2I\alpha\tau A\left[1 + \mathcal{V}\cos\left(\frac{2\pi p_o n}{N} + 2\overline{\Delta\phi}(\Delta x)\right)\right] \tag{B.23}$$

B.2 Mean Square Value of $< \vec{\theta}_s^2 >$

Using Equations 2.41 and 2.46, the mean square value of *s*-tilt can be expressed as:

$$\left\langle \vec{\theta}_s^2 \right\rangle = \left\langle \left(\frac{1}{kd}\right)^2 \left(\hat{x}\iint \frac{\Delta\phi(x,y,\Delta x)}{\Delta x} W(x,y)\mathrm{d}x\mathrm{d}y + \hat{y}\iint \frac{\Delta\phi(x,y,\Delta x)}{\Delta y} W(x,y)\mathrm{d}x\mathrm{d}y\right)^2 \right\rangle \tag{B.24}$$

Which simplifies to yield:

$$\left\langle \vec{\theta}_s^2 \right\rangle = \left\langle \frac{1}{kd^2\Delta x} \iint \Delta\phi(x,y,\Delta x)W(x,y)\mathrm{d}x\mathrm{d}y \cdot \frac{1}{kd^2\Delta x} \iint \Delta\phi(x,y,\Delta x)W(x,y)\mathrm{d}x\mathrm{d}y \right.$$
$$\left. + \frac{1}{kd^2\Delta y} \iint \Delta\phi(x,y,\Delta y)W(x,y)\mathrm{d}x\mathrm{d}y \cdot \frac{1}{kd^2\Delta y} \iint \Delta\phi(x,y,\Delta y)W(x,y)\mathrm{d}x\mathrm{d}y \right\rangle \quad \text{(B.25)}$$

Examination of Equation B.25 reveals that the two added terms are essentially the same. Therefore, the second term can be dropped and accounted for by multiplying the first by two. Doing this and combining the four resulting integrals yields:

$$\left\langle \vec{\theta}_s^2 \right\rangle = \left\langle \frac{2}{k^2d^4\Delta x^2} \iiii \Delta\phi(x_1,y_1,\Delta x)\Delta\phi(x_2,y_2,\Delta x)W(x_1,y_1)W(x_2,y_2)\mathrm{d}x_1\mathrm{d}y_1\mathrm{d}x_2\mathrm{d}y_2 \right\rangle \quad \text{(B.26)}$$

Since $W(x,y)$ is deterministic, $\Delta\phi$ is the only random term. Hence, the expected value operator can be moved inside the integrals to yield:

$$\left\langle \vec{\theta}_s^2 \right\rangle = \frac{2}{k^2d^4\Delta x^2} \iiii \left\langle \Delta\phi(x_1,y_1,\Delta x)\Delta\phi(x_2,y_2,\Delta x) \right\rangle W(x_1,y_1)W(x_2,y_2)\mathrm{d}x_1\mathrm{d}y_1\mathrm{d}x_2\mathrm{d}y_2 \quad \text{(B.27)}$$

An expression for $\langle \Delta\phi(x_1,y_1,\Delta x)\Delta\phi(x_2,y_2,\Delta x) \rangle$ is therefore needed. Recalling the definition for $\Delta\phi$:

$$\Delta\phi(x,y,\Delta x) = \phi(x - \frac{\Delta x}{2}, y) - \phi(x + \frac{\Delta x}{2}, y) \quad \text{(B.28)}$$

The correlation function becomes:

$$\langle \Delta\phi(x_1,y_1,\Delta x)\Delta\phi(x_2,y_2,\Delta x) \rangle = \left\langle \left[\phi(x_1 - \frac{\Delta x}{2}, y_1) - \phi(x_1 + \frac{\Delta x}{2}, y_1) \right] \right.$$
$$\left. \cdot \left[\phi(x_2 - \frac{\Delta x}{2}, y_2) - \phi(x_2 + \frac{\Delta x}{2}, y_2) \right] \right\rangle \quad \text{(B.29)}$$

which can be expanded to be:

$$\begin{aligned}\langle \Delta\phi(x_1,y_1,\Delta x)\Delta\phi(x_2,y_2,\Delta x)\rangle = \Big\langle & \phi\left(x_1-\frac{\Delta x}{2},y_1\right)\phi\left(x_2-\frac{\Delta x}{2},y_2\right) \\ & -\phi\left(x_1-\frac{\Delta x}{2},y_1\right)\phi\left(x_2+\frac{\Delta x}{2},y_2\right) \\ & -\phi\left(x_1+\frac{\Delta x}{2},y_1\right)\phi\left(x_2-\frac{\Delta x}{2},y_2\right) \\ & +\phi\left(x_1+\frac{\Delta x}{2},y_1\right)\phi\left(x_2+\frac{\Delta x}{2},y_2\right)\Big\rangle \end{aligned} \qquad \text{(B.30)}$$

An expression for these correlation functions was found in Chapter III, Equation 3.32, to be:

$$\langle \phi(x_1,y_1)\phi(x_2,y_2)\rangle = -\frac{6.88}{2}\left(\frac{\sqrt{(x_2-x_1)^2+(y_2-y_1)^2}}{r_o}\right)^{5/3} + \Gamma_\phi(0,0) \qquad \text{(B.31)}$$

Therefore, by substitution of Equation B.31 and pulling out the constants, Equation B.30 becomes:

$$\begin{aligned}\langle \Delta\phi(x_1,y_1,\Delta x)\Delta\phi(x_2,y_2,\Delta x)\rangle = \frac{6.88}{2r_o^{5/3}}\Bigg[& \sqrt{\left(x_2+\frac{\Delta x}{2}-x_1+\frac{\Delta x}{2}\right)^2+(y_2-y_1)^2}^{\frac{5}{3}} \\ & +\sqrt{\left(x_2-\frac{\Delta x}{2}-x_1-\frac{\Delta x}{2}\right)^2+(y_2-y_1)^2}^{\frac{5}{3}} \\ & -\sqrt{\left(x_2-\frac{\Delta x}{2}-x_1+\frac{\Delta x}{2}\right)^2+(y_2-y_1)^2}^{\frac{5}{3}} \\ & -\sqrt{\left(x_2+\frac{\Delta x}{2}-x_1-\frac{\Delta x}{2}\right)^2+(y_2-y_1)^2}^{\frac{5}{3}}\Bigg] \end{aligned} \qquad \text{(B.32)}$$

Substituting Equation B.32 into Equation B.27, after some algebraic simplification, yields:

$$\begin{aligned}\left\langle \tilde{\theta}_s^2 \right\rangle = \frac{2}{k^2d^4\Delta x^2}\cdot\frac{6.88}{2r_o^{5/3}}\iiint\Bigg[& \sqrt{(x_2-x_1+\Delta x)^2+(y_2-y_1)^2}^{\frac{5}{3}}+\sqrt{(x_2-x_1-\Delta x)^2+(y_2-y_1)^2}^{\frac{5}{3}} \\ & -2\sqrt{(x_2-x_1)^2+(y_2-y_1)^2}^{\frac{5}{3}}\Bigg] W(x_1,y_1)W(x_2,y_2)\mathrm{d}x_1\mathrm{d}y_1\mathrm{d}x_2\mathrm{d}y_2 \end{aligned} \qquad \text{(B.33)}$$

Recalling Equation 2.42, the aperture function, Equation B.33 becomes:

$$\left\langle \vec{\theta}_s^2 \right\rangle = \frac{6.88}{k^2 d^4 \Delta x^2 r_o^{5/3}} \iiint \left[\sqrt{(x_2 - x_1 + \Delta x)^2 + (y_2 - y_1)^2}^{\frac{5}{3}} + \sqrt{(x_2 - x_1 - \Delta x)^2 + (y_2 - y_1)^2}^{\frac{5}{3}} \right.$$
$$\left. -2\sqrt{(x_2 - x_1)^2 + (y_2 - y_1)^2}^{\frac{5}{3}} \right]$$
$$\times \text{rect}\left(\frac{x_1}{d}\right) \text{rect}\left(\frac{x_2}{d}\right) \text{rect}\left(\frac{y_1}{d}\right) \text{rect}\left(\frac{y_2}{d}\right) dx_1 dy_1 dx_2 dy_2 \qquad \text{(B.34)}$$

Equation B.34 can be written in dimensionless form by making the following substitutions:

$$\begin{aligned} \xi_i &= \frac{x_i}{d/2} \quad \rightarrow \quad dx_i = \frac{d}{2} d\xi_i, \\ \psi_i &= \frac{y_i}{d/2} \quad \rightarrow \quad dy_i = \frac{d}{2} d\psi_i \quad \text{and} \\ s &= \frac{\Delta x}{r_o} \end{aligned} \qquad \text{(B.35)}$$

After some simplification, Equation B.34 then becomes

$$\left\langle \vec{\theta}_s^2 \right\rangle = \frac{6.88}{2^4 2^{5/3} k^2 d^{1/3} r_o^{5/3}} \left(\frac{d/r_o}{s}\right)^2$$
$$\times \iiint \left[\sqrt{\left(\xi_2 - \xi_1 + 2\frac{s}{d/r_o}\right)^2 + (\psi_2 - \psi_1)^2}^{\frac{5}{3}} + \sqrt{\left(\xi_2 - \xi_1 - 2\frac{s}{d/r_o}\right)^2 + (\psi_2 - \psi_1)^2}^{\frac{5}{3}} \right.$$
$$\left. -2\sqrt{(\xi_2 - \xi_1)^2 + (\psi_2 - \psi_1)^2}^{\frac{5}{3}} \right] \text{rect}\left(\frac{\xi_1}{2}\right) \text{rect}\left(\frac{\xi_2}{2}\right) \text{rect}\left(\frac{\psi_1}{2}\right) \text{rect}\left(\frac{\psi_2}{2}\right)$$
$$\times d\xi_1 d\psi_1 d\xi_2 d\psi_2 \qquad \text{(B.36)}$$

Note that all the terms inside the integrals are dimensionless, which allows solving Equation B.36 to simply be an exercise in calculus. Therefore, the following variable substitution will be defined:

$$\begin{aligned} \Delta\xi = \xi_2 - \xi_1 \text{ and } \Sigma\xi = \frac{\xi_2 + \xi_1}{2} \quad &\rightarrow \quad \xi_1 = \Sigma\xi - \frac{1}{2}\Delta\xi \text{ and } \xi_2 = \Sigma\xi + \frac{1}{2}\Delta\xi \\ \Delta\psi = \psi_2 - \psi_1 \text{ and } \Sigma\psi = \frac{\psi_2 + \psi_1}{2} \quad &\rightarrow \quad \psi_1 = \Sigma\psi - \frac{1}{2}\Delta\psi \text{ and } \psi_2 = \Sigma\psi + \frac{1}{2}\Delta\psi \end{aligned} \qquad \text{(B.37)}$$

This choice allows the Jacobian to be one. Equation B.36 then becomes:

$$\left\langle \vec{\theta}_s^2 \right\rangle = \frac{6.88}{2^4 2^{5/3} k^2 d^{1/3} r_o^{5/3}} \left(\frac{d/r_o}{s}\right)^2 \times \iint \left[\left| \left(\Delta\xi + 2\frac{s}{d/r_o}\right)^2 + \Delta\psi^2 \right|^{\frac{5}{6}} + \left| \left(\Delta\xi - 2\frac{s}{d/r_o}\right)^2 + \Delta\psi^2 \right|^{\frac{5}{6}} - 2\left|\Delta\xi^2 + \Delta\psi^2\right|^{\frac{5}{6}} \right] \times \text{rect}\left(\frac{\Sigma\xi - \frac{1}{2}\Delta\xi}{2}\right) \text{rect}\left(\frac{\Sigma\xi + \frac{1}{2}\Delta\xi}{2}\right) \text{rect}\left(\frac{\Sigma\psi - \frac{1}{2}\Delta\psi}{2}\right) \text{rect}\left(\frac{\Sigma\psi + \frac{1}{2}\Delta\psi}{2}\right) \times d\Delta\xi d\Delta\psi d\Sigma\xi d\Sigma\psi \tag{B.38}$$

Note that all terms that depend on $\Sigma\psi$ can be separate out. So, just for a moment, we can look only at the integral:

$$\int \text{rect}\left(\frac{\Sigma\psi - \frac{1}{2}\Delta\psi}{2}\right) \text{rect}\left(\frac{\Sigma\psi + \frac{1}{2}\Delta\psi}{2}\right) d\Sigma\psi \tag{B.39}$$

which is identical to Equation A.20 in Appendix A.1. Thus, from Equation A.23, this simply becomes:

$$\int \text{rect}\left(\frac{\Sigma\psi - \frac{1}{2}\Delta\psi}{2}\right) \text{rect}\left(\frac{\Sigma\psi + \frac{1}{2}\Delta\psi}{2}\right) d\Sigma\psi = 2\text{tri}\left(\frac{\Delta\psi}{2}\right) \tag{B.40}$$

Similarly, all terms that depend on $\Sigma\xi$ can be separated from Equation B.38 to yield:

$$\int \text{rect}\left(\frac{\Sigma\xi - \frac{1}{2}\Delta\xi}{2}\right) \text{rect}\left(\frac{\Sigma\xi + \frac{1}{2}\Delta\xi}{2}\right) d\Sigma\xi = 2\text{tri}\left(\frac{\Delta\xi}{2}\right) \tag{B.41}$$

Substituting Equations B.40 and B.41 back into Equation B.38 yields:

$$\left\langle \vec{\theta}_s^2 \right\rangle = \frac{6.88}{2^2 2^{5/3} k^2 d^{1/3} r_o^{5/3}} \left(\frac{d/r_o}{s}\right)^2 \times \iint \left[\left| \left(\Delta\xi + 2\frac{s}{d/r_o}\right)^2 + \Delta\psi^2 \right|^{\frac{5}{6}} + \left| \left(\Delta\xi - 2\frac{s}{d/r_o}\right)^2 + \Delta\psi^2 \right|^{\frac{5}{6}} - 2\left|\Delta\xi^2 + \Delta\psi^2\right|^{\frac{5}{6}} \right] \times \left[\text{tri}\left(\frac{\Delta\psi}{2}\right)\right] \left[\text{tri}\left(\frac{\Delta\xi}{2}\right)\right] d\Delta\xi d\Delta\psi \tag{B.42}$$

Recalling the definition of the tri function, Equation A.27, setting the limits on the integration and performing some minor algebraic simplification, Equation B.42 becomes:

$$\left\langle \vec{\theta}_s^2 \right\rangle = \frac{6.88}{2^4 2^{5/3} k^2 d^{1/3} r_o^{5/3}} \left(\frac{d/r_o}{s}\right)^2 \int_{-2}^{2}\int_{-2}^{2} (2-|\Delta\xi|)(2-|\Delta\psi|) \left[\left|\left(\Delta\xi + 2\frac{s}{d/r_o}\right)^2 + \Delta\psi^2\right|^{\frac{5}{6}} + \left|\left(\Delta\xi - 2\frac{s}{d/r_o}\right)^2 + \Delta\psi^2\right|^{\frac{5}{6}} - 2\left|\Delta\xi^2 + \Delta\psi^2\right|^{\frac{5}{6}}\right] d\Delta\xi d\Delta\psi \quad \text{(B.43)}$$

Which could be written as:

$$\left\langle \vec{\theta}_s^2 \right\rangle = \frac{0.13544 f_v\left(s\frac{r_o}{d}\right)}{k^2 d^{1/3} r_o^{5/3}} \quad \text{(B.44)}$$

where $f_v\left(s\frac{r_o}{d}\right)$ is defined to be:

$$f_v(x) \equiv (x)^{-2} \int_{-2}^{2}\int_{-2}^{2} (2-|\Delta\xi|)(2-|\Delta\psi|) \left[\left|((\Delta\xi + 2x)^2 + \Delta\psi^2\right|^{\frac{5}{6}} + \left|((\Delta\xi - 2x)^2 + \Delta\psi^2\right|^{\frac{5}{6}} - 2\left|(\Delta\xi^2 + \Delta\psi^2\right|^{\frac{5}{6}}\right] d\Delta\xi d\Delta\psi \quad \text{(B.45)}$$

B.3 Derivation of Cross-Correlation of z-tilt and s-tilt, $\left\langle \vec{\theta}_t \cdot \vec{\theta}_s \right\rangle$

From Equation 4.23

$$\left\langle \vec{\theta}_t \cdot \vec{\theta}_s \right\rangle = \left\langle \left[\hat{x}\frac{\int x\phi(x,y)W(x,y)dxdy}{\frac{kd^4}{12}} + \hat{y}\frac{\int y\phi(x,y)W(x,y)dxdy}{\frac{kd^4}{12}}\right] \cdot \left[\hat{x}\frac{\int \Delta\phi(x,y,\Delta x)W(x,y)dxdy}{\Delta x k d^2} + \hat{y}\frac{\int \Delta\phi(x,y,\Delta y)W(x,y)dxdy}{\Delta y k d^2}\right] \right\rangle \quad \text{(B.46)}$$

Performing the dot product yields:

$$\left\langle \vec{\theta}_t \cdot \vec{\theta}_s \right\rangle = \left\langle \left(\frac{1}{\Delta x k d^2}\iint \Delta\phi(x,y,\Delta x)W(x,y)dxdy\right) \cdot \left(\frac{12}{kd^4}\iint x\phi(x,y)W(x,y)dxdy\right) + \left(\frac{1}{\Delta y k d^2}\iint \Delta\phi(x,y,\Delta y)W(x,y)dxdy\right) \cdot \left(\frac{12}{kd^4}\iint y\phi(x,y)W(x,y)dxdy\right)\right\rangle \quad \text{(B.47)}$$

Again, the first two integral pairs are essentially identical to the second two pairs. Hence, the second two integral pairs can be dropped and accounted for by multiplying the first two integral pairs by two. Combining the remaining integrals and pulling out the constants yields:

$$\left\langle \vec{\theta}_t \cdot \vec{\theta}_s \right\rangle = \left\langle \frac{2 \cdot 12}{\Delta x k^2 d^6} \iiint x_2 \Delta\phi(x_1, y_1, \Delta x)\phi(x_2, y_2) W(x_1, y_1) W(x_2, y_2) \mathrm{d}x_1 \mathrm{d}x_2 \mathrm{d}y_1 \mathrm{d}y_2 \right\rangle \quad \text{(B.48)}$$

Since ϕ and $\Delta\phi$ are the only random terms, the expected value operators can be moved inside the integrals to yield:

$$\left\langle \vec{\theta}_t \cdot \vec{\theta}_s \right\rangle = \frac{24}{\Delta x k^2 d^6} \iiint x_2 \left\langle \Delta\phi(x_1, y_1, \Delta x)\phi(x_2, y_2) \right\rangle W(x_1, y_1) W(x_2, y_2) \mathrm{d}x_1 \mathrm{d}x_2 \mathrm{d}y_1 \mathrm{d}y_2 \quad \text{(B.49)}$$

Therefore, an expression for $\langle \Delta\phi(x_1, y_1, \Delta x)\phi(x_2, y_2) \rangle$ is needed. Again recalling Equation 2.13, this correlation function can be written as:

$$\langle \Delta\phi(x_1, y_1, \Delta x)\phi(x_2, y_2) \rangle = \left\langle \phi\left(x_1 - \frac{\Delta x}{2}, y_1\right) \phi(x_2, y_2) - \phi\left(x_1 + \frac{\Delta x}{2}, y_1\right) \phi(x_2, y_2) \right\rangle \quad \text{(B.50)}$$

After using Equation 3.32, this simplifies to:

$$\langle \Delta\phi(x_1, y_1, \Delta x)\phi(x_2, y_2) \rangle = \frac{6.88}{2 r_o^{5/3}} \left[\sqrt{\left(x_2 - x_1 + \frac{\Delta x}{2}\right)^2 + (y_2 - y_1)^2}^{\frac{5}{3}} - \sqrt{\left(x_2 - x_1 - \frac{\Delta x}{2}\right)^2 + (y_2 - y_1)^2}^{\frac{5}{3}} \right] \quad \text{(B.51)}$$

Substituting Equation B.51 into Equation B.49 yields:

$$\left\langle \vec{\theta}_t \cdot \vec{\theta}_s \right\rangle = \frac{24}{\Delta x k^2 d^6} \cdot \frac{6.88}{2 r_o^{5/3}} \iiint x_2 W(x_1, y_1) W(x_2, y_2) \left(\sqrt{\left(x_2 - x_1 + \frac{\Delta x}{2}\right)^2 + (y_2 - y_1)^2}^{\frac{5}{3}} - \sqrt{\left(x_2 - x_1 - \frac{\Delta x}{2}\right)^2 + (y_2 - y_1)^2}^{\frac{5}{3}} \right) \mathrm{d}x_1 \mathrm{d}x_2 \mathrm{d}y_1 \mathrm{d}y_2 \quad \text{(B.52)}$$

Recalling the definition of the subaperture function, Equation 2.42, Equation B.52 becomes:

$$\left\langle \vec{\theta}_t \cdot \vec{\theta}_s \right\rangle = \frac{12 \cdot 6.88}{\Delta x k^2 d^6 r_o^{5/3}} \iiiint x_2 \text{rect}\left(\frac{x_1}{d}\right) \text{rect}\left(\frac{x_2}{d}\right) \text{rect}\left(\frac{y_1}{d}\right) \text{rect}\left(\frac{y_2}{d}\right) \times \left[\sqrt{\left(x_2 - x_1 + \frac{\Delta x}{2}\right)^2 + (y_2 - y_1)^2}^{\frac{5}{3}} - \sqrt{\left(x_2 - x_1 - \frac{\Delta x}{2}\right)^2 + (y_2 - y_1)^2}^{\frac{5}{3}} \right] \times dx_1 dx_2 dy_1 dy_2 \tag{B.53}$$

As before, the integral in Equation B.53 will be normalized with the same variable substitution that was used in Section B.2, Equation B.35. After some simplification, Equation B.53 becomes:

$$\left\langle \vec{\theta}_t \cdot \vec{\theta}_s \right\rangle = \frac{12 \cdot 6.88}{2^5 2^{5/3} k^2 d^{1/3} r_o^{5/3}} \frac{d/r_o}{s} \iiiint \xi_2 \text{rect}\left(\frac{\xi_1}{2}\right) \text{rect}\left(\frac{\xi_2}{2}\right) \text{rect}\left(\frac{\psi_1}{2}\right) \text{rect}\left(\frac{\psi_2}{2}\right) \times \left[\left| \left(\xi_2 - \xi_1 + \frac{s}{d/r_o}\right)^2 + (\psi_2 - \psi_1)^2 \right|^{\frac{5}{6}} - \left| \left(\xi_2 - \xi_1 - \frac{s}{d/r_o}\right)^2 + (\psi_2 - \psi_1)^2 \right|^{\frac{5}{6}} \right] \times d\xi_1 d\xi_2 d\psi_1 d\psi_2 \tag{B.54}$$

Again, following similar steps in as Section B.2, the variable substitution defined by Equation B.37 is made, allowing Equation B.54 to become:

$$\left\langle \vec{\theta}_t \cdot \vec{\theta}_s \right\rangle = \frac{12 \cdot 6.88}{2^5 2^{5/3} k^2 d^{1/3} r_o^{5/3}} \frac{d/r_o}{s} \iiiint \left(\frac{1}{2}\Delta\xi + \Sigma\xi\right) \times \left[\left| \left(\Delta\xi + \frac{s}{d/r_o}\right)^2 + \Delta\psi^2 \right|^{\frac{5}{6}} - \left| \left(\Delta\xi - \frac{s}{d/r_o}\right)^2 + \Delta\psi^2 \right|^{\frac{5}{6}} \right] \times \text{rect}\left(\frac{\Sigma\xi - \frac{1}{2}\Delta\xi}{2}\right) \text{rect}\left(\frac{\Sigma\xi + \frac{1}{2}\Delta\xi}{2}\right) \text{rect}\left(\frac{\Sigma\psi - \frac{1}{2}\Delta\psi}{2}\right) \times \text{rect}\left(\frac{\Sigma\psi + \frac{1}{2}\Delta\psi}{2}\right) d\Delta\xi d\Sigma\xi d\Delta\psi d\Sigma\psi \tag{B.55}$$

Examination of Equation B.55 shows that all terms that depend on $\Sigma\psi$ can easily be separated. Thus, just as in Section B.2, we can just look at the integral:

$$\int \text{rect}\left(\frac{\Sigma\psi + \frac{1}{2}\Delta\psi}{2}\right) \text{rect}\left(\frac{\Sigma\psi - \frac{1}{2}\Delta\psi}{2}\right) d\Sigma\psi \tag{B.56}$$

This is identical to Equation B.39 and simply becomes:

$$\int \text{rect}\left(\frac{\Sigma\psi + \frac{1}{2}\Delta\psi}{2}\right) \text{rect}\left(\frac{\Sigma\psi - \frac{1}{2}\Delta\psi}{2}\right) d\Sigma\psi = 2\text{tri}\left(\frac{\Delta\psi}{2}\right) \tag{B.57}$$

Hence, Equation B.55 becomes:

$$\begin{aligned}\left\langle \vec{\theta}_t \cdot \vec{\theta}_s \right\rangle = \frac{12 \cdot 6.88}{2^4 2^{5/3} k^2 d^{1/3} r_o^{5/3}} \frac{d/r_o}{s} \iint \left(\frac{1}{2}\Delta\xi + \Sigma\xi\right) \\ \times \left[\left|\left(\Delta\xi + \frac{s}{d/r_o}\right)^2 + \Delta\psi^2\right|^{\frac{5}{6}} - \left|\left(\Delta\xi - \frac{s}{d/r_o}\right)^2 + \Delta\psi^2\right|^{\frac{5}{6}}\right] \\ \times \text{rect}\left(\frac{\Sigma\xi - \frac{1}{2}\Delta\xi}{2}\right) \text{rect}\left(\frac{\Sigma\xi + \frac{1}{2}\Delta\xi}{2}\right) \text{tri}\left(\frac{\Delta\psi}{2}\right) \\ \times d\Delta\xi d\Sigma\xi d\Delta\psi\end{aligned} \tag{B.58}$$

To aid in the visualization of the next steps, Equation B.58 will be written as:

$$\begin{aligned}\left\langle \vec{\theta}_t \cdot \vec{\theta}_s \right\rangle = \frac{12 \cdot 6.88}{2^4 2^{5/3} k^2 d^{1/3} r_o^{5/3}} \frac{d/r_o}{s} \Bigg[\iint \frac{1}{2}\Delta\xi \left[\left|\left(\Delta\xi + \frac{s}{d/r_o}\right)^2 + \Delta\psi^2\right|^{\frac{5}{6}} - \left|\left(\Delta\xi - \frac{s}{d/r_o}\right)^2 + \Delta\psi^2\right|^{\frac{5}{6}}\right] \\ \times \text{rect}\left(\frac{\Sigma\xi - \frac{1}{2}\Delta\xi}{2}\right) \text{rect}\left(\frac{\Sigma\xi + \frac{1}{2}\Delta\xi}{2}\right) \text{tri}\left(\frac{\Delta\psi}{2}\right) d\Delta\xi d\Sigma\xi d\Delta\psi \\ + \iint \Sigma\xi \left[\left|\left(\Delta\xi + \frac{s}{d/r_o}\right)^2 + \Delta\psi^2\right|^{\frac{5}{6}} - \left|\left(\Delta\xi - \frac{s}{d/r_o}\right)^2 + \Delta\psi^2\right|^{\frac{5}{6}}\right] \\ \times \text{rect}\left(\frac{\Sigma\xi - \frac{1}{2}\Delta\xi}{2}\right) \text{rect}\left(\frac{\Sigma\xi + \frac{1}{2}\Delta\xi}{2}\right) \text{tri}\left(\frac{\Delta\psi}{2}\right) d\Delta\xi d\Sigma\xi d\Delta\psi \Bigg]\end{aligned} \tag{B.59}$$

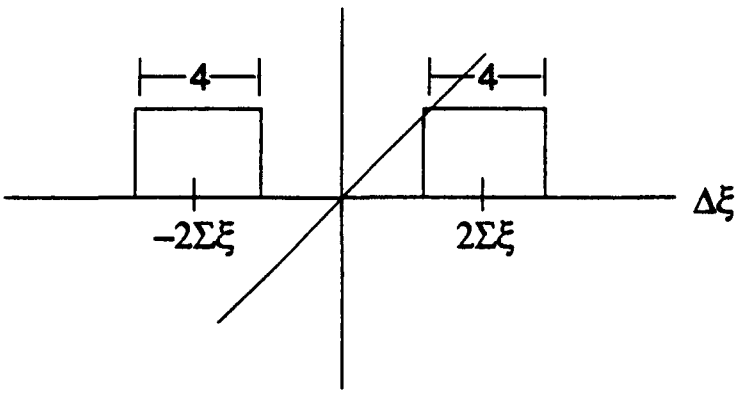

Figure B.1. Plot Showing Integration of an Odd Function over a Symmetric Period.

In the first triple integral of Equation B.59, the terms depended on $\Sigma\xi$ are easily separated to form the common result:

$$\int \text{rect}\left(\frac{\Sigma\xi - \frac{1}{2}\Delta\xi}{2}\right) \text{rect}\left(\frac{\Sigma\xi + \frac{1}{2}\Delta\xi}{2}\right) d\Sigma\xi = 2\text{tri}\left(\frac{\Delta\xi}{2}\right) \tag{B.60}$$

The $\Sigma\xi$ terms in the second triple integral can also be separated as:

$$\int \Sigma\xi \text{rect}\left(\frac{\Sigma\xi - \frac{1}{2}\Delta\xi}{2}\right) \text{rect}\left(\frac{\Sigma\xi + \frac{1}{2}\Delta\xi}{2}\right) d\Sigma\xi \tag{B.61}$$

While Equation B.61 is not as trivial as the others, examination of Figure B.1 reveals that it is merely the integration of an odd function, $\Sigma\xi$, over a symmetric interval, and hence the integral is zero.

$$\int \Sigma\xi \text{rect}\left(\frac{\Sigma\xi - \frac{1}{2}\Delta\xi}{2}\right) \text{rect}\left(\frac{\Sigma\xi + \frac{1}{2}\Delta\xi}{2}\right) d\Sigma\xi = 0 \tag{B.62}$$

Therefore, the second triple integral in Equation B.59 goes to zero and, after substituting in Equation B.60, Equation B.59 becomes:

$$\left\langle \vec{\theta}_t \cdot \vec{\theta}_s \right\rangle = \frac{12 \cdot 6.88}{2^3 2^{5/3} k^2 d^{1/3} r_o^{5/3}} \frac{d/r_o}{s} \iint \frac{1}{2} \Delta\xi \left[\left| \left(\Delta\xi + \frac{s}{d/r_o} \right)^2 + \Delta\psi^2 \right|^{\frac{5}{6}} - \left| \left(\Delta\xi - \frac{s}{d/r_o} \right)^2 + \Delta\psi^2 \right|^{\frac{5}{6}} \right] \times \mathrm{tri}\left(\frac{\Delta\xi}{2} \right) \mathrm{tri}\left(\frac{\Delta\psi}{2} \right) \mathrm{d}\Delta\xi \mathrm{d}\Delta\psi \tag{B.63}$$

Recalling the definition of tri functions, Equation A.27, Equation B.63 becomes:

$$\left\langle \vec{\theta}_t \cdot \vec{\theta}_s \right\rangle = \frac{12 \cdot 6.88}{2^6 2^{5/3} k^2 d^{1/3} r_o^{5/3}} \frac{d/r_o}{s} \int_{-2}^{2} \int_{-2}^{2} \Delta\xi \left(2 - |\Delta\xi|\right) \left(2 - |\Delta\psi|\right) \times \left[\left| \left(\Delta\xi + \frac{s}{d/r_o} \right)^2 + \Delta\psi^2 \right|^{\frac{5}{6}} - \left| \left(\Delta\xi - \frac{s}{d/r_o} \right)^2 + \Delta\psi^2 \right|^{\frac{5}{6}} \right] \times \mathrm{d}\Delta\xi \mathrm{d}\Delta\psi \tag{B.64}$$

Equation B.64 can be written as:

$$\left\langle \vec{\theta}_t \cdot \vec{\theta}_s \right\rangle = \frac{0.406325 f_c\left(s \frac{r_o}{d}\right)}{k^2 d^{1/3} r_o^{5/3}} \tag{B.65}$$

where $f_c\left(s \frac{r_o}{d}\right)$ is defined as:

$$f_c(x) = x^{-1} \int_{-2}^{2} \int_{-2}^{2} \Delta\xi \left(2 - |\Delta\xi|\right) \left(2 - |\Delta\psi|\right) \times \left[\left| (\Delta\xi + x)^2 + \Delta\psi^2 \right|^{\frac{5}{6}} - \left| (\Delta\xi - x)^2 + \Delta\psi^2 \right|^{\frac{5}{6}} \right] \mathrm{d}\Delta\xi \mathrm{d}\Delta\psi \tag{B.66}$$

Bibliography

1. Babcock, Horace. W. "The Possibility of Compensating Astronomical Seeing," *Publ. Astron. Soc. Pac.*, *65*:229–236 (October 1953).
2. Fried, D.L. "Optical Resolution Through a Randomly Inhomogeneous Medium for Very Long and Very Short Exposures," *Journal of the Optical Society of America*, *56*(10):1372–1379 (October 1966).
3. Fugate, Robert Q., editor. *Laser Guide Star Adaptived Optics Workshop*, *1*, 10-12 March 1992.
4. Fugate, Robert Q. "Laser Beacon Adaptive Optics," *Optics and Photonics News*, *4*(6):14–19 (June 1993).
5. Gardner, Chester S., et al. "Design and Performance Analysis of Adaptive Optical Telescopes Using Laser Guide Stars," *Proceedings of the IEEE*, *78*(11):1721–1742 (November 1990).
6. Gaskill, Jack D. *Linear Systems, Fourier Transforms, and Optics*. New York: John Wiley and Sons, 1978.
7. Goodman, Joseph W. *Introduction to Fourier Optics*. New York: McGraw-Hill Publishing Company, 1968.
8. Goodman, Joseph W. *Statistical Optics*. New York: John Wiley and Sons, 1985.
9. Greenwood, Darryl P. and David L. Fried. "Power spectra requirements for wave-front-compensative systems," *Journal of the Optical Society of America*, *66*(3):193–206 (March 1976).
10. Hardy, John W. "Active Optics: A New Technology for the Control of Light," *Proceedings of the IEEE*, *66*(6):651–697 (June 1978).
11. Hardy, J.W. and A. J. MacGovern. "Shearing interferometry : a flexible technique for wavefront measurement," *SPIE Proceedings on Interferometric Metrology*, *816*:180–195 (1987).
12. Kane, Timothy J., et al. "Wavefront detector optimization for laser guided adaptive telescopes," *Proceedings of the SPIE*, *1114*:160–171 (1989).
13. Kane, T.J. and C.S. Gradner. *Optimal Design of an Adaptive Optic Wavefront Sensor*. Technical Report, Urbana, Illinois: University of Illinois, May 1989.
14. Lee, R.W. and J. C. Harp. "Weak scattering in random media, with applications to remote probing," *Proc. IEEE*, *57*:375–406 (1969).
15. Merkle, Fritz. "Adaptive Optics." *International Trends in Optics* edited by Josehph W. Goodmann, chapter 26, 375–390, Academic Press, Inc., 1991.
16. Newton, Sir Issac. *Opticks* (Fourth Edition). Dover Publications, Inc., 1952.
17. Roggemann, Michael C. and David W. Tyler. "Unconventional Imaging," *Optics and Photonics News*, 17–21 (March 1992).
18. Taub, Herbert and Donald L. Schilling. *Principles of Communication Systems* (Second Edition). McGraw-Hill Book Company, 1986.
19. Tyson, R.K. *Principles of Adaptive Optics*. Boston: Academic Press, Inc., 1991.
20. Walkup, J.F. and J.W. Goodman. "Limitations of fringe-parameter estimation at low light levels," *Journal of the Optical Society of America*, *63*(4):399–407 (April 1973).

21. Wallner, Edward P. "Optimal wave-front correction using slope measurements," *Journal of the Optical Society of America*, *73*(12):1771–1776 (December 1983).

22. Welsh, B. M. and M. C. Roggemann. "Evaluating the Performance of Adaptive Optical Telescopes." *NATO Advanced Study Institute, Adaptive Optics for Astronomy*, edited by D. Alloin and J.-M. Mariotti. Kluwer Academic Publishers, 1993.

23. Welsh, Byron M. and Chester S. Gardner. "Performance analysis of adaptive-optics systems using laser guide stars and slope sensors," *Journal of the Optical Society of America A*, *6*(12):1913–1923 (December 1989).

24. Yura, H.T. and M.T. Tavis. "Centroid anisoplanatism," *Journal of the Optical Society of America A*, *2*(5):765–773 (May 1985).

REPORT DOCUMENTATION PAGE

Form Approved
OMB No. 0704-0188

1. AGENCY USE ONLY (Leave blank)	2. REPORT DATE	3. REPORT TYPE AND DATES COVERED
	December 1993	Master's Thesis

4. TITLE AND SUBTITLE
Performance Comparison of Shearing Interferometer and Hartmann Wave Front Sensors

5. FUNDING NUMBERS

6. AUTHOR(S)
Timothy L. Pennington

7. PERFORMING ORGANIZATION NAME(S) AND ADDRESS(ES)
Air Force Institute of Technology, WPAFB OH 45433-6583

8. PERFORMING ORGANIZATION REPORT NUMBER
AFIT/GE/ENG/93D-31

9. SPONSORING/MONITORING AGENCY NAME(S) AND ADDRESS(ES)
Dr. Brent Ellerbroek
3550 Aberdeen Ave. S.E.
Phillips Lab/LIG
Kirtland AFB, NM 87117-5776

10. SPONSORING/MONITORING AGENCY REPORT NUMBER

11. SUPPLEMENTARY NOTES

12a. DISTRIBUTION/AVAILABILITY STATEMENT
Distribution Unlimited

12b. DISTRIBUTION CODE

13. ABSTRACT (Maximum 200 words)

The resolution of optical imaging systems is severely degraded from the diffraction limit by the random effects of the atmosphere. Techniques exist to compensate for the atmospheric turbulence, one of which is adaptive optics. A critical component in the adaptive optics system is the wavefront sensor. Presently, two types of sensors are being used–the Hartmann-Shack Wavefront Sensor and the Shearing Interferometer. Previous studies have compared these two sensors and found them to perform identically for a point source. However, to date, no comparison has been performed for an extended source and subaperture spacing larger than the correlation length of the atmosphere, r_o. This thesis has examined this problem and compared these two sensors for the above conditions. Results indicate that the sensors have comparable performance when an infinite number of photons are available. However, the photon limited cases indicate superior performance by the Hartmann Sensor.

14. SUBJECT TERMS	15. NUMBER OF PAGES
Atmospheric Optics, Hartmann, Shearing Interferometer, Adaptive Optics	91
	16. PRICE CODE

17. SECURITY CLASSIFICATION OF REPORT	18. SECURITY CLASSIFICATION OF THIS PAGE	19. SECURITY CLASSIFICATION OF ABSTRACT	20. LIMITATION OF ABSTRACT
UNCLASSIFIED	UNCLASSIFIED	UNCLASSIFIED	UL